Title
Neuronal Activity Regulates the Nuclear Proteome to Promote Activity-Dependent Transcription

Author
Herbst, Wendy

Publication Date
2021

Peer reviewed|Thesis/dissertation

UNIVERSITY OF CALIFORNIA

Los Angeles

Neuronal Activity Regulates the Nuclear Proteome to Promote Activity-Dependent Transcription

A dissertation submitted in partial satisfaction of the requirements for the degree Doctor of Philosophy in Neuroscience

by

Wendy Alice Herbst

2021

ABSTRACT OF THE DISSERTATION

Neuronal Activity Regulates the Nuclear Proteome to Promote Activity-Dependent Transcription

by

Wendy Alice Herbst

Doctor of Philosophy in Neuroscience

University of California, Los Angeles, 2021

Professor Kelsey Martin, Chair

The formation and plasticity of neuronal circuits relies on dynamic activity-dependent gene expression. While recent work has revealed the identity of important transcriptional regulators and of genes that are transcribed and translated in response to activity, relatively little is known about the cell biological mechanisms by which activity alters the nuclear proteome of neurons to link neuronal stimulation to transcription. Using nucleus-specific proteomic mapping in silenced and stimulated neurons, we uncovered an understudied mechanism of nuclear proteome regulation: activity-dependent proteasome-mediated degradation. We found that the tumor suppressor protein PDCD4 undergoes rapid stimulus-induced degradation in the nucleus of neurons. We demonstrate that degradation of PDCD4 is required for normal activity-dependent transcription, and that PDCD4 target genes include those encoding proteins critical for synapse formation, remodeling, and transmission. Our findings highlight the importance of the nuclear proteasome in regulating the activity-dependent nuclear proteome, and point to a specific role for PDCD4 as a regulator of activity-dependent transcription in neurons.

The dissertation of Wendy Alice Herbst is approved.

Samantha J. Butler

S. Lawrence Zipursky

James A. Wohlschlegel

Thomas J. O'Dell

Kelsey C. Martin, Committee Chair

University of California, Los Angeles

2021

TABLE OF CONTENTS

LIST OF FIGURES

LIST OF TABLES

ACKNOWLEDGEMENTS

I would like to thank Dr. Kelsey Martin for being an incredible mentor to me throughout my Ph.D. journey. Thank you for your guidance, insightful advice, kindness, and support. I'm so grateful to have worked in your lab, and am constantly inspired by your thoughtful perspectives on cell biology and neuroscience, as well as your commitment to rigorous, high-quality science. I've learned so much about science and about being a scientist in your lab.

I'd also like to thank all members of the Martin Lab, past and present. I especially want to thank Dr. Jennifer Achiro, who is a co-author on my manuscript and performed the RNA-sequencing data analysis, in addition to providing thoughtful feedback throughout the preparation and revision of the manuscript. A huge thank you to Dr. Jennifer Achiro, Dr. Sylvia Neumann, and Marika Watanabe for all of your scientific advice, as well as friendship.

Thanks to Weixian Deng and the Wohlschlegel lab for performing the mass spectrometry and data analysis, as well as the Technology Center for Genomics & Bioinformatics (TCGB) at UCLA for performing the RNA sequencing.

I would like to thank my committee members: Dr. Samantha Butler, Dr. Larry Zipursky, Dr. James Wohlschlegel, and Dr. Tom O'Dell. Thank you for all of your important feedback at my committee meetings over the years. It has been incredibly helpful having all of you on my committee.

Thank you to the UCLA Neuroscience Interdepartmental Program, especially student affairs officer Jenny Lee, for all of the support and encouragement. And thank you to my fellow classmates from the 2014 entering year for all the camaraderie.

I would like to formally acknowledge my funding from the National Institute of Mental Health (NRSA F31) and from the ARCS foundation.

The work described in Chapters 2-3 has been submitted for publication, with the author list as follows: Wendy A. Herbst, Weixian Deng, James A. Wohlschlegel, Jennifer M. Achiro, and Kelsey C. Martin. The work was conceived by W.A.H. and K.C.M., the work was performed by W.A.H. (APEX2 and PDCD4 neuron experiments), W.D. (mass spectrometry), and J.M.A. (RNA-seq data analysis), written and revised by W.A.H., J.M.A., and K.C.M., and supervised by K.C.M. and J.A.W.

On a personal note, I'd like to thank my family. To my husband, Nicholas Penthorn, thanks for making this cross-country journey with me as we both pursued our Ph.Ds. at UCLA. It was really special to go through these parallel journeys, in physics and in neuroscience, together. Thanks for brightening each day and for being a supportive partner. To my parents, Barbara Lipsky and Patrick Herbst, as well as my brother, Steven Herbst, thank you for all your love and support throughout the years, and for always being a phone call away during graduate school.

CURRICULUM VITAE

Education

College of William and Mary — August 2010 – May 2014

B.S. in Neuroscience — GPA 3.94

Research Experience

Graduate Student Researcher, UCLA — April 2015 – August 2021

Department of Biological Chemistry — Dr. Kelsey Martin

Undergraduate Research, College of William & Mary — January 2011 – June 2014

Department of Biology — Dr. Margaret Saha

Awards

NIH NRSA (F31) Fellowship — 2017 – 2020

Achievement Rewards for College Scientists (ARCS) Foundation Award — 2016 – 2019

NSF Graduate Research Fellowship Honorable Mention — 2016

Publications

1) Herbst WA, Deng W, Wohlschlegel JA, Achiro JM, Martin KC. Neuronal activity regulates the nuclear proteome to promote activity-dependent transcription. J Cell Bio. **In Revision.**
2) Herbst WA, Martin KC. 2017. Regulated transport of signaling proteins from synapse to nucleus. Curr Opin Neurobiol 45: 78-84.

Presentations

1) Herbst WA, Deng W, Wohlschlegel JA, Martin KC. Activity-dependent regulation and role of PDCD4 in neurons. UCLA Biological Chemistry Seminar Series; Los Angeles, CA. 2020.
2) Herbst WA, Deng W, Wohlschlegel JA, Martin KC. Identification of activity-dependent nucleocytoplasmic shuttling and protein degradation in neuronal nuclei. Janelia Research Campus, Cell Biology of Neurons and Circuits II, Selected Short Talk & Poster Presentation. Ashburn, VA. 2019.
3) Herbst WA, Wohlschlegel JA, Martin KC. Identification of neuronal activity-dependent synapse-to-nucleus signaling proteins. UCLA Biological Chemistry Seminar Series; Los Angeles, CA. 2018.
4) Herbst WA, Vashisht AA, Rajbhandari AK, Fanselow MS, Houser CR, Wohlschlegel JA, Martin KC. Systematic identification of activity-dependent synaptonuclear signaling proteins in the hippocampus. Society for Neuroscience Poster Presentation; Washington DC, 2017

Chapter 1: Introduction

"Memories, even your most precious ones, fade surprisingly quickly. But I don't go along with that. The memories I value most, I don't ever see them fading."

Kazuo Ishiguro, *Never Let Me Go*

Synaptic plasticity, long-term potentiation, and memory

Humans have a remarkable capacity to remember information and events for a lifetime. Memories, which are formed during experiences or when learning new information and skills, are essential for navigating through everyday life and for constructing meaning out of one's life. Memory deficits, caused by aging and neurodegenerative diseases, can strip individuals of their identities and independence. The question of how memories are stored in the brain has been a subject of interest for centuries. In the 1890s, the neuroscientist Ramón y Cajal speculated that learning may require the formation of new connections between neurons (Ramón y Cajal, 1894). This concept was further developed in the 1940s, when Konorski and Hebb proposed that synaptic connections between neurons are strengthened in response to repeated stimulation (Konorski, 1948; Hebb, 1949). This activity-dependent change in the *strength* of synaptic connections, as well as the activity-dependent change in the *number* of synaptic connections, is known as synaptic plasticity. In subsequent decades, synaptic plasticity was demonstrated to be an important underlying mechanism of memory formation (Takeuchi et al., 2014). An early model for studying the mechanisms of memory was the sea slug *Aplysia californica*. This organism displays a simple form of long-term memory, wherein the animal's gill withdrawal reflex can undergo sensitization when the touch has previously been paired with a painful

stimulus, or habituation when the touch is has been delivered previously without pairing to a painful stimulus. Sensitization is associated with *increased* synaptic connections, whereas habituation is associated with *decreased* synaptic connections between the presynaptic sensory neurons and postsynaptic motor neurons (Bailey and Chen, 1988). Synaptic plasticity occurs *in vivo* in the brain during memory formation, as indicated by the both detection of new synapses (Giachero et al., 2013; Heinrichs et al., 2013) and increases in synaptic strength (Whitlock, 2006; Gruart, 2006; Clarke et al., 2010) that occur during memory formation. Synaptic plasticity is required for memory formation, as it has been demonstrated that genetic or pharmacological disruptions to the proteins involved in synaptic plasticity subsequently disrupt memory formation (Morris et al., 1986; Sakimura et al., 1995; Tsien et al., 1996b). With the use of optogenetics, synaptic plasticity has also been demonstrated to be sufficient to produce memories. Liu et al. labeled neurons that were activated and involved in synaptic plasticity during a context-specific memory task, and found that re-activation of these neurons was sufficient to produce the memory, even in the absence of the context (Liu et al., 2014). Moreover, interventions to increase the concentration and activity of proteins involved in synaptic plasticity subsequently enhance memory formation (Lee and Silva, 2009).

Many studies of synaptic plasticity have focused on a specific region of the brain, the hippocampus. The hippocampus was shown to be important for long-term memory formation when a patient named Henry Molaison underwent a hippocampal lesion surgery in an attempt to prevent severe seizures, and the damage to the hippocampus resulted in a permanent inability to form new long-term episodic memories (Scoville and Milner, 1957). Other case studies in humans, as well as studies in animal models, have confirmed the importance of the hippocampus in memory formation (Bird and Burgess, 2008). In order to elucidate the mechanisms of synaptic

plasticity, an experimental model was developed in which electrophysiological techniques are used to stimulate hippocampal neurons and measure the strength of synaptic connections. In a landmark paper, Bliss and Lømo described the phenomenon of long-term potentiation (LTP), in which a high-frequency stimulation synapses results in a long-lasting increase in synaptic strength (Bliss and Lømo, 1973). Similarly, the phenomenon of long-term depression (LTD) was described, in which a low-frequency stimulation of synapses results in a long-lasting decrease in synaptic strength (Ito and Kano, 1982; Dudek and Bear, 1992). Together, LTP and LTD can alter the strength of connections between neurons and produce the long-lasting changes in neural circuitry that are important for memory formation.

Long-term potentiation is often mediated by changes that occur in the postsynaptic neuron. In brief, glutamatergic transmission activates AMPA receptors, which depolarize the postsynaptic compartment via influx of sodium ions. A strong stimulation will sufficiently depolarize the compartment, such that the magnesium block on NMDA receptors is relieved and glutamatergic transmission can then activate NMDARs, eliciting sodium and calcium ion influx (Nicoll, 2017). Calcium is an important second messenger, which binds to the calcium-sensitive binding protein calmodulin (CaM), activating many kinases and phosphatases, including CaM kinase II (CaMKII). Once active, CaMKII phosphorylates many targets, including AMPARs and related regulatory proteins, leading to increased synaptic localization and conductance of AMPARs (Lisman et al., 2002) and thereby increasing the strength of synaptic connection by increasing the strength of the postsynaptic response. This mechanism is important for producing changes that are responsible for the early stages of LTP. Later stages of LTP are transcription- and translation-dependent.

Transcription is required for long-term potentiation and memory

Long-lasting changes in synaptic plasticity, LTP, and memory require activity-dependent gene expression. When transcriptional inhibitors are applied during the LTP-inducing stimulation, synaptic strength increases only briefly, before returning to baseline levels (Nguyen et al., 1994; Nguyen and Kandel, 1997; Chotiner et al., 2003). Similarly, when transcription inhibitors are delivered *in vivo* during a training session for a memory task in animal models, the animals are unable to form a long-term memory of the training session (Pedreira, 1996; Wüstenberg et al., 1998; Bailey et al., 1999). Notably, long-lasting LTP is impaired only when transcriptional inhibitors are applied during and shortly after the stimulation, but not when inhibitors are applied at later time points, demonstrating that there is a critical window of transcription following stimulation (Nguyen et al., 1994). Indeed, there is a large burst of transcription in response to neuronal stimulation (Brigidi et al., 2019; Tyssowski et al., 2018), long-term potentiation (Coba et al., 2008; Chen et al., 2017), and memory formation (Cho et al., 2016; Rao-Ruiz et al., 2019), which involving the regulation of thousands of genes. Immediate early genes (IEGs) are transcribed rapidly and as a direct response to stimulation. IEGs typically encode transcription factors, such as c-Fos, c-Jun, Egr1, Npas4, and Nr4a1, as well as effector genes that encode products that are directly relevant to the synapse, such as the cytoskeleton-associated protein Arc, the neurotrophic growth factor Bdnf, and the scaffolding protein Homer1a (Benito and Barco, 2015). Other genes are transcribed at later timepoints, often as transcriptional targets of the IEG transcription factors. While the immediate early genes are thought to be a generic response to neuronal activity irrespective of stimulus-type, the selection of late-response genes that are up-regulated is thought to be cell-type specific and tailored to the function of the neuron (Yap and Greenberg, 2018). Gene knockout studies of activity-dependent

genes demonstrate a role for activity-dependent genes in synaptic plasticity and memory (Fleischmann et al., 2003; Plath et al., 2006). Ultimately, activity-dependent transcription is important for generating the proteins that regulate the function of the synapse, which leads to changes in synapse number and strength.

Activity-dependent signaling from synapses to the nucleus

Given that transcription is required for synaptic plasticity and memory, signals from stimulated synapses must reach the nucleus, to regulate transcription. Neurons employ rapid signaling mechanisms, such as electrochemical signaling and calcium waves (Bading, 2013), as well as the slower signaling mechanism that involves the physical transport of signaling proteins from synapses to the nucleus (Herbst and Martin, 2017). Electrochemical signaling occurs on the order of milliseconds (Bengtson and Bading, 2012) and involves synaptic input producing an excitatory post-synaptic potential (EPSP) and triggering an action potential, which back-propagates to the soma and depolarizes the neuron, eliciting calcium influx through voltage-gated calcium channels (VGCCs) (Bading, 2013). Calcium waves involve synaptic inputs activating IP_3 signaling or calcium influx through VGCCs, which stimulates IP_3 receptors and ryanodine receptors on the endoplasmic reticulum (ER). Stimulation of these receptors elicits the release of calcium from the ER, and this increase in cytosolic calcium is then propagated along the ER via calcium-induced calcium release (Bengtson and Bading, 2012). Both electrochemical signaling and calcium waves ultimately produce an increase of intracellular calcium in the somatic cytoplasm and in the nucleus.

Following electrochemical signaling or calcium waves, an increase in calcium concentration leads to the activation of many calcium-sensitive kinases and phosphatases, via the

calcium-sensitive binding protein calmodulin (CaM) (Deisseroth et al., 2003). Calmodulin activates the family of CaM kinases (CaMKs), which are important for phosphorylating many activity-dependent targets, including transcription factors in the nucleus (Cohen et al., 2015). Notably, CaMKIV activates the transcription factor CREB by phosphorylation at serine 133, thereby enabling CREB-binding protein (CBP) to bind to CREB and promote transcription by acetylating histones (West et al., 2001). CREB is an important transcription factor in neurons, and promotes the transcription of many activity-dependent genes, including *c-fos*, *Arc*, and *Bdnf* (Ortega-Martínez, 2015). In addition to calcium-dependent signaling pathways, increases in calcium concentration can regulate certain transcriptional factors directly, such as the transcriptional repressor DREAM (Carrión et al., 1999).

The transport of signaling proteins from stimulated synapses to the nucleus occurs on the order of minutes or hours (Mikenberg et al., 2007; Dieterich et al., 2008; Ch'ng et al., 2012; Dinamarca et al., 2016; Kravchick et al., 2016a). This mechanism typically involves active transport of signaling proteins by dynein along microtubules (Mikenberg et al., 2007; Ch'ng et al., 2012) and the importin-mediated nuclear translocation of proteins through the nuclear pore complex (Dieterich et al., 2008; Dinamarca et al., 2016). Synapse-to-nucleus signaling proteins are often transcription factors (Mikenberg et al., 2007; Lai et al., 2008) or other proteins that regulate transcription (Ch'ng et al., 2012; Karpova et al., 2013). CRTC1, an exemplar synapse-to-nucleus signaling protein, localizes to synapses but undergoes activity-dependent dephosphorylation and nuclear translocation in response to stimulation (Ch'ng et al., 2012; Nonaka et al., 2014). Once in the nucleus, CRTC1 serves as a transcriptional co-activator for CREB and promotes the expression of activity-dependent genes (Ch'ng et al., 2012; Parra-Damas et al., 2014). The caldendrin-binding protein Jacob also localizes to synapses, and

undergoes activity-dependent translocation to the nucleus (Dieterich et al., 2008). Interestingly, the type of stimulation and subsequent phosphorylation state of Jacob is important for determining the function of Jacob in the nucleus; depending on which residues are phosphorylated, Jacob either enhances or attenuates CREB-dependent transcription (Karpova et al., 2013).

The different mechanisms of synapse-to-nucleus signaling –electrochemical signaling, calcium waves, and signaling proteins– all possess unique spatiotemporal signaling capabilities. Electrochemical signaling is a rapid signaling mechanism and is therefore ideal for encoding firing frequency information, but this signaling mechanism does not contain synapse-specific information, because the entire neuron is depolarized. Calcium waves are likely to contain some spatial information, as calcium waves propagate through the endoplasmic reticulum of a specific dendritic branch or the axon. Synapse-to-nucleus signaling proteins are the slowest mechanism, which may allow for a larger time window over which gene expression is impacted. Synapse-to-nucleus signaling proteins provide the most spatial information, as they can originate from individual stimulated synapses (Zhai et al., 2013; Ch'ng et al., 2015) and the phosphorylation state of these proteins can provide information about the type of stimulation received at that synapse (Ch'ng et al., 2012; Karpova et al., 2013). Both electrochemical signaling and synapse-to-nucleus signaling proteins can each be sufficient to produce activity-dependent changes in gene expression. Certain synaptic stimuli that do not produce electrochemical signaling or calcium waves can still undergo changes in gene expression, due to the translocation of signaling proteins (Zhai et al., 2013; Martin et al., 1997). Similarly, action potentials are sufficient to produce changes in gene expression in the absence of synaptic connections, underscoring the importance of electrochemical signaling (Eshete and Fields, 2001).

What are the mechanisms linking neuronal stimulation at synapses to changes in transcription in the nucleus?

A large body of work has described the activity-dependent changes in gene expression that occur in response to neuronal stimulation (Brigidi et al., 2019; Chen et al., 2017; Dörrbaum et al., 2020; Fernandez-Albert et al., 2019; Hrvatin et al., 2018; Lacar et al., 2016; Tyssowski et al., 2018). While the activity-dependent transcriptome has been well-characterized, less work has focused on the upstream changes that occur in the nucleus to produce these changes in transcription. Elucidating the mechanisms that link stimulation at neuronal synapses to changes in the nucleus will provide insight into how transcription is regulated in response to stimulation. The present study investigates this question by systematically characterizing, to our knowledge for the first time, the changes that occur in the nuclear proteome in response to neuronal activity (**Chapter 2**). We discovered that the tumor suppressor protein PDCD4 undergoes stimulus-induced proteasome-mediated degradation in the nucleus of neurons, with important consequences for activity-dependent transcription (**Chapter 3**). Lastly, we investigate an exemplar synapse-to-nucleus signaling protein CRTC1 by generating CRISPR/Cas9 conditional knockout mice (**Chapter 4**).

Chapter 2:

Identification of the neuronal activity-dependent nuclear proteome

INTRODUCTION

Activity-dependent transcription is critical for neural circuit function:

Stimulus-induced gene expression allows neurons to adapt their structure and function in response to a dynamically changing external environment (Yap and Greenberg, 2018; Holt et al., 2019; Gallegos et al., 2018). Activity-dependent transcription is critical to neural circuit function, from synapse formation during development (West and Greenberg, 2011; Flavell et al., 2006; Wayman et al., 2006; Polleux et al., 2007; Lin et al., 2008) to synaptic plasticity in the mature brain (Bloodgood et al., 2013; Chen et al., 2017; Ramanan et al., 2005; Tyssowski et al., 2018; Yap and Greenberg, 2018). During synapse development, activity-dependent transcription plays an important role at multiple steps, including axon guidance (Kashani et al., 2006; Graef et al., 2003), dendrite morphogenesis (Gaudillière et al., 2004; Aizawa et al., 2004), and synapse formation and elimination (Flavell et al., 2006; Lin et al., 2008). In the mature nervous system, activity-dependent transcription is required for synaptic plasticity and long-term potentiation (**Chapter 1**).

Neuronal activity can regulate gene expression in the nucleus through chromatin modification and transcriptional regulation and in the cytoplasm through regulation of RNA localization, stability, and translation (Martin and Ephrussi, 2009). The extreme morphological polarity and compartmentalization of neurons pose a cell biological challenge to the activity-

dependent regulation of gene expression: how are stimuli received at one site coupled to changes in gene expression within specific subcellular compartments? To produce activity-dependent changes in transcription, signals must be relayed from the site where the signal is received, at the synapse, to the nucleus. To better understand the activity-dependent mechanisms linking neuronal stimulation to changes in the nucleus, the present study compares the nuclear proteomes of silenced neurons and stimulated neurons, to identify activity-dependent changes.

Activity-dependent changes in the nuclear proteome:

Neuronal activity can change the concentration of nuclear proteins via a variety of mechanisms, from nucleocytoplasmic shuttling of signaling proteins, to synthesis or degradation of nuclear proteins. As such, when comparing the nuclear proteomes of silenced and stimulation neurons, a protein could be differentially expressed between the two conditions due to changes in shuttling, protein synthesis, or degradation.

Upon neuronal stimulation, many signaling proteins undergo nuclear import. This includes the nuclear import of synapse-to-nucleus signaling proteins, which originate at synapses and, upon stimulation, translocate to the nucleus (**Chapter 1**). Some examples of activity-dependent synapse-to-nucleus signaling proteins include: the transcriptional co-activator CRTC1 (Ch'ng et al., 2012), the CREB regulator Jacob (Dieterich et al., 2008), the nucleolus regulator AIDA-1D (Jordan et al., 2007), and the transcriptional regulator RNF10 (Dinamarca et al., 2016). Interestingly, one synapse-to-nucleus signaling protein, the transcriptional repressor CTBP1, only translocates to the nucleus upon neuronal *silencing*, and is tethered to synapses by neuronal stimulation (Ivanova et al., 2015). In addition to synapse-to-nucleus transport, there is also activity-dependent transport of signaling proteins from the nearby somatic cytoplasm into

the nucleus, including transport of the signaling protein CAMK2G (Ma et al., 2014) and the transcription factor NFAT (Wild et al., 2019). Proteins can also undergo activity-dependent nuclear export from the nucleus to the cytoplasm. Several histone de-acetylases are exported from the nucleus upon neuronal stimulation, thereby relieving an inhibitory brake on transcription (Chawla et al., 2003; Schlumm et al., 2013). Taken together, these examples demonstrate the array of nucleocytoplasmic shuttling that occurs are a result of neuronal activity.

Neuronal activity can also stimulate the proteasome-mediated degradation of nuclear proteins. There are well-known examples of stimulus-induced degradation of cytoplasmic proteins, for example, the degradation of the PKA regulatory subunit or inhibitor kappa B (Hegde et al., 1993; Mattson and Meffert, 2006), but degradation of nuclear proteins also occurs. Examples of nuclear proteins that undergo proteasome-mediated degradation include the repressor CREB1B, the methyltransferase DNMT3A1, and the transcription factor JUN (Upadhya et al., 2004; Bayraktar et al., 2020; Kravchick et al., 2016a). However, these studies have not examined if the proteins are degraded specifically in the nucleus, or exported from the nucleus and then degraded in the cytoplasm.

Neuronal activity can also stimulate the synthesis of new nuclear proteins. Numerous genes are transcribed and translated in response to neuronal stimulation, and many of these genes encode transcription factors or other proteins that, once translated in the cytoplasm, are imported into the nucleus (Yap and Greenberg, 2018). Examples of activity-dependent nuclear proteins that are synthesized in response to activity include the transcription factors NPAS4, FOS, and EGR1 (Lin et al., 2008; Sheng et al., 1990; Duclot and Kabbaj, 2017). It is important to note that the activity-dependent increase in nuclear abundance of these proteins is *downstream* of changes in transcription, and therefore increases in the nuclear concentration of these proteins occur

subsequent to the initial activity-dependent changes in nuclear signaling proteins. While the activity-dependent transcriptome and translatome of neurons has been extensively characterized (Brigidi et al., 2019; Chen et al., 2017; Dörrbaum et al., 2020; Fernandez-Albert et al., 2019; Hrvatin et al., 2018; Lacar et al., 2016; Tyssowski et al., 2018), less work has focused on the upstream changes that occur in the nucleus, specifically identifying the population of proteins that undergo activity-dependent changes in nuclear abundance due to regulated transport or stability, which can in turn influence transcription. In the present study, we characterize the nuclear proteomes of silenced and stimulated neurons in the presence of a protein synthesis inhibitor, in order to eliminate the activity-dependent changes that occur downstream of transcription and translation. We instead focus on identifying pre-existing proteins that undergo changes in nuclear localization or stability in response to activity. By characterizing stimulus-induced changes in the nuclear proteome, this study provides insight into how activity-dependent transcription is regulated.

Identifying the nuclear proteome using APEX2 proximity biotinylation:

Traditional methods of examining the nuclear proteome involves subcellular fractionation to biochemically isolate the nuclei from the other cellular components. In brief, this technique involves homogenization of the cells followed by separation of organelles by density centrifugation through a sucrose cushion (Guimarães de Araújo and Huber, 2007). Obtaining a pure nuclear fraction from neuronal samples is challenging because, in our hands, we found that synaptic components, including PSD95, pellet with the nuclear fraction using standard protocols (Yuanxiang et al., 2014). In protocols that *do* produce pure nuclear fractions (Uchida et al., 2017; Grabowski, 2005), we were unable to detect activity-dependent increases in the known synapse-

to-nucleus signaling protein CRTC1 when comparing nuclear samples from silenced and stimulated neurons, despite confirming successful nuclear translocation of CRTC1 in parallel immunostaining experiments. We speculate that dynamic, activity-dependent nucleocytoplasmic shuttling proteins are sensitive to biochemical fractionation, and can leak out of the nucleus during fractionation protocols.

Proximity biotinylation techniques are a promising alternative to subcellular fractionation. One such technique, APEX2 proximity biotinylation, involves expression of an engineered ascorbate peroxidase (APEX) in living cells (Hung et al., 2016). To target APEX2 to a specific subcellular compartment of interest, APEX2 can be fused to localization signals, such as a nuclear localization signal (NLS). The cells are incubated with the labeling substrate biotin phenol, which, in the presence of hydrogen peroxide, is converted to biotin-phenoxyl radicals by APEX2. Biotin-phenoxyl covalently tags proteins that are in close proximity (20 nm) to the APEX2 enzyme (Rhee et al., 2013). Because proteins are only labeled if they are in the same subcellular space as APEX2, the biotinylated proteins can be captured from whole cell lysates, avoiding the need for subcellular fractionation. In addition to being specific to the desired subcellular compartment, APEX2 can also be expressed in the desired cell type of interest through the use of specific promoters. This is a major advantage over subcellular fractionation, as the nuclei of neurons and glia in heterogeneous samples is challenging to separate biochemically. In contrast to previous proximity labeling techniques that require many hours for labeling (Uezu et al., 2016; Sears et al., 2019), APEX2 labeling occurs rapidly during a 1-minute labeling period. This rapid labeling is advantageous for capturing dynamic, activity-dependent processes at precise time points. The development of APEX2 promixity biotinylation technology

enabled us to interrogate, for the first time, activity-dependent changes in the nuclear proteome of neurons.

RESULTS

Identification of the nuclear proteome from silenced and stimulated neurons using APEX2 proximity biotinylation and mass spectrometry

To identify proteins that undergo activity-dependent changes in nuclear localization or abundance, we analyzed the nuclear proteomes of silenced and stimulated cultured rat forebrain neurons. In developing this assay, we used CREB Regulated Transcriptional Coactivator 1 (CRTC1) as a positive control, as we have previously shown that glutamatergic activity drives the synapse-to-nucleus import of CRTC1, and that neuronal silencing decreases CRTC1 nuclear abundance (Ch'ng et al., 2012, 2015). We initially used nuclear fractionation to capture the nuclear proteins but discovered that CRTC1 leaked out of the nucleus during the assay. This suggested that nuclear fractionation was not a suitable method and led us to instead use APEX2 proximity biotinylation (Hung et al., 2016), an *in situ* proximity ligation assay, to identify activity-dependent changes in the nuclear proteome. To specifically label the nuclear proteome, we fused the engineered ascorbate peroxidase APEX2 to two SV40 nuclear localization signals (Kalderon et al., 1984) (NLSs, **Fig 2.1A**). APEX2 proximity ligation was advantageous for these experiments for the following reasons: 1) APEX2 biotinylated proteins can be captured directly by streptavidin pulldown, avoiding the need for subcellular fractionation, 2) biotinylation occurs rapidly (1-minute labeling period), and 3) APEX2 can be expressed in a specific cell type of interest. We designed a neuron-specific nuclear-localized APEX2 construct (**Fig 2.1A**) and transduced cultured rat forebrain neurons with adeno-associated virus (AAV) expressing

APEX2-NLS. Immunofluorescence of transduced neurons revealed that APEX2-NLS was expressed specifically in the nucleus (**Fig 2.1B**). We optimized the multiplicity of infection of AAV to achieve high transduction efficiency without overexpression of the construct (important as higher doses of AAV led to APEX2-NLS expression in the cytoplasm). When all three components of the labeling reaction were supplied (APEX2-NLS, biotin-phenol, and H_2O_2), proteins were biotinylated specifically in neuronal nuclei (**Fig 2.1B**). No labeling was detected in the absence of APEX2-NLS, biotin-phenol, or H_2O_2.

To identify proteins that undergo activity-dependent changes in nuclear abundance, we silenced neurons for 1 hour with the voltage-gated sodium channel antagonist tetrodotoxin (TTX) or stimulated neurons for 1 hour with bicuculline (Bic), which inhibits $GABA_A$ receptors and drives glutamatergic transmission. We also inhibited protein synthesis using cycloheximide (CHX) in these experiments because many of the genes that are rapidly transcribed and translated in response to activity encode nuclear proteins (Yap and Greenberg, 2018; Heinz and Bloodgood, 2020; Alberini, 2009). We were concerned that the translation of activity-dependent genes would overshadow – and thereby hinder the detection of – the upstream changes that occur in the nuclear proteome resulting from alterations in nuclear protein localization or stability. We confirmed that the CHX treatment used throughout this study impairs protein translation, as detected by the strong reduction of new protein synthesis as detected by AHA labeling (**Fig 2.2A-B**) as well as the complete inhibition of activity-dependent FOS induction (**Fig 2.2C-D**).

After silencing or stimulating neurons for 1 hour and performing the 1-minute labeling reaction (**Fig 2.3A)**, protein lysates were collected for analysis by western blot and mass spectrometry. In neurons expressing APEX2-NLS, many proteins at a variety of molecular weights were biotinylated in both TTX and Bic conditions, whereas very few proteins were

biotinylated in the No-APEX control, as detected by western blot (**Fig 2.3B**). The bands detected in the No-APEX control were at molecular weights of known endogenously biotinylated proteins (Hung et al., 2016). In all experiments, we also confirmed by immunocytochemistry that the APEX2-NLS construct localized to the nucleus during both experimental conditions (**Fig 2.4A-B**). For mass spectrometry, biotinylated proteins were captured using streptavidin pulldown and the nuclear proteomes were characterized using the TMT-MS3-SPS acquisition method (**Ting et al., 2011**) through LC-MS. We detected 4,407 proteins, and of those, 2,860 proteins were significantly enriched above the No-APEX negative control with log2 fold change (FC) > 3 and adjusted p-value < 0.05. In order to assess nuclear enrichment of the samples, we performed Gene Ontology (GO) cellular component analysis on the list of 2,860 proteins that were enriched above No-APEX (which could be matched to 2,615 unique gene IDs). Approximately 80% of the top 100 most abundant proteins detected in the study contained the GO term "nucleus", and over 60% of the entire list of 2,615 proteins contained the GO term "nucleus" (**Fig 2.4C-D**). We performed GO cellular component enrichment analysis and found that most of the top enriched terms were components of the nucleus (**Fig 2.4D**).

When comparing Bic and TTX conditions, 23 proteins were differentially expressed in the nucleus with log2FC > 0.5 or log2FC < -0.5 and p-value < 0.05 (**Table 2.1**). The highest-ranked protein by log2FC enriched in the Bic versus TTX nuclear proteome was the synapse-to-nucleus signaling protein, CRTC1 (Ch'ng et al., 2015; Nonaka et al., 2014; Sekeres et al., 2012) (**Fig 2.5A**). The next highest-ranked proteins were: the serine/threonine kinase TLK1, a component of Cajal bodies COIL, the pre-mRNA splicing enzyme PPWD1, and the transcriptional repressor GON4L (**Fig 2.5A**). The highest-ranked proteins enriched in the TTX versus Bic nuclear proteome were HDAC4 and HDAC5, both of which have been reported to

undergo nuclear export following neuronal stimulation (Chawla et al., 2003; Schlumm et al., 2013) (**Fig 2.5B**). The next highest-ranked protein was the tumor suppressor protein PDCD4 (see **Chapter 3**), followed by the ER-associated protein TMEM147 and a component of DNA maintenance, SMC5 (**Fig 2.5B**). Using immunocytochemistry (ICC), we confirmed that CRTC1 increased in the nucleus and HDAC4 decreased in the nucleus following Bic stimulation (**Fig 2.5C-F**). These findings demonstrate that the nucleus-specific APEX2 proximity ligation assay successfully captured activity-dependent changes in the nuclear proteome of neurons.

DISCUSSION

In this study, we sought to test how neuronal activity at the synapse changes the nuclear proteome to regulate activity-dependent transcription. While advances in transcriptomic technologies have enabled the identification of genes that undergo activity-dependent changes in expression (Brigidi et al., 2019; Chen et al., 2017; Fernandez-Albert et al., 2019; Tyssowski et al., 2018), the systematic identification of proteins that undergo changes in subcellular localization and/or stability has been more challenging. We implemented a new proximity-ligation approach to characterize changes in the nuclear proteome triggered by neuronal stimulation. Our results provide the first, to our knowledge, unbiased characterization of the population of proteins that undergo changes in nuclear abundance following neuronal silencing and/or glutamatergic stimulation, and does so in a manner that is independent of translation or transcription. We detected activity-dependent changes in the known nucleocytoplasmic shuttling proteins, CRTC1 and HDAC 4/5 (Ch'ng et al., 2012; Chawla et al., 2003), demonstrating the validity of this neuron-specific, subcellular compartment-specific assay.

In total, we identified 23 proteins that are differentially expressed when comparing the nuclei of silenced neurons and stimulated neurons. We investigated one candidate protein, PDCD4, in further detail (**Chapter 3**). The relatively small number of proteins identified could indicate that few proteins undergo activity-dependent changes in nuclear abundance, or it could indicate that there are technical limitations of the mass spectrometry approach. In the former case, it is important to note that this study characterized the neuronal nuclear proteome in response one type of stimulation, captured at one time point. Many proteins may only be regulated in response to specific types of stimulation, and the activity-dependent changes of different proteins might occur during disparate time windows. For example, CRTC1 rapidly translocates to the nucleus within minutes after bicuculline stimulation, but is also quickly exported from the nucleus after the stimulus has ended (Ch'ng et al., 2012). In contrast, importin β1 translocates to the nucleus on a slower time course, reaching the nucleus 30 minutes after a brief glutamate stimulation has ended (Thompson et al., 2004). Moreover, different stimuli such as LTP and LTD activate distinct signaling pathways, with the repressor CREB2 translocating to the nucleus following LTD but not LTP stimulation (Lai et al., 2008).

The relatively few changes detected in the activity-dependent nuclear proteome of neurons may also be due to technical limitations of our assay. While some activity-dependent changes in the nucleus are large and easy-to-detect, such as the 4-fold increase in nuclear CRTC1 (Ch'ng et al., 2012) or the 2-fold nuclear export of HDAC4 (Chawla et al., 2003), other biological changes may have a much smaller magnitude. For example, in order to detect the nuclear translocation of NFκB, the nuclear export inhibitor LMB was applied to trap translocated NFκB in the nucleus, enabling the detection of small amounts of protein in the nucleus (Mikenberg et al., 2007). Moreover, nuclear translocation of the Notch intracellular domain is

notoriously difficult to detect (Struhl and Adachi, 1998). While TMT-MS3-SPS has improved upon the quantitative capabilities of mass spectrometry (Ting et al., 2011), it remains technically challenging to detect small changes in protein expression.

The current study characterizes the nuclear proteome of neurons in response to bicuculline stimulation. Given that different signaling proteins may respond to distinct types of stimulation, future studies should characterize the nuclear proteome following a variety of stimulations. Notably, it would be important to examine the effect of LTP and LTD induction on the nuclear proteome, in order to investigate the role of the nucleus in different types of synaptic plasticity. While the current study characterizes the nuclear proteome in cultured neurons, future studies could expand this method to a more physiological model, such as the use of acute hippocampal slices. In order to label proteins, APEX2 proximity biotinylation requires a brief application of H_2O_2, which poses technical challenges for labeling tissue. The H_2O_2 needs to be applied long enough to penetrate the tissue, but long applications of H_2O_2 can cause cell death via oxidative stress. Nonetheless, APEX2 and other peroxide-based proximity biotinylation assays have been performed on dissected tissue samples (Li et al., 2020a; Mannix et al., 2019). Proximity biotinylation methods that do not require H_2O_2 typically have slow labeling kinetics that would not be suitable to capture dynamic processes, but recent advances have been made in increasing the kinetics of these enzymes (Cho et al., 2020).

While my current studies focused on the role of a single candidate protein identified by mass spectrometry (PDCD4, see **Chapter 3**), future work will be needed to characterize the other candidate proteins. For each candidate protein, it will be important to determine if the activity-dependent change in nuclear expression is due to nucleocytoplasmic shuttling or protein degradation. Moreover, the function of the candidate proteins can be addressed, in order to

provide insight into the signaling mechanisms regulating transcription in the nucleus. Preliminary immunocytochemistry from our lab suggested that two other proteins, the kinase TLK1 and the transcriptional repressor CBX6, undergo activity-dependent changes in nuclear expression.

METHODS

Primary Neuronal Cultures:

All experiments were performed using approaches approved by the UCLA Animal Research Committee. Forebrain from postnatal day 0 Sprague-Dawley rats (Charles River) was dissected in cold Hanks' Balanced Salt Solution (HBSS, Thermo Fisher) supplemented with 10 mM HEPES buffer and 1 mM sodium pyruvate. Sex was not determined and tissue from male and female pups were pooled. The tissue was chopped finely and digested in 1x trypsin solution (Thermo Fisher) in HBSS (supplemented with 120 µg/mL DNase and 1.2 mM $CaCl_2$) for 15 minutes at 37°C. The tissue was washed and triturated in Dulbecco's Modified Eagle Medium (Thermo Fisher) + 10% Fetal Bovine Serum (Omega Scientific) before plating on poly-DL-lysine (PDLL)-coated (0.1 mg/mL, Sigma) 10 cm dishes or 24-well plates containing acid-etched PDLL-coated coverslips (Carolina Biologicals). Neurons were plated at a density of 1 forebrain per 10 cm dish (for mass spectrometry experiments) or 1/2 forebrain per entire 24-well plate (for immunocytochemistry, RNA-seq, and western blot experiments). Neurons were cultured in Neurobasal-A (Thermo Fisher) supplemented with 1x B-27 (Thermo Fisher), 0.5 mM glutaMAX (Thermo Fisher), 25 µM monosodium glutamate (Sigma), and 25 µM β-mercaptoethanol (Sigma) and incubated at 37°C, 5% CO_2. When applicable, neurons were transduced with AAV at DIV 13. All experiments were performed at DIV 20.

Generation of Plasmids and AAV:

To create hSyn NLS-APEX2-EGFP-NLS, APEX2 was amplified from the pcDNA3 APEX2-NES plasmid (gift from Alice Ting, Addgene plasmid #49386) with three sequential sets of primers to add SV40 NLS to both the N-terminus and C-terminus of APEX2 (primer sets 1-3, **Table 2.2**). The design of using NLS on both sides of APEX2 was based on the design of Cas9-NLS (Swiech et al., 2015). NLS-APEX2-NLS was then inserted into the pAAV-hSyn-EGFP plasmid (gift from Bryan Roth, Addgene plasmid #50465) between the BamHI and EcoRI sites, replacing the EGFP insert. The final hSyn NLS-APEX2-EGFP-NLS construct was created by amplifying hSyn NLS-APEX2-NLS (primer set 4, **Table 2.2**) and EGFP (primer set 5, **Table 2.2**), and joining the two products at NheI and SacI. AAV9 was generated for APEX2-NLS at Penn Vector Core.

Pharmacological Treatments:

Neurons were pre-incubated with cycloheximide (CHX, 60 μM, Sigma) for 15 min before the start of the experiment and maintained in the media throughout the duration of the experiment, incubated at 37 °C. To silence the neurons, 1 μM tetrodotoxin (TTX, Tocris) was applied to the neurons for 1 hr. To stimulate the neurons, 40 μM (-)-bicuculline methiodide (Bic, Tocris) was applied to the neurons for 1 hr.

APEX2 Proximity Biotinylation, Streptavidin Pulldown, and On-Bead Tryptic Digestion:

For APEX2 mass spectrometry experiments, 3 biological replicates (sets of cultures) were prepared, with 3 samples in each replicate (APEX + Bic, APEX + TTX, and No APEX).

Neurons were TTX-silenced or Bic-stimulated for 1 hour in the presence of CHX (as above). During the final 30 minutes of the treatment, neurons were incubated with 500 µM biotin-phenol (APExBIO) at 37 °C. During the final 1 minute, labeling was performed by adding H_2O_2 to a final concentration of 1 mM. To stop the labeling reaction, neurons were washed three times in large volumes of quencher solution (phosphate-buffered saline with 10 mM sodium azide, 10 mM sodium ascorbate, and 5 mM Trolox).

Neurons were lysed with RIPA (50 mM Tris, 150 mM NaCl, 0.1% SDS, 0.5% sodium deoxycholate, 1% Triton X-100, pH 7.5) containing protease inhibitor cocktail (Sigma), phosphatase inhibitor cocktail (Sigma), and quenchers. Lysates were treated with benzonase (200 U/mg protein, Sigma) for 5 min and then clarified by centrifugation at 15,000 g for 10 min. Samples were concentrated with Amicon centrifugal filter tubes (3K NMWL, Millipore) to at least 1.5 mg/mL protein and quantified using Pierce 660 nm protein assay kit (Thermo Fisher).

For each sample, 2 mg of lysate was incubated with 220 µL Pierce streptavidin magnetic beads (Thermo Fisher) for 60 min at room temperature. Samples were washed twice with RIPA, once with 1M KCl, once with 0.1 M sodium carbonate, once with 2 M Urea 10 mM Tris-HCl pH 8.0, and twice with RIPA according to (Hung et al., 2016).

The streptavidin beads bound by biotinylated proteins were then washed three times with 8 M Urea 100 mM Tris-HCl pH 8.5 and three times with pure water, and then the samples were resuspended in 100 µl 50 mM TEAB. Samples were reduced and alkylated by sequentially incubating with 5 mM TCEP and 10 mM iodoacetamide for 30 minutes at room temperature in the dark on a shaker set to 1000 rpm. The samples were incubated overnight with 0.4 µg Lys-C and 0.8 µg trypsin protease at 37° C on a shaker set to 1000 rpm. Streptavidin beads were

removed from peptide digests, and peptide digests were desalted using Pierce C18 tips (100 µl bead volume), dried, and then reconstituted in water.

Tandem Mass Tag (TMT) Labeling:

The desalted peptide digests were labeled by TMT reagents according to the manufacturer's instructions (TMT10plex™ Isobaric Label Reagent Set). Essentially, peptides were incubated with acetonitrile reconstituted TMT labeling reagent for 1 hour and then quenched by adding hydroxylamine. Sample-label matches are: NoAPEX replicate #1 labeled with TMT126, APEX+Bic replicate #1 labeled with TMT127N, APEX+TTX replicate #1 labeled with TMT127C, APEX+TTX replicate #2 labeled with TMT128N, NoAPEX replicate #2 labeled with TMT128C, NoAPEX replicate #3 labeled with TMT129N, APEX+Bic replicate #2 labeled with TMT129C, APEX+Bic replicate #3 labeled with TMT130N, APEX+TTX replicate #3 labeled with TMT130C. Labeled samples were then combined, dried and reconstituted in 0.1% TFA for high pH reversed phase fractionation.

High pH Reversed Phase Fractionation:

High pH reversed phase fractionation was performed according to the manufacturer's instructions (Pierce High pH Reversed-Phase Peptide Fractionation Kit). Essentially, peptides were bound to the resin in the spin column and then eluted by stepwise incubations with 300 µl of increasing acetonitrile concentrations. The eight fractions were combined into four fractions (fractions 1 & 5, 2 & 6, 3 & 7, 4 & 8). Fractions were then dried by vacuum centrifugation and reconstituted in 5% formic acid for mass spectrometry analysis.

LC-MS Data Acquisition:

A 75 µm x 25 cm custom-made C18 column was connected to a nano-flow Dionex Ultimate 3000 UHPLC system. A 140-minute gradient of increasing acetonitrile (ACN) was delivered at a 200 nL/min flow rate as follows: 1 – 5.5% ACN phase from minutes 0 – 5, 5.5 – 27.5% ACN from minutes 5 – 128, 27.5 – 35% ACN from minutes 128 – 135, 35 – 80% ACN from minutes 135 – 136, 80% ACN hold from minutes 136 – 138 and then down to 1% ACN from minutes 138 – 140. An Orbitrap Fusion Lumos Tribrid mass spectrometer TMT-MS3-SPS method was used for data acquisition. Full MS scans were acquired at 120K resolution in Orbitrap with the AGC target set to 2e5 and a maximum injection time set to 50 ms. MS2 scans were collected in Ion Trap with Turbo scan rate after isolating precursors with an isolation window of 0.7 m/z and CID fragmentation using 35% collision energy. MS3 scans were acquired in Obitrap at 50K resolution and 10 synchronized selected precursor ions were pooled for each scan using 65% HCD energy for fragmentation. For data dependent acquisition, a 3-second cycle time was used to acquire MS/MS spectra corresponding to peptide targets from the preceding full MS scan. Dynamic exclusion was set to 30 seconds.

MS/MS Database Search:

MS/MS database searching was performed using MaxQuant (1.6.10.43) (Cox and Mann, 2008) against the rat reference proteome from EMBL (UP000002494-10116 RAT, Rattus norvegicus, 21649 entries). The search included carbamidomethylation on as a fixed modification and methionine oxidation and N-terminal acetylation as variable modifications. The digestion mode was set to trypsin and allowed a maximum of 2 missed cleavages. The precursor mass tolerances were set to 20 and 4.5 ppm for the first and second searches, respectively, while

a 20-ppm mass tolerance was used for fragment ions. Datasets were filtered at 1% FDR at both the PSM and protein-level. Quantification type was set to reporter ion MS3 with 10plex TMT option.

Statistical Inference in Mass Spectrometry Data:

MSStatsTMT (1.4.1) (Huang et al., 2020) was used to analyze the MaxQuant TMT-MS3 data in the APEX2 proximity labeling experiment to statistically assess protein enrichment. TTX channels were used for MS run level normalization. The "msstats" method was then used for protein summarization. P-values for t-tests were corrected for multiple hypothesis testing using the Benjamini-Hochberg adjustment. We identified proteins that were enriched above the No APEX negative control using a log2FC > 3 and adjusted p-value < 0.05 cutoff above the No APEX condition. Of this protein list, we then identified proteins that were differentially expressed when comparing between Bic and TTX conditions using log2FC > 0.5 or log2FC < -0.5 and p-value < 0.05. It is important to note that we used a non-adjusted p-value cutoff when identifying candidate proteins that were differentially expressed between the TTX-silenced and Bic-stimulated conditions, because only HDAC4 and six other proteins had a significant adjusted p-value when using these cutoffs. Even CRTC1, a protein that has been shown to undergo activity-dependent changes in multiple studies (Ch'ng et al., 2012, 2015; Nonaka et al., 2014) and confirmed again in the present study, did not reach adjusted p-value significance, suggesting that we do not have the statistical power to detect certain activity-dependent changes. Because we used non-adjusted p-values to identify candidate proteins, it is especially important to experimentally validate any potential candidate protein.

Western Blot:

Protein lysates were boiled in loading buffer (10% glycerol, 1% SDS, 60 mM Tris HCl pH 7.0, 0.1 M DTT, 0.02% bromophenol blue) for 10 min at 95°C and run on at 8% polyacrylamide gel for 90 min at 120 V. Samples were wet-transferred onto a 0.2 µm nitrocellulose membrane for 16 hours at 40 mA. The membrane blocked with Odyssey Blocking Buffer and then incubated with IRDye 800CW Streptavidin (1:1,000) for 1 hour at room temperature. The membrane was imaged using the Odyssey Infrared imaging system (LI-COR).

Immunocytochemistry (ICC):

Neurons were fixed with 4% paraformaldehyde in phosphate-buffer saline (PBS) for 10 min, permeabilized in 0.1% Triton X-100 in PBS for 5 min, and blocked in 10% goat serum in PBS for 1 hour. Neurons were incubated with primary antibodies: chicken MAP2 (PhosphoSolutions #1100-MAP2, 1:1000), rabbit CRTC1 (Bethyl #A300-769, 1:1000), rabbit HDAC4 (CST #7628, 1:100), and rabbit FOS (CST #2250, 1:500) for 3-4 hours at room temperature or overnight at 4°C. Neurons were washed with PBS, and incubated at 1:1000 with secondary antibodies: anti-chicken Alexa Fluor 647, anti-rabbit Alexa Fluor 555 or Streptavidin Alexa Fluor 555, and Hoechst 33342 stain for 1 hour at room temperature. Neurons were washed with PBS, and mounted on slides with Aqua-Poly/Mount (Polysciences) for confocal imaging.

Protein Synthesis Assay (AHA Labeling):

Neurons were washed once in warm Tyrode's solution (140 mM NaCl, 10 mM HEPES, 5 mM KCl, 3 mM $CaCl_2$, 1 mM $MgCl_2$, 20 mM glucose, pH 7.4) and then incubated in methionine-free Hibernate A (BrainBits) supplemented with 1x B-27 for 30 min at 37°C, 0%

CO2 (due to the buffering conditions of Hibernate A). Neurons were then incubated in 4 mM AHA (L-Azidohomoalanine, Thermo Fisher) or the non-labeling control 4 mM methionine (Sigma) for 2 hrs in Hibernate A at 37°C, 0% CO2. When applicable, 60 μm CHX was pre-incubated for 15 min before the start of the AHA-labeling and remained in the media throughout the duration of the experiment. Neurons were washed twice in cold Tyrode's solution, fixed with 4% paraformaldehyde in phosphate-buffered saline (PBS) for 10 min, permeabilized in 0.1% Triton X-100 in PBS for 5 min, and washed three times in 3% bovine serum albumin in PBS. The Click-IT reaction was performed using the Click-iT Cell Reaction Buffer Kit (Thermo Fisher) and Alexa Fluor 488 Alkyne (Thermo Fisher) according to manufacturer's instructions, with a 30 min reaction at room temperature using 5 μM Alexa Fluor 488 alkyne. Neurons were washed three times in 3% bovine serum albumin in PBS, and then proceeded to the normal ICC protocol above, starting at the goat serum blocking step.

Confocal Imaging:

Samples were imaged using a Zeiss LSM 700 confocal microscope with a 40x / 1.3 NA and 63x 1.4 NA oil objective and 405 nm, 488 nm, 555 nm, and 639 nm lasers, using Zen microscopy software. All images were acquired using the 40x objective, except for the AHA incorporation protein synthesis experiments, which were imaged using the 63x objective. Identical image acquisition settings were used for all images within an experiment. For each image acquisition, the experimenter viewed the MAP2 and Hoechst channels to select a field-of-view, and was blind to the experimental channel (GFP, streptavidin, CRTC1, HDAC4, etc.).

Image Analysis:

ICC images were processed using ImageJ (Schindelin et al., 2012). An ImageJ macro was used to create regions of interest (ROIs) for neuronal nuclei. In brief, the Hoechst signal was used to outline the nucleus, and the MAP2 signal was used to select neurons and exclude non-neuronal cells. To create ROIs for neuronal cytoplasm, the cell body of each neuron was manually outlined using the MAP2 signal and then the nuclear ROI was subtracted from the total cell body ROI. The ROIs were used to calculate the mean intensity in the channel of interest (GFP, CRTC1, HDAC4, etc) for the nucleus and cytoplasm of each neuron. Within each ICC experimental replicate, the measured values from all ROIs were normalized to the median value of the control condition (basal).

Quantification and Statistical Analysis:

For ICC experiments, the quantification of signal intensity is displayed in violin plots using GraphPad Prism. The medians are indicated with thick lines and the quartiles are indicated with thin lines. "n" refers to the number of neurons in each condition, and all individual data points were plotted on the graphs. Our sample sizes were not pre-determined. A non-parametric statistical test (Mann-Whitney U test) was used to calculate statistical significance because our data were not normally distributed, as indicated by the violin plots. A Bonferroni correction was used to adjust for multiple hypothesis testing.

FIGURE LEGENDS

Figure 2.1 Design of APEX2-NLS to label nuclear proteins in cultured neurons.

A) Design of APEX2-NLS construct. hSyn = human synapsin promoter, NLS = SV40 nuclear localization signal.

B) Immunocytochemistry (ICC) of cultured rat forebrain neurons after APEX2 proximity biotinylation labeling. Nuclear proteins were biotinylated (streptavidin, red) by the combined presence of APEX2-NLS (GFP, green), biotin-phenol (BP), and H_2O_2. Scale bar = 10 µm.

Figure 2.2 Cycloheximide effectively inhibits protein synthesis.

A) Metabolic labeling and ICC of control, CHX-treated, and non-labeled cells. Protein synthesis was measured by AHA incorporation and Click-IT Alexa Fluor 488 alkyne reaction. The Alexa Fluor 488 signal intensity is displayed using a look up table. Scale bar = 10 µm.

B) Violin plots of normalized somatic Click-IT intensity. Control n = 90, CHX n = 63 cells, No Label n = 7 cells, from 2 sets of cultures. Control median = 1.00, CHX median = 0.32, No Label median = 0.05. Control vs CHX $p < 0.0001$.

C) FOS ICC of basal and Bic-stimulated neurons, in the presence or absence of cycloheximide (CHX). Scale bar = 10 µm.

D) Violin plots of normalized nuclear FOS ICC intensity. Basal n = 28, Bic n = 40 cells, CHX-Basal n = 32, CHX-Bic n = 26 cells, from 1 set of cultures. Basal median = 1.00, Bic median = 4.484, CHX-Basal median = 0.8941, CHX-Bic median = 0.8307. Basal vs Bic $p < 0.0001$, CHX-Basal vs CHX-Bic $p = 0.3064$.

Statistical significance is indicated by ****$p < 0.0001$, from Mann-Whitney U test.

Figure 2.3 Labeling the nuclear proteomes of silenced and stimulated neurons.

A) Workflow for labeling nuclear proteins from silenced and stimulated neurons. APEX2 labeling diagram based on (Hung et al., 2016).

B) Western blot of cultured neuron protein lysates from No APEX, APEX+TTX, or APEX+Bic conditions, stained with streptavidin.

Figure 2.4 APEX2-NLS is localized to the nucleus and labels nuclear proteins.

A) Localization of APEX2-NLS GFP in TTX-silenced and Bic-stimulated neurons, in the presence of CHX. Scale bar = 30 µm.

B) Violin plots of APEX2-NLS GFP nucleocytoplasmic localization (nuc / cyto ratio) in TTX-silenced and Bic-stimulated neurons, in the presence of CHX. TTX n = 116, Bic n = 120 cells, from 9 sets of cultures. TTX median = 4.31, Bic median = 4.00. TTX vs Bic p = 0.0562.

C) Bar graphs displaying the percentage of proteins containing the GO term "nucleus" (GO:0005634), from the list of proteins detected by APEX2-NLS mass spectrometry. The list of proteins detected by mass spectrometry was ranked according to MS/MS count abundance, and separate bar graphs are displayed for the top 50 proteins, top 100 proteins, and so on.

D) Cellular component GO analysis of the APEX2-NLS mass spectrometry, with the top 18 terms listed in order of fold enrichment. Nuclear cellular components are listed in blue.

Figure 2.5 Comparing the nuclear proteomes of silenced and stimulated neurons.

A) The top five proteins enriched in the nucleus of Bic-stimulated neurons, as ranked by Bic vs TTX log2FC.

B) The top five proteins enriched in the nucleus of TTX-silenced neurons, as ranked by Bic vs TTX log2FC.

C) CRTC1 ICC of basal, TTX-silenced, and Bic-stimulated neurons. Scale bar = 10 µm.

D) Violin plots of normalized nuclear CRTC1 ICC intensity. Basal n = 28, TTX n = 21, Bic n = 22 cells, from 1 set of cultures. Basal median = 1.00, TTX median = 0.33, Bic median = 2.64. Basal vs Bic $p < 0.0001$, TTX vs Bic $p < 0.0001$.

E) HDAC4 ICC of basal, TTX-silenced, and Bic-stimulated neurons. Scale bar = 10 μm.

F) Violin plots of normalized nuclear HDAC4 ICC intensity. Basal n = 28, TTX n = 24, Bic n = 26 cells, from 1 set of cultures. Basal median = 1.00, TTX median = 1.79, Bic median = 0.61. Basal vs Bic $p = 0.0006$, TTX vs Bic $p < 0.0001$.

Statistical significance is indicated by ***$p < 0.001$ and ****$p < 0.0001$, from Mann-Whitney U test with Bonferroni correction.

Table 2.1

Candidate proteins that are differentially expressed in the nucleus of silenced vs stimulated neurons.

Table 2.2

Primers used for cloning APEX2-NLS.

Figure 2.1

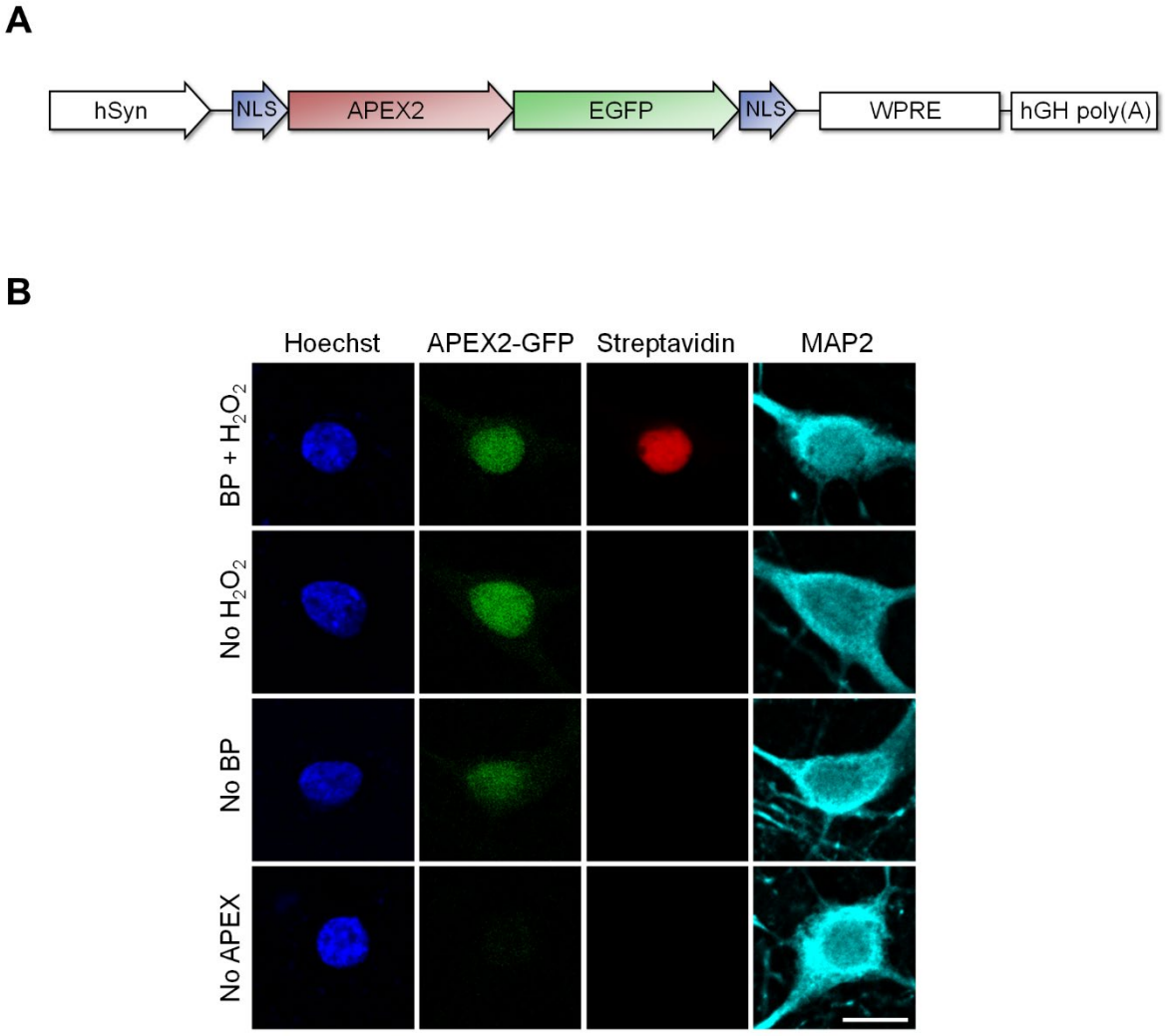
A
hSyn
NLS
APEX2
EGFP
NLS
WPRE
hGH poly(A)
B
Hoechst
APEX2-GFP
Streptavidin
MAP2
BP + H2O2
No H2O2
No BP
No APEX

Figure 2.2

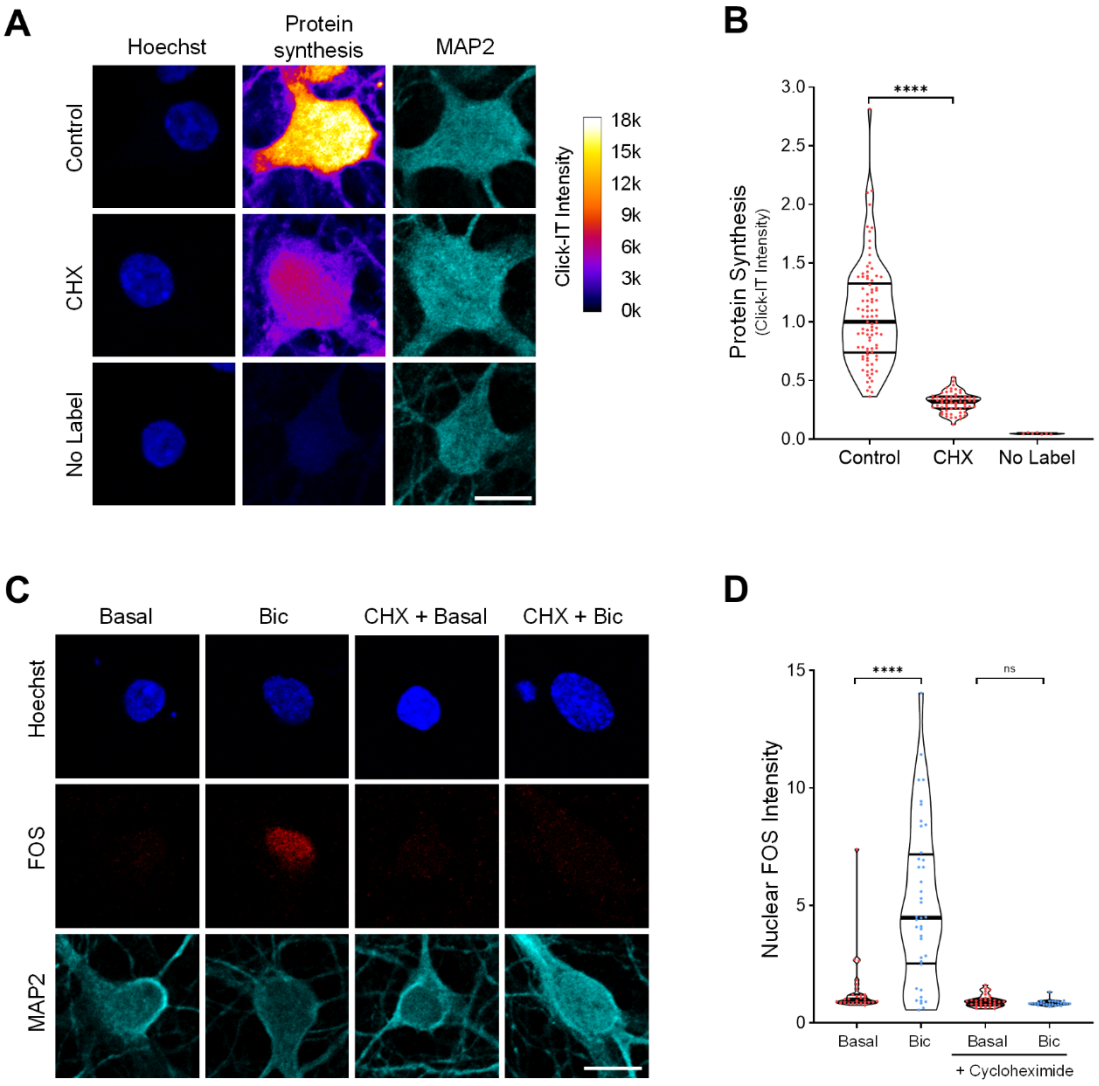
A
Hoechst
Protein synthesis
MAP2
Control
CHX
No Label
Click-IT Intensity
18k
15k
12k
9k
6k
3k
0k
B
Protein Synthesis
(Click-IT Intensity)
3.0
2.5
2.0
1.5
1.0
0.5
0.0
****
Control
CHX
No Label
C
Basal
Bic
CHX + Basal
CHX + Bic
Hoechst
FOS
MAP2
D
Nuclear FOS Intensity
15
10
5
0
****
ns
Basal
Bic
Basal
Bic
+ Cycloheximide

Figure 2.3

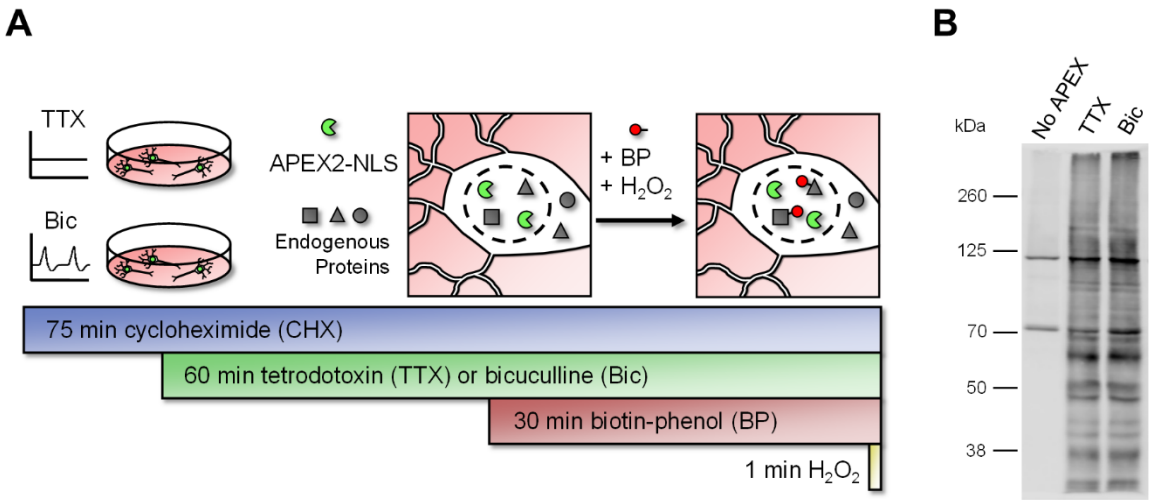
A
TTX
Bic
APEX2-NLS
Endogenous Proteins
+ BP
+ H2O2
75 min cycloheximide (CHX)
60 min tetrodotoxin (TTX) or bicuculline (Bic)
30 min biotin-phenol (BP)
1 min H2O2
B
kDa
No APEX
TTX
Bic
260
125
70
50
38

Figure 2.4

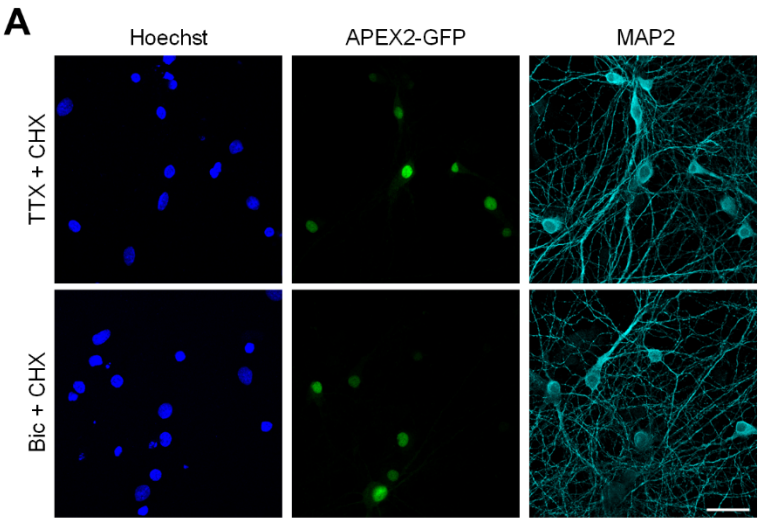

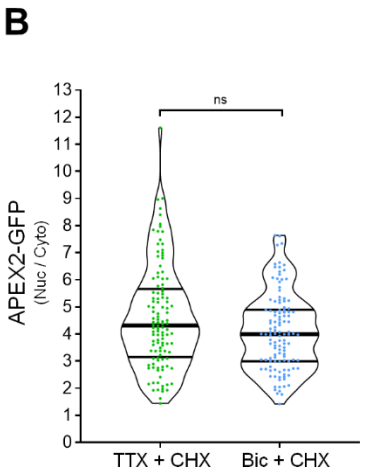

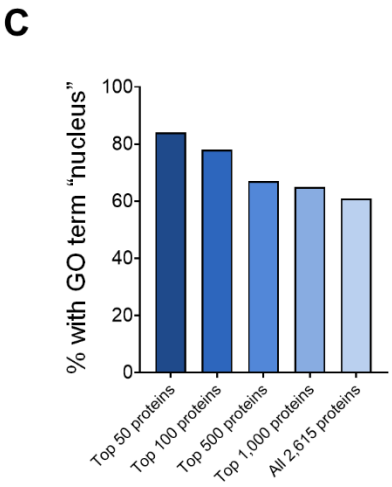

D

GO Cellular Component	# Terms in Dataset	# Terms Expected	Fold Enrichment	FDR
Supraspliceosomal Complex	4	.49	**8.17**	3.75E-02
Proteasome Activator Complex	4	.49	**8.17**	3.74E-02
Dendritic Filopodium	5	.61	**8.17**	1.50E-02
Barr Body	4	.49	**8.17**	3.73E-02
NURF Complex	6	.73	**8.17**	5.94E-03
Paraspeckles	6	.73	**8.17**	5.92E-03
Presynaptic Endocytic Zone	12	1.59	**7.54**	4.16E-05
Proteasome Regulatory Particle, Base Subcomplex	11	1.47	**7.49**	1.06E-04
Presynaptic Endocytic Zone Membrane	8	1.10	**7.26**	1.56E-03
PTW/PP1 Phosphatase Complex	6	.86	**7.00**	9.56E-03
Transcription Factor TFIIIC Complex	5	.73	**6.81**	2.32E-02
pICln-Sm Protein Complex	5	.73	**6.81**	2.32E-02
Nuclear Stress Granule	5	.73	**6.81**	2.31E-02
NuRD Complex	13	1.96	**6.64**	4.24E-05
CHD-type Complex	13	1.96	**6.64**	4.21E-05
Cyclin/CDK Positive Transcription Elongation Factor Complex	8	1.22	**6.53**	2.39E-03
Nuclear Lamina	8	1.22	**6.53**	2.38E-03
nBAF Complex	12	1.84	**6.53**	1.06E-04

Figure 2.5

A

Top proteins enriched in nucleus of Bic-stimulated neurons:

Symbol	Description	Log2FC Bic vs TTX	P-value
CRTC1	CREB Regulated Transcription Coactivator 1	1.21	0.0085
TLK1	Tousled Like Kinase 1	0.92	0
COIL	Coilin	0.79	0.0069
PPWD1	Peptidylprolyl Isomerase Domain And WD Repeat Containing 1	0.73	0.0016
GON4L	Gon-4 Like	0.73	0.0293

B

Top proteins enriched in nucleus of TTX-silenced neurons:

Symbol	Description	Log2FC Bic vs TTX	P-value
HDAC5	Histone Deacetylase 5	-1.04	0.0042
HDAC4	Histone Deacetylase 4	-0.93	0.0024
PDCD4	Programmed Cell Death 4	-0.89	0.0190
TMEM147	Transmembrane Protein 147	-0.84	0.0430
SMC5	Structural Maintenance Of Chromosomes 5	-0.82	0.0309

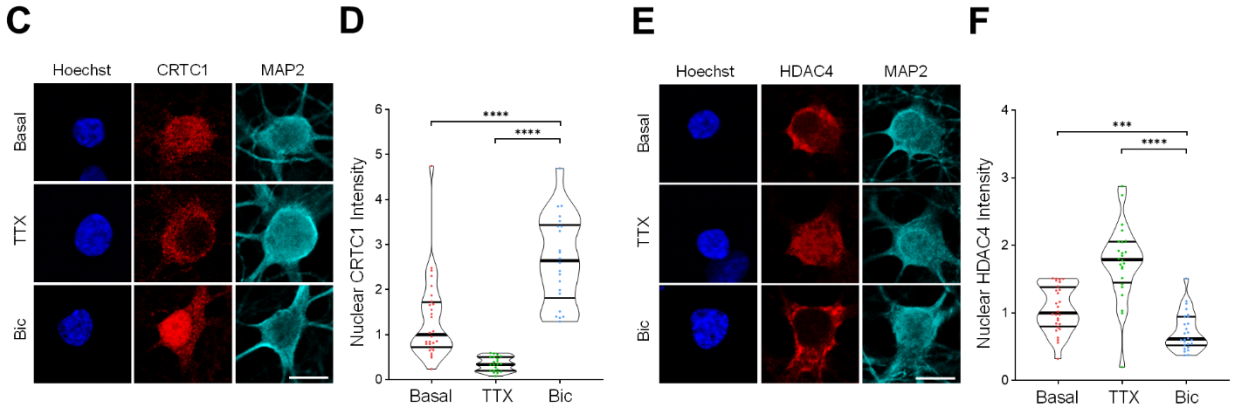

Table 2.1

Symbol	Log2FC (Bic vs TTX)	p-value
Crtc1	1.2067	0.008512
Hdac5	-1.0441	0.004163
Hdac4	-0.9263	0.002427
Tlk1	0.9155	0
Pdcd4	-0.8862	0.019014
Tmem147	-0.8393	0.042954
Smc5	-0.8245	0.03094
Coil	0.7947	0.006852
Czib	-0.7533	0.025884
Ppwd1	0.7280	0.001598
Gon4l	0.7258	0.029297
Ubxn2b	0.6990	0.030829
Hykk	-0.6864	3.50E-05
Serpine2	-0.6666	0.030284
Nop16	0.6638	0.00127
Larp6	0.6129	0.015253
Neurod2	0.5989	0.032162
Grk2	0.5698	0.023994
Chmp5	0.5436	0.0089
Tlk1	0.5306	0.008924
Ufc1	-0.5205	1.48E-20
Akirin2	0.5190	0.023126
Nelfe	-0.5126	0

Table 2.2

Primer	Sequence (5’ -> 3’)
Cloning Primer 1F (NLS-APEX2-NLS)	AGAAGAAACGTAAGGTCGAAGCGTCCGGAAAGTCTTACCCAACTGTGAGTG
Cloning Primer 1R (NLS-APEX2-NLS)	TCTTCTTCTTAGGACTGGCATCAGCAAACCCAAGCT
Cloning Primer 2F (NLS-APEX2-NLS)	CAAGGATGACGATGATAAGTCGCCCAAGAAGAAACGTAAGGTCGAAGC
Cloning Primer 2R (NLS-APEX2-NLS)	CTGGCCTCCACCTTTCTCTTCTTCTTAGGACTGGCATCAGC
Cloning Primer 3F (NLS-APEX2-NLS)	GTTGTTGGATCCCGCCACCATGGACTACAAGGATGACGATGATAAGTCGCC
Cloning Primer 3R (NLS-APEX2-NLS)	GGTGGTGAATTCTTAGCTGGCCTCCACCTTTCTCTTCTT
Cloning Primer 4F (hSyn-NLS-APEX2-NLS)	GGTGGTGAGCTCAGTCCTAAGAAGAAGAGAAAGGTGG
Cloning Primer 4R (hSyn-NLS-APEX2-NLS)	GTTGTTGCTAGCCTCGCTACCACCGGCATCAGCAAACCCAAGC
Cloning Primer 5F (EGFP)	GTTGTTGCTAGCGGAGGGTCAGTGAGTAAGGGCGAGGAGCT
Cloning Primer 5R (EGFP)	GGTGGTGAGCTCCTTGTACAGCTCGTCCATGCC

Chapter 3:

Activity-dependent regulation and role of PDCD4 in neurons

INTRODUCTION

PDCD4 is a tumor suppressor protein and translational repressor in the cytoplasm:

Programme**d** **C**ell **D**eath **4**, or PDCD4, was initially discovered in a cDNA screen of genes upregulated during apoptosis in several cell lines (Shibahara et al., 1995). Upregulation of PDCD4 is correlated with apoptosis (Zhang et al., 2006), while both overexpression and knockout of PDCD4 can promote pro-apoptotic pathways (Zhang et al., 2006; Eto et al., 2012). Moreover, PDCD4 has been demonstrated to be a tumor suppressor protein. Low concentrations of PDCD4 have been reported to correlate with invasion, proliferation, and metastasis of many types of cancers, including colon, lung, breast, and ovarian cancer (Allgayer, 2010; Chen et al., 2003; Wang and Yang, 2018; Wei et al., 2012). In mouse models and cell lines, knockdown and knockout of PDCD4 promotes tumor growth (Schmid et al., 2008; Cmarik et al., 1999), while overexpression of PDCD4 suppresses tumor growth (Jansen et al., 2005; Yang et al., 2003b).

Many studies have shown that PDCD4 functions as a translational repressor (Wang and Yang, 2018; Matsuhashi et al., 2019). Through its MA-3 domains, PDCD4 binds to the RNA helicase EIF4A, thereby preventing EIF4A from binding to EIF4G and participating in cap-dependent translation (Yang et al., 2003a). Because PDCD4 inhibits the participation of an RNA helicase in translation, PDCD4 is thought to impair translation of highly structured mRNAs. In particular, PDCD4 inhibits translation of *p53* and *Sin1* (Wedeken et al., 2011; Wang et al.,

2017). PDCD4's repression of *Sin1* translation impairs mTORs signaling and subsequent cancer growth, while PDCD4's repression of *p53* translation promotes apoptosis (Wang and Yang, 2018). In addition to binding to EIF4A, PDCD4 can bind directly to certain mRNAs, including *Bcl* and *XIAP*, and sterically inhibit their translation (Liwak et al., 2012). Recent PDCD4 knockdown and ribosome profiling experiments in retinal pigment epithelial cells have revealed that PDCD4 represses the translation of 62 genes involved in a variety of functions including extracellular matrix regulation, immune response, and metabolic processes (Haas et al., 2020).

PDCD4 may function as a transcriptional repressor in the nucleus:

While the role of PDCD4 as a translation repressor in the cytoplasm has been well characterized, less is known about the role of PDCD4 in the nucleus. Several studies have observed that PDCD4 also localizes to the nucleus and, in some cell lines and tissues, is localized predominately to the nucleus (Böhm et al., 2003; Palamarchuk et al., 2005; Fassan et al., 2011; Madera et al., 2020). Previous studies have indicated that PDCD4 can inhibit AP-1-dependent transcription, although there is conflicting evidence as to whether this inhibition occurs as a result of direct actions of PDCD4 in the nucleus (Bitomsky et al., 2004) or via an indirect role, e.g. in regulating the translation of signaling proteins in the cytoplasm (Yang et al., 2006). In Bitomsky et al., PDCD4 expression prevented the phosphorylation and activation of c-Jun (a component of AP-1-dependend transcription), and PDCD4 was demonstrated to bind directly to c-Jun, which the authors proposed was important for preventing Jun N-terminal kinase (JNK) from phosphorylating c-Jun. However, in Yang et al., PDCD4 inhibited JNK activation by inhibiting the translation of upstream signaling proteins in this pathway, and overexpression of

an upstream signaling protein, MAP4K1, rescued c-Jun activation and subsequent AP-1-dependent transcription.

However, other studies have provided evidence for role for PDCD4 regulating transcription directly in the nucleus. In cancer cell lines, PDCD4 binds directly to the transcription factor TWIST1 within the nucleus, inhibiting the DNA binding domain and preventing expression of TWIST1 transcriptional targets (Shiota et al., 2009). In fibroblasts, PDCD4 was demonstrated to interact with the CSL repressive complex in the nucleus, to bind to the promoters of CSL target genes, and to negatively regulate canonical Notch/CSL targets including *Hes1* (Jo et al., 2016). PDCD4 also interacts with the transcriptional regulator DAXX, is co-localized with DAXX in the nucleus, and promotes DAXX turnover by disrupting the interaction of DAXX with the de-ubiquitinylating enzyme HAUSP (Kumar et al., 2013). Of note, PDCD4 can also regulate transcription via a cytoplasmic role. Here, PDCD4 has been shown to bind to, and inhibit the nuclear translocation of, the NFκB p65 subunit (Hwang et al., 2014).

PDCD4 expression is regulated by multiple mechanisms:

PDCD4 expression is regulated at multiple levels: transcriptional regulation of the *Pdcd4* gene, miRNA-mediated translational repression of *Pdcd4* mRNA, nucleocytoplasmic shuttling of PDCD4 protein, and phosphorylation- and ubiquitin-mediated degradation of PDCD4 by the proteasome (Wang and Yang, 2018; Matsuhashi et al., 2019). Given that our study was conducted in the presence of the protein synthesis inhibitor cycloheximide, we considered it unlikely that the observed activity-dependent decrease in nuclear PDCD4 was due to changes in transcription and/or translation. We thus focused on the regulation of PDCD4 by nucleocytoplasmic shuttling and proteasome-mediated degradation.

PDCD4 can be localized to either the nucleus or cytoplasm of cells, depending on the cell and tissue type (Lankat-Buttgereit and Göke, 2009). Notably, the subcellular localization of PDCD4 can change in response to certain conditions. In fibroblasts, PDCD4 is normally localized to the nucleus but translocates to the cytoplasm upon serum starvation (Böhm et al., 2003). This nuclear export of PDCD4 was demonstrated to be mediated by CRM1, and the inhibitor Leptomycin B (LMB) blocked the starvation-induced nuclear export of PDCD4 (Böhm et al., 2003). Serum starvation-induced nuclear export was further confirmed by Palamarchuk et al. 2005, who additionally demonstrated that phosphorylation on serine 457 was required for nuclear localization of PDCD4 (Palamarchuk et al., 2005).

PDCD4 has also been shown to undergo proteasome-mediated degradation. Dorrello et al. reported that total PDCD4 levels decrease in response to serum stimulation of a glioblastoma cell line, and found that this decrease was blocked by the proteasome inhibitor MG132 (Dorrello et al., 2006). In keratinocytes, decreases in PDCD4 concentration in response to tumor-promoting TPA treatment was also found to be blocked by MG132 (Schmid et al., 2008). PDCD4 contains a canonical motif for binding to the E3 ubiquitin ligase βTRCP1/2, a ligase that binds to proteins and ubiquitinates them, marking them for degradation by the proteasome. Similar to disruption of the proteasome, knockdown of βTRCP was also found to prevent PDCD4 degradation (Dorrello et al., 2006). The binding of βTRCP to target proteins is typically mediated by phosphorylation at sites on the βTRCP-binding motif on the target protein (Cardozo and Pagano, 2004). Indeed, individual phospho-null serine-to-alanine mutations within and adjacent to this region at either serine 67, 71, or 76 completely prevented the degradation of PDCD4 (Dorrello et al., 2006). This region of PDCD4 contains canonical phosphorylation consensus sites for the kinases S6K1 and PKC; Ser71 is a consensus site for PKC, and Ser67 and

Ser76 are consensus sites for S6K1 (Matsuhashi et al., 2019). Previous studies have demonstrated that, depending on the signaling pathways involved, S6K1 or PKC is required for the degradation of PDCD4 (Matsuhashi et al., 2014; Dorrello et al., 2006; Nakashima et al., 2010; Schmid et al., 2008). For PDCD4 degradation following EGF-treatment, S6K1 is required, while for PDCD4 degradation following TPA-treatment, PKC is required (Matsuhashi et al., 2019, 2014; Nakashima et al., 2010).

Recent evidence for a role of PDCD4 in neurons:

Despite being expressed at significant levels in the brain, especially in the hippocampus and cortex (Lein et al., 2007; Li et al., 2020b), few studies have addressed the role of PDCD4 in the nervous system. PDCD4 expression in neurons is altered by injury and stress, with prenatal ethanol exposure upregulating total PDCD4 protein in the developing rat cortex (Narasimhan et al., 2013; Riar et al., 2014), stroke upregulating PDCD4 in the adult rat cortex (Shan et al., 2021), and spinal cord injury downregulating PDCD4 protein expression (Jiang et al., 2017). In these injury models, upregulation of PDCD4 impaired translation (Narasimhan et al., 2013), while downregulation of PDCD4 was neuroprotective (Shan et al., 2021) and promoted neurite growth (Jiang et al., 2017).

Recently, a role for PDCD4 in stress-induced depression was demonstrated in a mouse model (Li et al., 2020b). PDCD4 was upregulated in response to chronic stress, and overexpression of PDCD4 induced decreased *Bdnf* translation, loss of dendritic spines, and increased depressive-like behaviors, while PDCD4 knockout prevented these stress-induced changes. PDCD4 was proposed to serve as a brake on *Bdnf* translation, with downstream consequences for spine function and behavior. Additionally, in Di Paolo et al. 2020, a role for

PDCD4 in axon outgrowth was demonstrated, with PDCD4 knockdown increasing axon length and PDCD4 overexpression decreasing axon length in mouse cultured cortical neurons. In ribosome profiling of differentiated PC12 neuron-like cells, PDCD4 knockdown increased the translation of ~250 genes, including neurite-growth related genes such as *Bdnf* (Di Paolo et al., 2020). Both studies support the idea that PDCD4 negatively regulates neuronal growth and function, by acting as a repressor of translation.

While these studies demonstrate that PDCD4 expression is regulated by stress and injury, it is unknown if neuronal activity itself regulates PDCD4 expression. Activity-dependent regulation of PDCD4 would provide an exciting link between neuronal stimulation and regulation of gene expression, with potential relevance for activity-dependent processes such as synapse development and synaptic plasticity. Moreover, the previous work has focused on the role of PDCD4 as a translational repressor in the cytoplasm, but the role of PDCD4 as a potential regulation of transcription in the nucleus of neurons has not yet been studied.

RESULTS

Neuronal stimulation decreases PDCD4 protein concentration in the nucleus and cytoplasm of neurons

Among the proteins that underwent activity-dependent changes in nuclear concentration in our APEX2-NLS mass spectrometry study (**Chapter 2**), the PDCD4 protein was significantly enriched in the TTX-treated nuclear proteome compared to the Bic-treated nuclear proteome. To validate this finding, we characterized the expression of PDCD4 protein in cultured neurons using ICC, and found that PDCD4 was present both in the nucleus and cytoplasm of neurons (**Fig 3.1A**). Bic stimulation significantly decreased PDCD4 protein expression in the nucleus by

~50% (**Fig 3.1B**), with a smaller decrease of ~20% in the cytoplasm (**Fig 3.1C**). The decrease of PDCD4 occurred within 15 minutes of Bic stimulation, and PDCD4 protein levels continued to decrease further with longer incubations of Bic up to 3 hours (**Fig 3.1D**). After washout of a 1-hour Bic stimulation, PDCD4 protein expression gradually returned towards baseline levels, although PDCD4 protein concentration was still 25% below baseline 24 hours after washout (**Fig 3.1E**).

In complementary experiments, we transduced neurons with AAV expressing C-terminal HA-tagged PDCD4 (**Fig 3.2A**) and characterized PDCD4-HA expression by western blot and ICC. By western blot, we found that total PDCD4-HA protein levels decreased by ~50% following Bic stimulation (**Fig 3.2B**). By ICC, both nuclear and cytoplasmic PDCD4-HA decreased by ~40% (**Fig 3.2C-D**). To further validate the Bic-induced decrease in PDCD4, we also created an N-terminal V5-tagged PDCD4 plasmid (**Fig 3.2A**) and transfected the construct in neurons. Consistent with the results from endogenous PDCD4 and transduced C-terminally HA-tagged PDCD4, both nuclear and cytoplasmic V5-PDCD4 decreased by ~40% with Bic stimulation (**Fig 3.2E-F**). These results show that exogenously expressed PDCD4 concentration in neurons is regulated by activity, and that the decrease in PDCD4 represents a decrease in the protein rather than cleavage into multiple fragments.

We also found that depolarization of neurons with 40 mM KCl for 5 min significantly decreased PDCD4 protein concentration by ~40% in the nucleus (**Fig 3.3A**) and ~30% in the cytoplasm (**Fig 3.3B**), as detected immediately after the 5 min treatment. Altogether, these results indicate that increases in glutamatergic transmission and depolarization lead to a rapid and long-lasting reduction in PDCD4 abundance in the nucleus and, to a lesser extent, the cytoplasm of neurons.

PDCD4 undergoes proteasome-mediated degradation following neuronal stimulation

In non-neuronal cells, PDCD4 has been reported to undergo miRNA-mediated translational repression (Asangani et al., 2008; Frankel et al., 2008; Ning et al., 2014), stimulus-induced nuclear export (Böhm et al., 2003)), and stimulus-induced proteasome-mediated degradation (Dorrello et al., 2006). Since the assay we used to detect activity-dependent changes in the nuclear proteome was conducted in the presence of the protein synthesis inhibitor CHX, we considered it unlikely that the Bic-induced decrease in PDCD4 was due to miRNA-mediated translational repression. To confirm this, we conducted PDCD4 ICC of TTX-silenced and Bic-stimulated neurons in the presence or absence of CHX. While CHX potently blocked the activity-dependent increase in FOS immunoreactivity (**Chapter 2**), it did not block the Bic-induced decrease in PDCD4 (**Fig 3.4A-B**), thereby ruling out a role for activity-dependent miRNA-mediated translational regulation.

To investigate the mechanism underlying the decrease in nuclear PDCD4, we tested if the decrease in nuclear abundance was due to activity-dependent increases in nuclear export. Nuclear export of PDCD4 is mediated by the nuclear export protein, CRM1, and sensitive to the nuclear export inhibitor, leptomycin B (LMB) (Böhm et al., 2003). Long incubation with LMB successfully caused nuclear accumulation of PDCD4 in unstimulated neurons (**Fig 3.5A**), and yet LMB was unable to prevent the activity-dependent decrease of nuclear PDCD4 following stimulation (**Fig 3.5B**). This result demonstrates that regulated nuclear export is not required for the activity-dependent decrease of PDCD4.

We next hypothesized that regulated ubiquitin proteasome-mediated degradation may explain the Bic-induced decrease of PDCD4. To test this idea, we incubated TTX-silenced and

Bic-stimulated neurons with the proteasome inhibitors epoximicin (Epox) or bortezomib (Bort). As shown in **Fig 3.6A-B**, the proteasome inhibitors impaired Bic-induced decreases of PDCD4 in both nucleus and cytoplasm of neurons, indicating that neuronal activity decreases PDCD4 concentrations via proteasome-mediated degradation (**Fig 3.6A-B**). The finding that the nuclear export inhibitor LMB did not block the Bic-induced decrease of PDCD4 in the nucleus (**Fig 3.5B**) indicates that activity regulates proteasome-mediated degradation of nuclear PDCD4 directly in the nucleus, rather than by nuclear export of PDCD4 followed by degradation in the cytoplasm.

The E3 ubiquitin ligases βTRCP1/2 have been shown to be required for the proteasome-mediated degradation of PDCD4 in the T98G glioblastoma cell line (Dorrello et al., 2006). βTRCP1/2 belong to the family of Cullin-RING E3 ubiquitin ligases, which require neddylation in order to be activated (Merlet et al., 2009). To determine if this family of ligases is involved in the activity-dependent decrease of PDCD4 in neurons, we used the neddylation inhibitor MLN4924 (MLN) and found that it blocked the Bic-induced decrease of PDCD4 in the nucleus and cytoplasm (**Fig 3.6C**) of neurons. This result further supports the finding that PDCD4 undergoes proteasome-mediated degradation following Bic stimulation, likely through ubiquitination by βTRCP1/2.

PDCD4 S71A mutation and PKC inhibition prevent the activity-dependent decrease of PDCD4

To understand how neuronal activity at synapses leads to proteasome-mediated degradation of PDCD4 in the nucleus, we focused on PDCD4's βTRCP-binding motif. Previous work in T98G glioblastoma cells has shown that phosphorylation of Ser67, Ser71, and/or Ser76 in βTRCP-binding region of PDCD4 is necessary for βTRCP binding and subsequent

proteasome-mediated degradation of PDCD4 (Dorrello et al., 2006). To test if a mutation in PDCD4 at one of these sites would prevent the activity-dependent decrease of PDCD4 in neurons, we expressed wild-type (WT) and mutant (S71A) PDCD4-HA in cultured neurons using AAV (**Fig 3.7A-B**). Similar to endogenous PDCD4, we found that WT PDCD4-HA decreased following Bic stimulation, with a ~30% decrease in nuclear HA intensity and a ~15% decrease in cytoplasmic intensity, as detected by ICC (**Fig 3.7C-D**). In contrast, the PDCD4-HA S71A mutant did not undergo an activity-dependent decrease in either the nucleus or cytoplasm, but showed a slight activity-dependent increase in nuclear intensity (**Fig 3.7C**). In complementary experiments, we found that Bic stimulation resulted in a ~40% decrease of WT PDCD4-HA signal by western blot, while PDCD4-HA S71A did not decrease after stimulation (**Fig 3.7E**). These results suggest that phosphorylation of S71 in PDCD4's βTRCP-binding motif is necessary for its activity-dependent degradation in neurons.

The βTRCP-binding region in PDCD4 contains canonical phosphorylation consensus sites for the kinases S6K1 and PKC (**Fig 3.7A**); Ser71 is a consensus site for PKC, and Ser67 and Ser76 are consensus sites for S6K1 (Dorrello et al., 2006; Matsuhashi et al., 2014, 2019; Nakashima et al., 2010). To test which kinase phosphorylates PDCD4 with neuronal activity, we incubated cultures in the S6K inhibitor LY2584702 or the PKC inhibitor Ro-31-8425. We found that the S6K inhibitor LY2584702 did not prevent the Bic-induced decrease of PDCD4 (**Fig 3.8A-B**), despite its ability to potently inhibit the phosphorylation of a known S6K target, ribosomal protein S6 (**Fig 3.8C**). In contrast, the pan-PKC inhibitor Ro-31-8425 completely prevented the activity-dependent decrease (and slightly increased nuclear intensity) of PDCD4 (**Fig 3.8D-E**). These results suggest that in response to glutamatergic activity, PKC

phosphorylates PDCD4 at Ser71, which enables the ubiquitin ligase βTRCP1/2 to bind and promote the proteasome-mediated degradation of PDCD4.

Stimulus-induced degradation of PDCD4 regulates the expression of neuronal activity-dependent genes

The finding that synaptic activity dynamically regulates PDCD4 protein concentration in the nucleus in response to synaptic activity points to a nuclear function for PDCD4 in coupling neuronal activity with changes in transcription. To investigate a role for PDCD4 in the regulation of activity-dependent transcription, we performed RNA-seq of forebrain cultures transduced with either wild-type PDCD4 or degradation-resistant PDCD4 (S71A), following neuronal silencing with TTX or stimulation with Bic for 1 hour (**Fig 3.9**). Given that PDCD4 has a well-known role in regulating translation, we sought to distinguish between direct PDCD4-mediated transcriptional changes in the nucleus and the changes in expression that are downstream of PDCD4-mediated translational changes in the cytoplasm by performing the experiments in either the presence or absence of CHX. We detected robust Bic-induced increases in normalized read counts of transcripts for canonical immediate early genes such as *Npas4*, *Rgs2*, and *Egr4* in all biological replicates (WT Bic vs TTX: *Npas4* log2FC = 6.5, *Rgs2* log2FC = 2.4, *Egr4* log2FC = 3.1, **Fig 3.9A**). We identified 912 activity-dependent genes, defined as genes with significant differential expression between Bic and TTX for PDCD4 WT samples (459 upregulated, 453 downregulated; adjusted p-value < 0.05 for WT no CHX; **Fig 3.9B-D**). Clustering of activity-dependent genes by fold change across sample type revealed that most activity-dependent genes showed similar fold changes between PDCD4 WT and PDCD4 S71A samples (**Fig 3.9B**), especially for genes with relatively high activity-dependent fold changes (**Fig 3.9C**). However,

Fig 3.9B also shows that PDCD4 S71A altered activity-dependent changes in gene expression for a subset of genes. Specifically, we found that PDCD4 S71A led to a decrease in activity-induced differential expression for a substantial proportion of genes: 43% of activity-dependent upregulated genes (198 genes) and 57% of activity-dependent downregulated genes (260 genes) were not significantly upregulated or downregulated, respectively, in the PDCD4 S71A samples (**Fig 3.9D**). These results suggest that regulated degradation of PDCD4 is important for the expression of activity-dependent genes in neurons.

This inhibition of activity-dependent gene expression could be due to both a potential role for PDCD4 in transcriptional processes and secondary effects from PDCD4's regulation of translation of specific transcripts (Matsuhashi et al., 2019; Wang and Yang, 2018). To isolate effects at the transcriptional level, we focused on CHX-insensitive activity-dependent genes, that is, genes that showed activity-dependent differential expression in both the presence and absence of CHX (in WT, 459 genes after excluding 3 genes that showed differential expression in different directions +/- CHX). We ranked CHX-insensitive genes by their change in activity-dependent fold change between PDCD4 WT and PDCD4 S71A samples and identified 91 putative PDCD4 target genes that showed large differences in activity-dependent gene expression between wild-type and degradation-resistant PDCD4 samples (see Methods; **Fig 3.10A**). We validated the effect of PDCD4 on activity-dependent gene expression with RT-qPCR for two of the genes with the largest change between PDCD4 WT and PDCD4 S71A (*Scd1* and *Thrsp*; **Fig 3.10B**). We performed motif analysis of promoter sequences of the putative PDCD4 target genes and found similar motifs as in promoters of other CHX-insensitive activity-dependent genes (e.g. AP-1/TRE, ATF/CRE, Sp1/Klf motifs; **Fig 3.11**), suggesting there was not a specific transcription factor motif associated with putative PDCD4 targets genes. Gene

ontology (GO) analysis of the putative PDCD4 target genes showed enrichment for neuronal signaling terms such as “nervous system development” (GO:0007399; 28 genes; FDR = 9.28E-04) and “synapse” (GO:0045202; 18 genes; FDR = 6.54E-03), whereas, for comparison, other CHX-insensitive activity-dependent genes showed enrichment for terms related to transcription such as “regulation of gene expression” (GO:0010468; 169 genes; FDR = 3.11E-25) and “nuclear chromosome” (GO:0000228; 51 genes; FDR = 2.88E-09; **Fig 3.12A**). Putative PDCD4 targets included genes encoding proteins critical for synapse formation, remodeling and transmission such as Shank1, p35, Abhd17b, Gap43, Cofilin, Spectrin-β2, Myosin-Va, Dendrin, Jacob, SNAP-β, Voltage-dependent calcium channel-α2/δ1, α-tubulin, and β-actin (**Fig 3.12B**). Together, these results suggest that PDCD4 functions in the nucleus to regulate the expression of a subset of genes, and that inhibiting the stimulation-induced degradation of nuclear PDCD4 results in a suppression of the transcription of many activity-dependent genes important for neuronal synaptic function (**Fig 3.13**).

DISCUSSION

We found that synaptic activity led to proteasome-mediated degradation of the tumor suppressor protein PDCD4, with important consequences for activity-dependent transcription. The activity-dependent decrease of PDCD4 occurred in the nucleus and, to a lesser extent, in the cytoplasm. The finding that the nuclear export inhibitor LMB did not block the activity-dependent decrease of nuclear PDCD4 demonstrated that nuclear PDCD4 is degraded without leaving the nucleus. Many examples of activity-dependent degradation of proteins within the cytoplasm have been reported in neurons (Hegde et al., 1993; Banerjee et al., 2009; Jarome et al., 2011), but fewer cases of activity-dependent degradation of proteins within the nucleus have

been described (Upadhya et al., 2004; Bayraktar et al., 2020; Kravchick et al., 2016b). Nonetheless, the nucleus contains machinery for proteasome-mediated degradation and there are numerous examples of proteins that are degraded by the nuclear proteasome in non-neuronal cells, including transcriptional regulators and cell-cycle proteins (von Mikecz, 2006). Neuronal nuclei have also been shown to contain machinery for proteasome-mediated degradation (Mengual et al., 1996) and exhibit proteasomal activity, albeit with less activity than is present in the cytoplasm (Upadhya et al., 2006; Tydlacka et al., 2008). Activity-dependent nuclear proteasome-mediated degradation of transcriptional regulators represents an important mechanism by which synaptic activity regulates gene expression.

In neurons, synaptic activity leads to an increase in the activity of many kinases, including S6K and PKC (Callender and Newton, 2017; Biever et al., 2015). We found that a phospho-incompetent serine-to-alanine mutation at Ser71 prevented the activity-dependent degradation of PDCD4, and that phosphorylation by PKC, but not S6K was required for this activity-dependent degradation. This result is consistent with previous studies in other cell types, demonstrating that either S6K or PKC is required for PDCD4 phosphorylation depending on the signaling pathway (Matsuhashi et al., 2019, 2014; Dorrello et al., 2006; Nakashima et al., 2010; Schmid et al., 2008). The stimulus-specific requirement of either S6K or PKC for PDCD4 degradation raises the interesting possibility that different types of neuronal stimulation could trigger PDCD4 degradation via distinct signaling pathways. Supporting this idea, two studies in neurons have suggested that PDCD4 degradation may be regulated by S6K in response to injury and stress (Li et al., 2020b; Di Paolo et al., 2020), while our study demonstrated that PDCD4 degradation was mediated by PKC. PKC is typically activated at the cell surface (Gould and Newton, 2008), however, it can translocate from the cytoplasm to the nucleus after activation

and can be activated directly in the nucleus, where it phosphorylates nuclear targets including histones and transcription factors (Lim et al., 2015; Martelli et al., 2006).

PDCD4 has been well-characterized as a translational repressor in the cytoplasm of cancer cells (Wang et al., 2017; Wedeken et al., 2011; Yang et al., 2004). Low concentrations of PDCD4 have been reported to correlate with invasion, proliferation, and metastasis of many types of cancers (Allgayer, 2010; Chen et al., 2003; Wang and Yang, 2018; Wei et al., 2012). However, the role of PDCD4 in the nucleus is less well-characterized, even though the protein is predominantly localized in the nucleus of many cells (Böhm et al., 2003). Despite being highly expressed in neurons, few studies have examined the neuronal function of PDCD4 (Di Paolo et al., 2020; Li et al., 2020b; Narasimhan et al., 2013), and as far as we are aware, no previous study has identified a role for PDCD4 in activity-dependent transcription in neurons. In our study, we detected a larger activity-dependent decrease of PDCD4 in the nucleus than in the cytoplasm, and we found that blocking PDCD4 degradation suppressed activity-dependent gene expression. These findings suggest that the proteasome-mediated degradation of PDCD4 is important for regulating activity-dependent transcription following neuronal stimulation. Previous studies in non-neuronal cells have indicated that PDCD4 can inhibit AP-1-dependent transcription, although it is unclear whether this is a direct role in the nucleus (Bitomsky et al., 2004) or an indirect role regulating the translation of signaling proteins in the cytoplasm (Yang et al., 2006). PDCD4 has also been shown to bind to the transcription factors CSL (Jo et al., 2016) and TWIST1 (Shiota et al., 2009) and inhibit their transcriptional activity. Although activity-dependent degradation of cytoplasmic PDCD4 was weaker and less consistent than that of nuclear PDCD4, we cannot rule out the possibility that PDCD4 has a translation-independent role in the cytoplasm (such as binding to signaling proteins) that could indirectly regulate

transcription. However, we propose that PDCD4 has a direct role in regulating activity-dependent transcription in the nucleus, in addition to its well-characterized role as a translational repressor in the cytoplasm.

We identified 91 genes that are putative activity-dependent targets of PDCD4, including genes encoding proteins that are important for synaptic function. The activity-dependent downregulation of PDCD4 in neurons is reminiscent of the concept of "memory suppressor genes" (Abel and Kandel, 1998), genes that act as inhibitory constraints on activity-dependent neuronal plasticity. By analogy to its function during cancer metastases, decreases in PDCD4 in neurons would function to enable experience-dependent neuronal growth and remodeling. Dysregulated PDCD4 concentrations have also been reported to underlie a variety of metabolic disorders, including polycystic ovary syndrome, obesity, diabetes, and atherosclerosis, highlighting the critical role PDCD4 plays in regulating gene expression in multiple cell types (Lu et al., 2020). Our study provides the first transcriptomic profile of PDCD4 that is independent of PDCD4's role in translation. These results provides insight into the transcriptional targets of PDCD4, which is of relevance not only to neuroscience, but also to the study of PDCD4 in cancer.

Of note, we observed a rapid decrease and long-lasting decrease of PDCD4 following neuronal stimulation. PDCD4 was degraded within 5-15 minutes of stimulation and the decrease persisted for 24 hours following removal of the stimulus. The extended time period during which PDCD4 is downregulated indicates that transient neuronal stimuli can lead to persistent changes in PDCD4 concentration. This decrease of PDCD4 may have functional implications shorter-term and longer-term activity-dependent changes in transcription. Our transcriptomic study revealed that PDCD4 expression attenuates the activity-dependent expression of genes important

for synapse function, and so having low levels of PDCD4 for a long time window after stimulation may be important for facilitating long-term changes at the synapse. Some genes are transcribed rapidly in response to neuronal stimulation, while other genes respond at later time points (Yap and Greenberg, 2018; Tyssowski et al., 2018). Because PDCD4 is downregulated for many hours after stimulation, the removal of PDCD4 may be important for enabling transcription throughout this extended time period of activity-dependent transcription.

Our study identifies the tumor suppressor protein PDCD4 as a critical regulator of activity-dependent gene expression in neurons, highlighting a role for PDCD4 in regulating the transcription of genes involved in synapse formation, remodeling, and transmission. This new role is in addition to PDCD4's well-characterized role as a translational inhibitor (Wang and Yang, 2018), and future investigation of the mechanisms by which PDCD4 regulates transcription of these genes will provide further insight into the understudied role of PDCD4 as a transcriptional regulator. In addition to investigating these transcriptional mechanisms, future studies are needed to investigate the functional consequences of PDCD4-mediated transcription, by examining synapse density and volume following PDCD4 manipulation. Lastly, the activity-dependent regulation and role of PDCD4 should be examined in additional, more physiologically relevant models, such as acute hippocampal slice preparation or *in vivo* in the rodent brain. Such studies also promise to deepen our understanding of the specific cell and molecular biological mechanisms by which experience alters gene expression in neurons to enable the formation and function of neural circuits.

METHODS

Primary Neuronal Cultures:

All experiments were performed using approaches approved by the UCLA Animal Research Committee. Forebrain from postnatal day 0 Sprague-Dawley rats (Charles River) was prepared for neuronal cultures (**see Chapter 2**). When applicable, neurons were transfected with plasmids using Lipofectamine 2000 (Thermo Fisher) according to manufacturer's instructions at days in vitro (DIV) 2, or transduced with AAV at DIV 13. All experiments were performed at DIV 20.

Generation of Plasmids and AAV:

To create hSyn PDCD4-HA, rat PDCD4 was amplified from cultured neuron cDNA (PDCD4 Forward: 5' – TCGCCACCAT GGATGTAGAA AACGAGCAGA TAC – 3', PDCD4 Reverse: 5' – GTTGTTGAAT TCTCAAGCGT AATCTGGAAC ATCGTATGGG TAGTAGCTCT CAGGTTTAAG ACGACCTC – 3') with a C-terminal HA tag, and then inserted into the pAAV-hSyn-EGFP plasmid between NcoI and EcoRI, replacing the EGFP insert. The S71A mutation was created using site-directed mutagenesis (services by Genewiz) to mutate serine 71 (TCT) to alanine (GCT). The hSyn V5-PDCD4-HA construct was created by adding a V5 tag to the N-terminus of PDCD4-HA using PCR-based mutagenesis (services by Genewiz).

AAV9 was generated for APEX2-NLS, PDCD4-HA WT, and PDCD4-HA S71A at Penn Vector Core.

Pharmacological Treatments:

Neurons were pre-incubated with cycloheximide (CHX, 60 μM, Sigma) for 15 min, leptomycin B (LMB, 10 nM, Sigma) for 30 min, LY2584702 (1 μM, Cayman Chemical) or Ro-

31-8425 (5 μM, Sigma) for 1 hr, or epoxomicin (5 μM, Enzo Life Sciences), bortezomib (10 μM, APExBIO), or MLN4924 (50 nM, APExBIO) for 2 hrs before the start of each respective experiment and remained in the media throughout the duration of each experiment, incubated at 37 °C. For neurons treated with inhibitors dissolved in DMSO (epoxomicin, bortezomib, MLN4924, LY2584702, and Ro-31-8425), the final DMSO concentration in the media was 0.1% or less. For neurons treated with LMB, the final methanol concentration in the media was 0.08%. All control groups received an equivalent concentration of vehicle (DMSO or methanol). To silence the neurons, 1 μM tetrodotoxin (TTX, Tocris) was applied to the neurons for 1 hr. To stimulate the neurons, 40 μM (-)-bicuculline methiodide (Bic, Tocris) was applied to the neurons for 1 hr unless otherwise stated.

For KCl stimulations, neurons were pre-incubated with standard Tyrode's solution (140 mM NaCl, 10 mM HEPES, 5 mM KCl, 3 mM $CaCl_2$, 1 mM $MgCl_2$, 20 mM glucose, pH 7.4) containing 1 μM TTX for 15 min at room temperature, and then stimulated for 5 min with 40 mM KCl isotonic Tyrode's solution containing TTX. Control cells remained in the standard Tyrode's solution containing TTX throughout the experiment.

Control data from LMB (**Fig 3.5B**) and CHX (**Fig 3.4A-B**) experiments were combined to generate the data shown in **Fig 3.1B-C**. Two of the bortezomib experiments were performed concurrently with two of the MLN4924 experiments, and so these experiments partially share control data in **Fig 3.6B-C**. One of the LY2584702 experiments was performed concurrently with one of the bortezomib experiments, and so **Fig 3.6B** partially shares control data with **Fig 3.8A**.

Protein Extraction and Western Blot:

Neurons were washed in Tyrode's solution (140 mM NaCl, 10 mM HEPES, 5 mM KCl, 3 mM $CaCl_2$, 1 mM $MgCl_2$, 20 mM glucose, pH 7.4) and lysed with RIPA (50 mM Tris, 150 mM NaCl, 0.1% SDS, 0.5% sodium deoxycholate, 1% Triton X-100, pH 7.5) containing protease and phosphatase inhibitor cocktails (Sigma). Samples were clarified by centrifugation at 10,000 g for 10 min. Protein concentration was determined using the Pierce BCA protein assay kit (Thermo Fisher).

Protein lysates were boiled in loading buffer (10% glycerol, 1% SDS, 60 mM Tris HCl pH 7.0, 0.1 M DTT, 0.02% bromophenol blue) for 10 min at 95°C and run on at 8% polyacrylamide gel for 90 min at 120 V. Samples were wet-transferred onto a 0.2 µm nitrocellulose membrane for 16 hours at 40 mA. The membrane blocked with Odyssey Blocking Buffer (LI-COR) and incubated with primary antibodies: mouse HA (BioLegend #901513, 1:1000), mouse TUJ1 (BioLegend #801201, 1:1000), mouse S6 (CST #2317, 1:1000), rabbit phospho-S6 ser 235/236 (CST #4858, 1:2000) for 3-4 hours at room temperature or overnight at 4°C. The membrane was washed with TBST and incubated with secondary antibodies: anti-rabbit IRDye 800CW (1:10,000), anti-mouse IRDye 800CW (1:10,000), anti-mouse IRDye 680CW (1:10,000), for 1 hour at room temperature. The membrane was imaged using the Odyssey Infrared imaging system (LI-COR). Western blots were quantified using the Image Studio (LI-COR) rectangle tool. The relative intensity of each band was calculated by normalizing to a loading control (TUJ1). Within each experiment, all values were normalized to the control (basal) sample.

Immunocytochemistry (ICC):

Neurons were fixed with 4% paraformaldehyde in phosphate-buffer saline (PBS) for 10 min, permeabilized in 0.1% Triton X-100 in PBS for 5 min, and blocked in 10% goat serum in PBS for 1 hour. Neurons were incubated with primary antibodies: chicken MAP2 (PhosphoSolutions #1100-MAP2, 1:1000), rabbit PDCD4 (CST #9535, 1:600), mouse HA (BioLegend #901513, 1:1000), mouse V5 (Thermo Fisher #R960-25, 1:250), for 3-4 hours at room temperature or overnight at 4°C. Neurons were washed with PBS, and incubated at 1:1000 with secondary antibodies: anti-chicken Alexa Fluor 647, anti-rabbit Alexa Fluor 555, anti-mouse Alexa Fluor 555, and Hoechst 33342 stain for 1 hour at room temperature. Neurons were washed with PBS, and mounted on slides with Aqua-Poly/Mount (Polysciences) for confocal imaging.

Confocal Imaging:

Samples were imaged using a Zeiss LSM 700 confocal microscope with a 40x / 1.3 NA oil objective and 405 nm, 488 nm, 555 nm, and 639 nm lasers, using Zen microscopy software. Identical image acquisition settings were used for all images within an experiment. For each image acquisition, the experimenter viewed the MAP2 and Hoechst channels to select a field-of-view, and was blind to the experimental channel (HA, PDCD4, etc.). For each coverslip, images were taken at multiple regions throughout the coverslip, and 2-3 coverslips were imaged per condition. Images were collected from at least 3 experimental replicates (sets of cultures), unless otherwise stated.

Image Analysis:

ICC images were processed as described in the **Chapter 2** methods section. For experiments using transfected cells (V5 experiments), the measured intensity of each ROI was normalized to the co-transfection marker (nuclear GFP intensity), in order to normalize for differences in transfection efficiency between cells.

RNA Extraction, Library Preparation, RNA Sequencing, and Data Analysis:

Samples were prepared from 3 biological replicates (sets of cultures), with 8 samples in each replicate (WT Bic, WT TTX, S71A Bic, S71A TTX, CHX WT Bic, CHX WT TTX, CHX S71A Bic, CHX S71A TTX). RNA was extracted from neuronal cultures using the RNeasy Micro Kit (Qiagen) according to manufacturer's instructions. Libraries for RNA-Seq were prepared with Nugen Universal plus mRNA-Seq Kit (Nugen) to generate strand-specific RNA-seq libraries. Samples were multiplexed, and sequencing was performed on Illumina HiSeq 3000 to a depth of 25 million reads/sample with single-end 65 bp reads. Demultiplexing was performed using Illumina Bcl2fastq v2.19.1.403 software. The RNA-seq data discussed in this publication have been deposited in NCBI's Gene Expression Omnibus (Edgar et al., 2002) and are accessible through GEO Series accession number GSE163127 (https://www.ncbi.nlm.nih.gov/geo/query/acc.cgi?acc=GSE163127). Reads were aligned to Rattus_norvegicus reference genome version Rnor_6.0 (rn6), and reads per gene was quantified by STAR 2.27a (Dobin et al., 2013) using Rnor_6.0 gtf file. We used DESeq2 (Love et al., 2014) to obtain normalized read counts and perform differential expression analysis, including batch correction for replicate number. Putative PDCD4 target genes were identified by first focusing on genes which showed activity-dependent differential expression in both the presence and absence of CHX (CHX-insensitive activity-dependent genes; 459 genes after excluding 3 genes

which showed differential expression in different directions +/- CHX). We then calculated the PDCD4 activity-dependent change by taking the difference between the activity-dependent fold change of PDCD4 WT and PDCD4 S71A samples and normalizing:

PDCD4 change index = abs(*S*-*W*)/abs(*W*)

Where *S* is the PDCD4 S71A no CHX Bic vs TTX log2FC, and *W* is the PDCD4 WT no CHX Bic vs TTX log2FC. We defined putative PDCD4 target genes as those with a PDCD4 change index > 0.75. Motif analysis was performed using the findMotifsGenome command in HOMER (Heinz et al., 2010), using sequences from the TSS and upstream 500 bp as the promoter sequences for each gene. GO analysis was performed using the Gene Ontology Resource (Ashburner et al., 2000; Carbon et al., 2019) and PANTHER enrichment tools (Mi et al., 2019). Cartoon of putative PDCD4 targets was generated using BioRender.com.

RT-qPCR:

As above, RNA was extracted from neuronal cultures using the RNeasy Micro Kit (Qiagen). cDNA was synthesized from 500 ng RNA using SuperScript III First-Strand Synthesis System (Thermo Fisher) with random hexamers. A "No Reverse Transcriptase" sample was also prepared as a negative control. RT-qPCR was performed on the CFX Connect Real-Time System (Bio-Rad) using PowerUp SYBR Green Master Mix (Applied BioSystems). Primer pairs were designed for two housekeeping genes (*Hprt*, *Gapdh*) and two candidate genes (*Scd1*, *Thrsp*) using Primer3Plus (Untergasser et al., 2012) and NCBI Primer-BLAST (Ye et al., 2012). HPRT F 5' – AAGCTTGCTGGTGAAAAGGA – 3' , HPRT R 5' – CCGCTGTCTTTTAGGCTTTG –

3', GAPDH F 5' – GGCATTGCTCTCAATGACAA – 3', GAPDH R 5' – ATGTAGGCCATGAGGTCCAC – 3', SCD1 F 5' – ACCTTGCTCTGGGGGATATT – 3', SCD1 R 5' – CGGGCCCATTCATACACAT – 3', THRSP F 5' – CTTACCCACCTGACCCAGAA – 3', THRSP R 5' – CATCGTCTTCCCTCTCGTGT – 3'. RT-qPCR was performed on 6 sets of cultures, with technical triplicate reactions for each sample. For each gene, relative quantity was calculated using the formula: E^(ΔCt), where E was calculated from the primer efficiencies (E≈2) and ΔCt was calculated using $Ct_{TTX} - Ct_{Bic}$. Relative gene expression was calculated by normalizing the relative quantity of the gene of interest to the relative quantity of the housekeeping genes *Hprt* and *Gapdh*: $(E_{gene})^{\Delta Ct\ gene}$ / GeoMean[$(E_{HPRT})^{\Delta Ct\ HPRT}$, $(E_{GAPDH})^{\Delta Ct\ GAPDH}$].

Quantification and Statistical Analysis:

For ICC experiments, analyses were performed as described in the **Chapter 2** methods section.

For RT-qPCR experiments, all data points were displayed using GraphPad Prism, with solid lines indicating the median values. "n" refers to the biological replicates (sets of cultures), and all data points were plotted on the graphs. The Mann-Whitney U test (Prism) was used to calculate statistical significance.

For western blot experiments, all data points were displayed using GraphPad Prism, with solid lines indicating the median values. "n" refers to the biological replicates (sets of cultures), and all data points were plotted on the graphs. The Mann-Whitney U test (Prism) was used to calculate statistical significance.

FIGURE LEGENDS

Figure 3.1 Neuronal stimulation decreases PDCD4 protein concentration in the nucleus and cytoplasm of neurons.

A) PDCD4 immunocytochemistry (ICC) of basal, TTX-silenced, and Bic-stimulated neurons. Scale bar = 10 μm.

B) Violin plots of normalized nuclear PDCD4 ICC intensity. Basal n = 226, TTX n = 227, Bic n = 218 cells, from 6 sets of cultures. Basal median = 1.00, TTX median = 1.00, Bic median = 0.55. Basal vs Bic $p < 0.0001$, TTX vs Bic $p < 0.0001$.

C) Violin plots of normalized cytoplasmic PDCD4 ICC intensity in the same cells as in **B**. Basal median = 1.00, TTX median = 1.07, Bic median = 0.81. Basal vs Bic $p < 0.0001$, TTX vs Bic $p < 0.0001$.

D) Violin plots of normalized nuclear PDCD4 ICC intensity after varying durations of Bic stimulation. Basal n = 115, Bic 15 min n = 111, 30 min n = 102, 1 hr n = 97, 3 hr n = 92, 6 hr n = 91 cells, from 3 sets of cultures. Basal median = 1.00, Bic 15 min median = 0.71, 30 min median = 0.63, 1 hr median = 0.52, 3 hr median = 0.45, 6 hr median = 0.46. Basal vs Bic 15 min $p < 0.0001$, Basal vs Bic 30 min $p < 0.0001$, Basal vs Bic 1 hr $p < 0.0001$, Basal vs Bic 3 hr $p < 0.0001$, Basal vs Bic 6 hr $p < 0.0001$.

E) Violin plots of normalized nuclear PDCD4 ICC intensity at various timepoints after removal of a 1 hr Bic stimulation. Basal n = 124, Washout 0 hr n = 94, 1 hr n = 111, 4 hr n = 104, 24 hr n = 99 cells, from 3 sets of cultures. Basal median = 1.00, Washout 0 hr median = 0.51, 1 hr median = 0.57, 4 hr median = 0.73, 24 hr median = 0.75. Basal vs 0 hr $p < 0.0001$, Basal vs 1 hr $p < 0.0001$, Basal vs 4 hr $p < 0.0001$, Basal vs 24 hr $p < 0.0001$.

Statistical significance is indicated by ****p < 0.0001, from Mann-Whitney U test with Bonferroni correction.

Figure 3.2 Neuronal stimulation decreases PDCD4 protein concentration, as detected by epitope tagging.

A) PDCD4 protein, with locations of V5 tag, HA tag, and PDCD4 (D29C6) epitope (recognized by the PDCD4 Cell Signaling Technology antibody used in this study).

B) Top: Western blot of protein lysates from basal, TTX-silenced, and Bic-stimulated neurons transduced with PDCD4-HA AAV. The PDCD4-HA band is indicated with an arrow. We observe a faint non-specific band above the HA band. Bottom: Quantification of western blot, from 4 sets of cultures. HA intensity was normalized to TUJ1 intensity. Within each experiment, all samples were normalized to the basal sample. TTX/Basal median = 1.57, Bic/Basal median = 0.54. TTX vs Bic p = 0.0286.

C) Violin plots of normalized nuclear HA ICC intensity in neurons transduced with PDCD4-HA AAV. Basal n = 107, TTX n = 88, Bic n = 102 cells, from 3 sets of cultures. Basal median = 1.00, TTX median = 1.116, Bic median = 0.5972. Basal vs Bic p < 0.0001, TTX vs Bic p < 0.0001.

D) Violin plots of normalized cytoplasmic HA ICC intensity in the same cells as in **C**. Basal median = 1.00, TTX median = 1.203, Bic median = 0.5983. Basal vs Bic p < 0.0001, TTX vs Bic p < 0.0001.

E) Violin plots of normalized nuclear V5 ICC intensity in neurons transfected with V5-PDCD4 plasmid and co-transfected with GFP plasmid as a transfection marker. Basal n = 36, TTX n = 36, Bic n = 36 cells, from 2 sets of cultures. For each cell, the nuclear V5 intensity was

normalized to the nuclear GFP intensity, in order to normalize for differences in transfection efficiency between cells. Basal median = 1.00, TTX median = 0.9810, Bic median = 0.5760. Basal vs Bic $p < 0.0001$, TTX vs Bic $p < 0.0001$.

F) Violin plots of normalized cytoplasmic V5 ICC intensity in the same cells as in **E**. For each cell, the cytoplasmic V5 intensity was normalized to the nuclear GFP intensity, in order to normalize for differences in transfection efficiency between cells. Basal median = 1.00, TTX median = 1.237, Bic median = 0.6167. Basal vs Bic $p = 0.0002$, TTX vs Bic $p < 0.0001$.

Statistical significance is indicated by $*p < 0.05$, $***p < 0.001$, and $****p < 0.0001$, from Mann-Whitney U test with Bonferroni correction.

Figure 3.3 KCl depolarization decreases PDCD4 protein concentration in the nucleus and cytoplasm of neurons.

A) Violin plots of normalized nuclear PDCD4 ICC intensity. Control n = 118, KCl n = 110 cells, from 3 sets of cultures. Control median = 1.00, KCl median = 0.63. Control vs KCl $p < 0.0001$.

B) Violin plots of normalized cytoplasmic PDCD4 ICC intensity in the same cells as in **A**. Control median = 1.00, KCl median = 0.70. Control vs KCl $p < 0.0001$.

Statistical significance is indicated by $****p < 0.0001$, from Mann-Whitney U test.

Figure 3.4 Inhibition of protein synthesis does not prevent activity-dependent decrease of PDCD4.

A) Violin plots of normalized nuclear PDCD4 immunocytochemistry (ICC) intensity. Basal n = 117, TTX n = 118, Bic n = 109, CHX-Basal n = 123, CHX-TTX n = 120, CHX-Bic n = 104

cells, from 3 sets of cultures. Basal median = 1.00, TTX median = 0.9119, Bic median = 0.4924, CHX-Basal median = 0.8890, CHX-TTX median = 1.033, CHX-Bic median = 0.5375. Basal vs Bic $p < 0.0001$, TTX vs Bic $p < 0.0001$, CHX-Basal vs CHX-Bic $p < 0.0001$, CHX-TTX vs CHX-Bic $p < 0.0001$.

B) Violin plots of normalized cytoplasmic PDCD4 ICC intensity in the same cells as in **A**. Basal median = 1.00, TTX median = 0.9501, Bic median = 0.7138, CHX-Basal median = 1.112, CHX-TTX median = 1.191, CHX-Bic median = 0.8626. Basal vs Bic $p < 0.0001$, TTX vs Bic $p < 0.0001$, CHX-Basal vs CHX-Bic $p < 0.0001$, CHX-TTX vs CHX-Bic $p < 0.0001$.

Statistical significance is indicated by ****$p < 0.0001$, from Mann-Whitney U test with Bonferroni correction.

Figure 3.5 PDCD4 does not undergo nuclear export following neuronal stimulation.

A) Left: Schematic of CRM1-mediated nuclear export inhibitor leptomycin B (LMB) experiments. Right: Violin plots of normalized nuclear PDCD4 ICC intensity. Control n = 137, LMB n = 122 cells, from 3 sets of cultures. Control median = 1.00, LMB median = 1.513. Control vs LMB $p < 0.0001$.

B) Left: Violin plots of normalized nuclear PDCD4 immunocytochemistry (ICC) intensity. Basal n = 109, TTX n = 109, Bic n = 109, LMB-Basal n = 106, LMB-TTX n = 100, LMB-Bic n = 86 cells, from 3 sets of cultures. Basal median = 1.00, TTX median = 1.08, Bic median = 0.59, LMB-Basal median = 1.30, LMB-TTX median = 1.16, LMB-Bic median = 0.52. Basal vs Bic $p < 0.0001$, TTX vs Bic $p < 0.0001$, LMB-Basal vs LMB-Bic $p < 0.0001$, LMB-TTX vs LMB-Bic $p < 0.0001$. Right: Violin plots of normalized cytoplasmic PDCD4 ICC intensity in the same cells as in **left**. Basal median = 1.00, TTX median = 1.158, Bic median = 0.9127, LMB-Basal

median = 1.031, LMB-TTX median = 1.005, LMB-Bic median = 0.7122. Basal vs Bic p = 0.034, TTX vs Bic p < 0.0001, LMB-Basal vs LMB-Bic p < 0.0001, LMB-TTX vs LMB-Bic p < 0.0001.

Statistical significance is indicated by *p < 0.05 and ****p < 0.0001, from Mann-Whitney U test with Bonferroni correction.

Figure 3.6 PDCD4 undergoes proteasome-mediated degradation following neuronal stimulation.

A) Left: Schematic of proteasome inhibitor epoxomicin (epox) experiments. Center: Violin plots of normalized nuclear PDCD4 ICC intensity. Basal n = 113, TTX n = 106, Bic n = 103, Epox-Basal n = 107, Epox-TTX n = 94, Epox-Bic n = 86 cells, from 3 sets of cultures. Basal median = 1.00, TTX median = 1.18, Bic median = 0.62, Epox-Basal median = 0.97, Epox-TTX median = 0.99, Epox-Bic median = 0.88. Basal vs Bic p < 0.0001, TTX vs Bic p < 0.0001, Epox-Basal vs Epox-Bic p = 0.1662, Epox-TTX vs Epox-Bic p = 0.0174. Right: Violin plots of normalized cytoplasmic PDCD4 ICC intensity in the same cells as in **center**. Basal median = 1.00, TTX median = 1.174, Bic median = 0.8439, Epox-Basal median = 0.8789, Epox-TTX median = 0.9596, Epox-Bic median = 0.9077. Basal vs Bic p = 0.001, TTX vs Bic p < 0.0001, Epox-Basal vs Epox-Bic p = 1, Epox-TTX vs Epox-Bic p = 0.8258.

B) Left: Schematic of proteasome inhibitor bortezomib (bort) experiments. Center: Violin plots of normalized nuclear PDCD4 ICC intensity. Basal n = 131, TTX n = 111, Bic n = 120, Bort-Basal n = 100, Bort-TTX n = 98, Bort-Bic n = 116 cells, from 3 sets of cultures. Basal median = 1.00, TTX median = 1.09, Bic median = 0.60, Bort-Basal median = 1.00, Bort-TTX median = 1.04, Bort-Bic median = 0.94. Basal vs Bic p < 0.0001, TTX vs Bic p < 0.0001, Bort-Basal vs

Bort-Bic p = 0.6224, Bort-TTX vs Bort-Bic p = 0.2648. Right: Violin plots of normalized cytoplasmic PDCD4 ICC intensity in the same cells as in **center**. Basal median = 1.00, TTX median = 1.093, Bic median = 0.9226, Bort-Basal median = 0.9229, Bort-TTX median = 0.8904, Bort-Bic median = 0.9472. Basal vs Bic p = 0.0156, TTX vs Bic p < 0.0001, Bort-Basal vs Bort-Bic p = 1, Bort-TTX vs Bort-Bic p = 0.3544.

C) Left: Schematic of MLN4924 (MLN) experiments. MLN4924 inhibits neddylation, preventing the activation of Cullin-RING E3 ubiquitin ligases. Center: Violin plots of normalized nuclear PDCD4 ICC intensity. Basal n = 130, TTX n = 120, Bic n = 120, MLN-Basal n = 115, MLN-TTX n = 108, MLN-Bic n = 97 cells, from 3 sets of cultures. Basal median = 1.00, TTX median = 1.11, Bic median = 0.64, MLN-Basal median = 1.05, MLN-TTX median = 0.93, MLN-Bic median = 0.95. Basal vs Bic p < 0.0001, TTX vs Bic p < 0.0001, MLN-Basal vs MLN-Bic p = 0.329, MLN-TTX vs MLN-Bic p = 1. Right: Violin plots of normalized cytoplasmic PDCD4 ICC intensity in the same cells as in **center**. Basal median = 1.00, TTX median = 1.173, Bic median = 0.8955, MLN-Basal median = 0.8940, MLN-TTX median = 0.9603, MLN-Bic median = 0.8633. Basal vs Bic p = 0.0324, TTX vs Bic p < 0.0001, MLN-Basal vs MLN-Bic p = 0.6294, MLN-TTX vs MLN-Bic p = 0.11.

Statistical significance is indicated by *p < 0.05, **p < 0.01, and ****p < 0.0001, from Mann-Whitney U test with Bonferroni correction.

Figure 3.7 PDCD4 S71A mutation prevents the activity-dependent decrease of PDCD4.

A) PDCD4 protein sequence (amino acids 62-76). PKC and S6K1 phosphorylation sites are indicated in purple. Adapted from (Matsuhashi et al., 2019).

B) HA immunocytochemistry (ICC) of basal, TTX-silenced, and Bic-stimulated neurons transduced with PDCD4-HA WT, PDCD4-HA S71A AAV, or No AAV (negative control). Scale bar = 10 μm.

C) Violin plots of normalized nuclear HA ICC intensity. WT-Basal n = 144, WT-TTX n = 136, WT-Bic n = 147, S71A-Basal n = 158, S71A-TTX n = 140, S71A-Bic n = 122 cells, from 4 sets of cultures. WT-Basal median = 1.00, WT-TTX median = 1.13, WT-Bic median = 0.67, S71A-Basal median = 1.05, S71A-TTX median = 1.21, S71A-Bic median = 1.27. WT-Basal vs WT-Bic $p < 0.0001$, WT-TTX vs WT-Bic $p < 0.0001$, S71A-Basal vs S71A-Bic $p = 0.0034$, S71A-TTX vs S71A-Bic $p = 0.14$.

D) Violin plots of normalized cytoplasmic HA immunocytochemistry (ICC) intensity in the same cells as in **C**. WT-Basal median = 1.00, WT-TTX median = 1.161, WT-Bic median = 0.8621, S71A-Basal median = 0.9676, S71A-TTX median = 1.209, S71A-Bic median = 1.063. WT-Basal vs WT-Bic $p = 0.0012$, WT-TTX vs WT-Bic $p < 0.0001$, S71A-Basal vs S71A-Bic $p = 0.6704$, S71A-TTX vs S71A-Bic $p = 0.2012$.

E) Top: Western blot of protein lysates from basal and Bic-stimulated neurons transduced with PDCD4-HA WT or PDCD4-HA S71A. The PDCD4-HA band is indicated with an arrow. We observe a non-specific band above the HA band. Bottom: Quantification of western blot, from 4 sets of cultures. HA intensity was normalized to TUJ1 intensity. Within each experiment, each Bic sample was normalized to its respective basal sample. WT Bic/Basal median = 0.59, S71A Bic/Basal median = 0.90. WT vs S71A $p = 0.0286$.

Statistical significance is indicated by $*p < 0.05$, $**p < 0.01$, and $****p < 0.0001$, from Mann-Whitney U test with Bonferroni correction.

Figure 3.8 PKC inhibition prevents the activity-dependent decrease of PDCD4.

A) Left: Schematic of S6K inhibitor Ly2584702 (LY) experiments. Center: Violin plots of normalized nuclear PDCD4 ICC intensity. Basal n = 138, TTX n = 104, Bic n = 122, LY-Basal n = 112, LY-TTX n = 112, LY-Bic n = 107 cells, from 3 sets of cultures. Basal median = 1.00, TTX median = 1.11, Bic median = 0.74, LY-Basal median = 1.07, LY-TTX median = 1.04, LY-Bic median = 0.62. Basal vs Bic $p < 0.0001$, TTX vs Bic $p < 0.0001$, LY-Basal vs LY-Bic $p < 0.0001$, LY-TTX vs LY-Bic $p < 0.0001$. Right: Violin plots of normalized cytoplasmic PDCD4 ICC intensity in the same cells as in **center**. Basal median = 1.00, TTX median = 1.14, Bic median = 0.95, LY-Basal median = 1.05, LY-TTX median = 1.04, LY-Bic median = 0.76. Basal vs Bic $p = 0.4742$, TTX vs Bic $p = 0.0088$, LY-Basal vs LY-Bic $p < 0.0001$, LY-TTX vs LY-Bic $p < 0.0001$. Note that, in these experiments, the Basal vs Bic-induced decrease in cytoplasmic PDCD4 is not statistically significant for the untreated (no inhibitor) cells. The Bic-induced cytoplasmic decrease is smaller and less consistent than the nuclear decrease, with statistical significance in the control cells of **Fig 3.6A-C** but not **Fig 3.8A+C**. Nonetheless, there is a significant Bic-induced decrease of cytoplasmic PDCD4 in the treated (LY2584702) cells, demonstrating that S6K is not required for the Bic-induced decrease of PDCD4.

B) Western blot of protein lysates from neurons treated with or without LY2584702. Western blot was stained with antibodies for phospho-S6 (ser 235/236) and total S6 to confirm that LY2584702 inhibits S6K activity.

C) Left: Schematic of PKC inhibitor Ro-31-8425 (Ro) experiments. Center: Violin plots of normalized nuclear PDCD4 ICC intensity. Basal n = 101, TTX n = 101, Bic n = 96, Ro-Basal n = 81, Ro-TTX n = 95, Ro-Bic n = 87 cells, from 3 sets of cultures. Basal median = 1.00, TTX median = 1.08, Bic median = 0.71, Ro-Basal median = 0.87, Ro-TTX median = 0.93, Ro-Bic

median = 0.97. Basal vs Bic $p < 0.0001$, TTX vs Bic $p < 0.0001$, Ro-Basal vs Ro-Bic $p = 0.0114$, Ro-TTX vs Ro-Bic $p = 0.3892$. Right: Violin plots of normalized cytoplasmic PDCD4 ICC intensity in the same cells as in **center**. Basal median = 1.00, TTX median = 1.114, Bic median = 0.9326, Ro-Basal median = 1.059, Ro-TTX median = 1.172, Ro-Bic median = 1.195. Basal vs Bic $p = 0.2592$, TTX vs Bic $p = 0.0008$, Ro-Basal vs Ro-Bic $p = 0.0118$, Ro-TTX vs Ro-Bic $p = 0.9892$.

Statistical significance is indicated by $*p < 0.05$, $**p < 0.01$, $***p < 0.001$, and $****p < 0.0001$, from Mann-Whitney U test with Bonferroni correction.

Figure 3.9 Stimulus-induced degradation of PDCD4 regulates the expression of neuronal activity-dependent genes.

A) For each biological replicate, normalized read counts (from DESeq2) divided by transcript length are shown for the top 20 activity-dependent genes, ranked by adjusted p-value for PDCD4 WT no CHX samples. Each row represents a gene, and each column represents a biological replicate. The color of each box indicates transcript abundance (note: color is not scaled linearly in order to display full range of read counts).

B) Stimulation-induced log2 fold change (FC) for all 912 activity-dependent genes, clustered by fold change across sample type. Each row represents a gene and each column represents a sample type. The color legend represents Bic vs TTX log2FC with red representing upregulation, blue representing downregulation, and white indicating log2FC of zero.

C) For each activity-dependent gene, Bic versus TTX log2FC is plotted against -log10 of adjusted p-value, from PDCD4 WT samples (black) and PDCD4 S71A samples (red). Gene names for the top five activity-dependent genes by adjusted p-value are labeled. For both

PDCD4 WT and PDCD4 S71A samples, *Npas4* Bic vs TTX adjusted p-value was zero (-log10 of zero is not defined), therefore for display, the -log10 adjusted p-value for *Npas4* was set to 250 for both samples.

D) Activity-dependent upregulated genes (left bar) and activity-dependent downregulated genes (right bar) were categorized by the activity-dependent differential expression in PDCD4 S71A samples. The colors in each bar show the percentage of activity-dependent genes showing activity-dependent upregulation (red), no change (gray) or downregulation (blue) in PDCD4 S71A samples.

Figure 3.10 PDCD4 degradation regulates the expression of 91 activity-dependent genes.

A) Bic versus TTX log2FC for all 91 putative PDCD4 transcriptional regulation target genes, clustered by fold change across sample type. Each row represents a gene, and each column represents a sample type. The color legend represents Bic vs TTX log2FC with red representing upregulation, blue representing downregulation, and white indicating a log2FC of zero.

B) RT-qPCR of putative PDCD4 target genes, *Scd1* and *Thrsp*, from TTX-silenced and Bic-stimulated neurons that were transduced with PDCD4 WT or S71A, from 6 sets of cultures. Samples were normalized using two housekeeping genes, *Hprt* and *Gapdh*. The abundance of the target gene in each Bic sample was normalized to its respective TTX sample. *Scd1* WT CHX median = 1.702, *Scd1* S71A CHX median = 0.5776, *Scd1* WT median = 2.401, *Scd1* S71A median = 0.7672, *Thrsp* WT CHX median = 1.826, *Thrsp* S71A CHX median = 0.9080, *Thrsp* WT median = 1.522, *Thrsp* S71A median = 0.5995. *Scd1* CHX WT vs CHX S71A p = 0.0022, *Scd1* WT vs S71A p = 0.0260, *Thrsp* CHX WT vs CHX S71A p = 0.0043, *Thrsp* WT vs S71A p

= 0.0043. Statistical significance is indicated by *p < 0.05 and **p < 0.01, from Mann-Whitney U test.

Figure 3.11 Motif analyses of promoters of putative PDCD4 target genes.

Motif analyses of promoters of putative PDCD4 target genes (left column) and for comparison, other CHX-insensitive activity-dependent genes (right column) using HOMER software. The top panel shows the motif image logos, enrichment, and p-values for the top ten motifs by p-value for activity-dependent upregulated genes, and the bottom panel shows the same but for activity-dependent downregulated genes (only 8 motifs were significant for down-regulated genes).

Figure 3.12 Degradation-resistant PDCD4 suppresses activity-dependent changes in expression of synaptic genes.

A) GO analysis -log10 false discovery rate (FDR; circles) and percent of genes (bars) in terms from Biological Process (top four terms) and Cellular Compartment (bottom four terms) analyses (Ashburner et al., 2000; Carbon et al., 2019; Mi et al., 2019). Data from putative PDCD4 target genes (91 genes) are shown in orange and for comparison, data from other CHX-insensitive activity-dependent genes (368 genes) are shown in purple.

B) Diagram depicting a generic synapse and synaptic proteins. The labeled synaptic proteins are encoded by putative PDCD4 target genes (gene name indicated in parenthesis alongside protein). The activity-dependent changes in expression of these genes are inhibited by degradation-resistant PDCD4. The presynaptic terminal is shown above with neurotransmitter-loaded synaptic vesicles, and the postsynaptic terminal is shown below with neurotransmitter receptors in the postsynaptic membrane (one receptor is shown anchored to an unlabeled gray PSD-95

protein). Arrow next to gene name illustrates the direction of activity-dependent differential expression and dashed line with bar illustrates the suppression of this activity-dependent change in the PDCD4 S71A samples.

Figure 3.13 Summary diagram of the activity-dependent proteasome-mediated degradation of PDCD4.

In silenced neurons (left), PDCD4 is highly expressed and suppresses the expression of specific genes. In stimulated neurons (right), PDCD4 is phosphorylated by PKC and undergoes proteasome-mediated degradation, thereby facilitating the expression of specific genes important for neuron synaptic function.

Figure 3.1

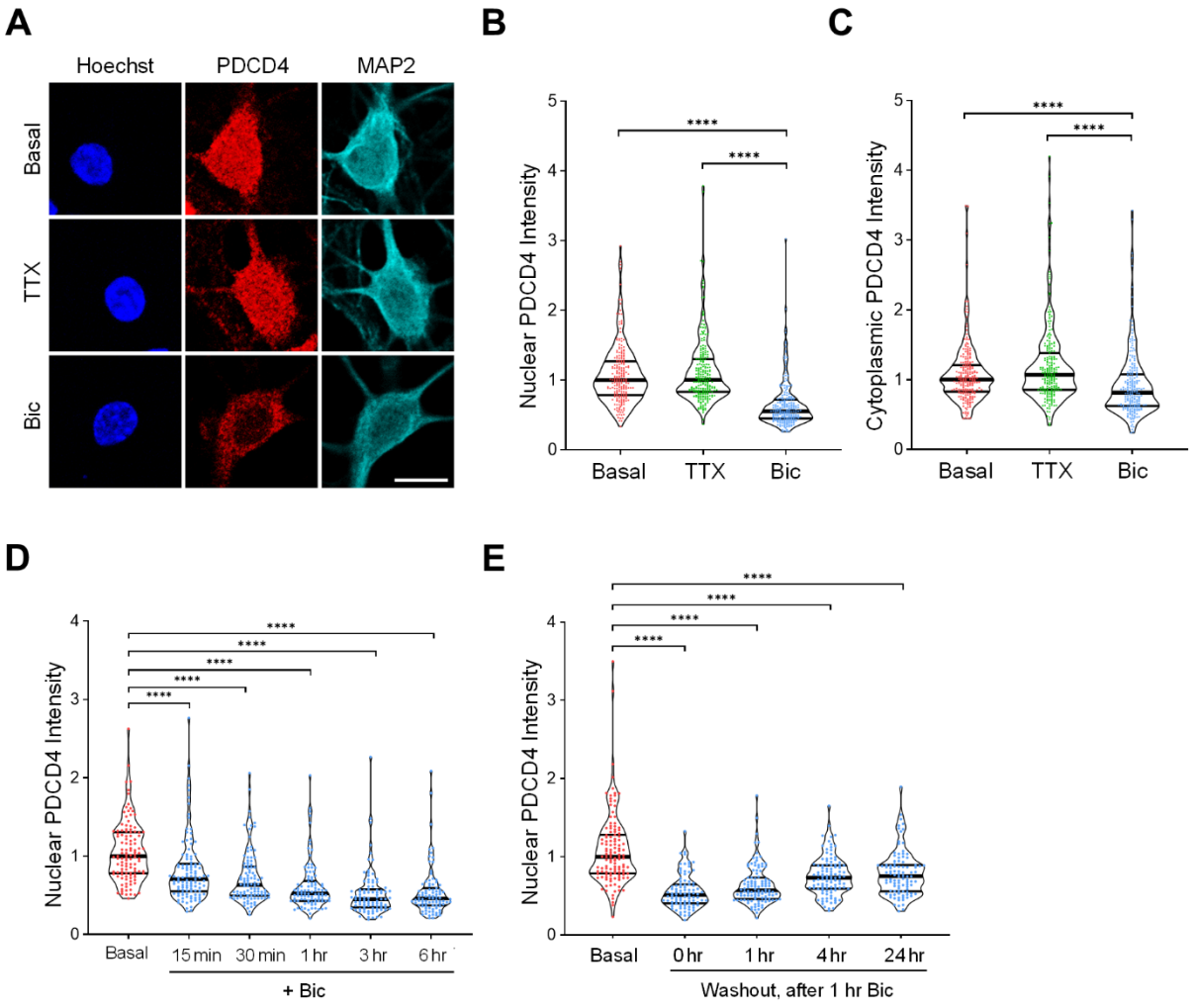
A
Hoechst
PDCD4
MAP2
Basal
TTX
Bic
B
Nuclear PDCD4 Intensity
Basal
TTX
Bic
C
Cytoplasmic PDCD4 Intensity
Basal
TTX
Bic
D
Nuclear PDCD4 Intensity
Basal
15 min
30 min
1 hr
3 hr
6 hr
+ Bic
E
Nuclear PDCD4 Intensity
Basal
0 hr
1 hr
4 hr
24 hr
Washout, after 1 hr Bic

Figure 3.2

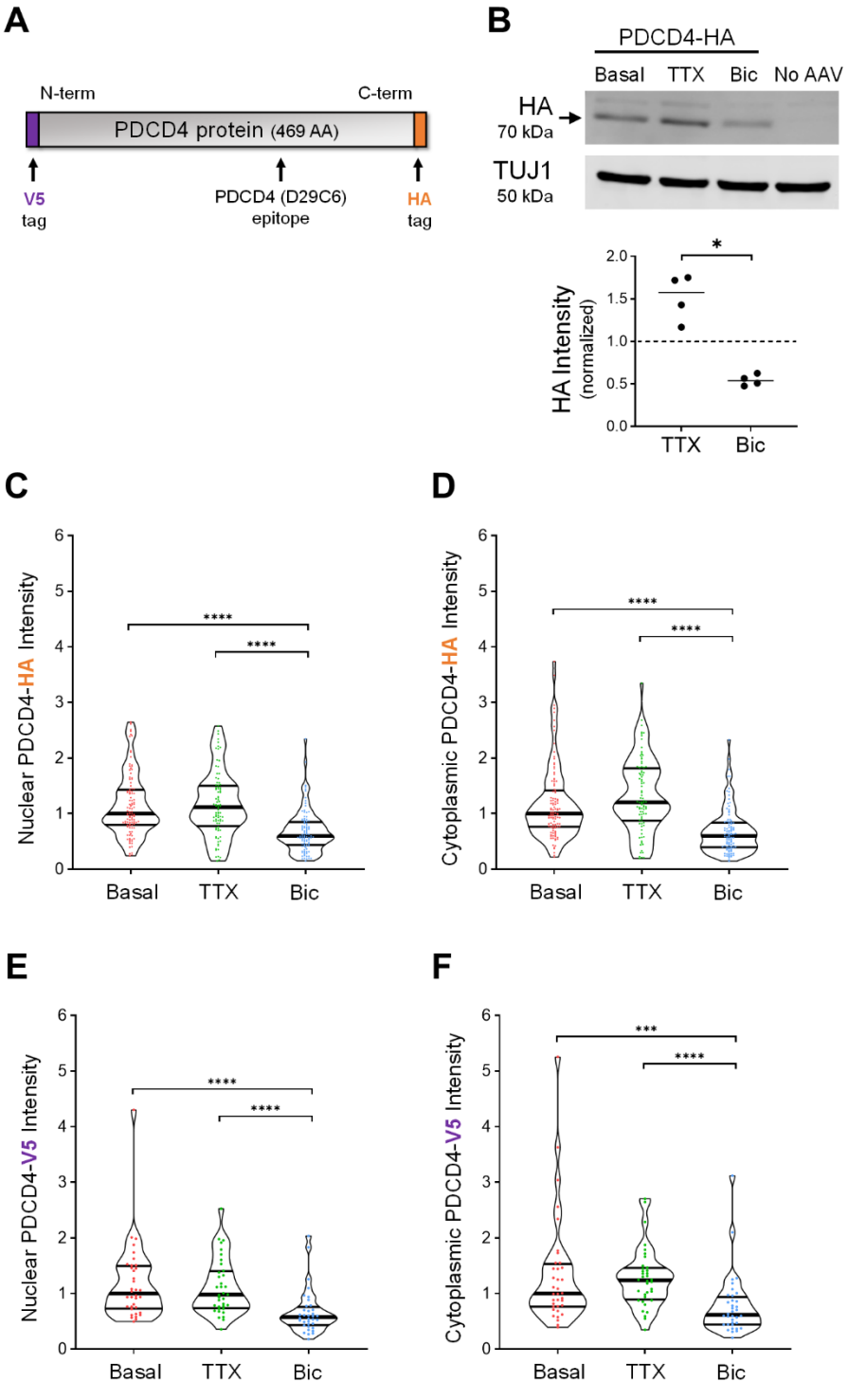
A
N-term
C-term
PDCD4 protein (469 AA)
V5 tag
PDCD4 (D29C6) epitope
HA tag
B
PDCD4-HA
Basal
TTX
Bic
No AAV
HA
70 kDa
TUJ1
50 kDa
HA Intensity (normalized)
TTX
Bic
C
Nuclear PDCD4-HA Intensity
D
Cytoplasmic PDCD4-HA Intensity
E
Nuclear PDCD4-V5 Intensity
F
Cytoplasmic PDCD4-V5 Intensity

Figure 3.3

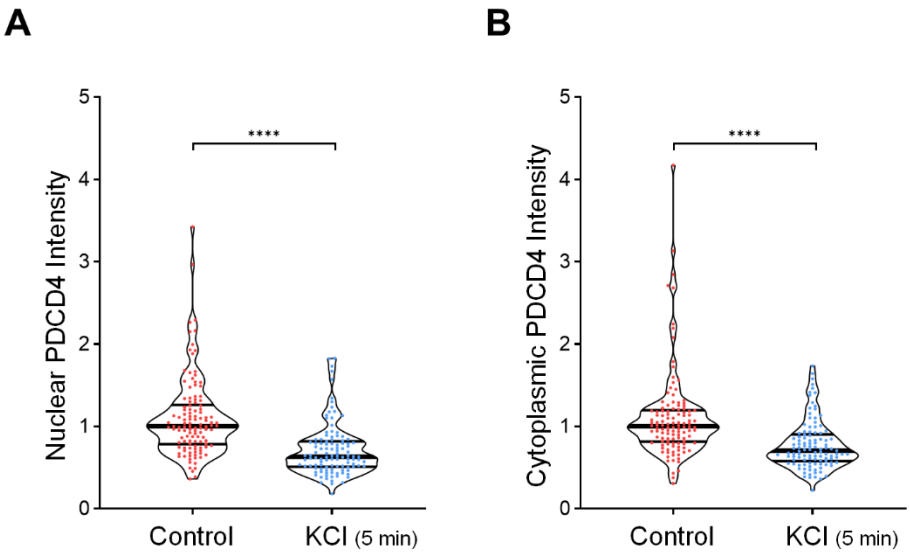
A
B
Nuclear PDCD4 Intensity
Cytoplasmic PDCD4 Intensity
0
1
2
3
4
5
****
Control
KCl (5 min)

Figure 3.4

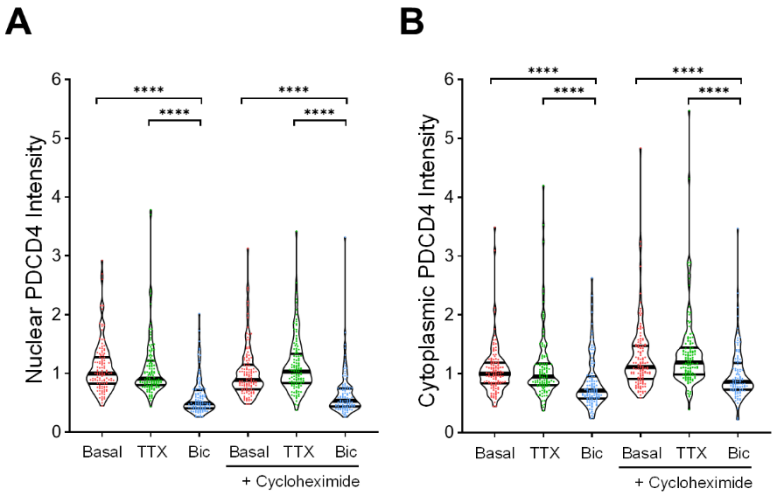
A
B
Nuclear PDCD4 Intensity
Cytoplasmic PDCD4 Intensity
0
1
2
3
4
5
6
****
Basal
TTX
Bic
Basal
TTX
Bic
+ Cycloheximide

Figure 3.5

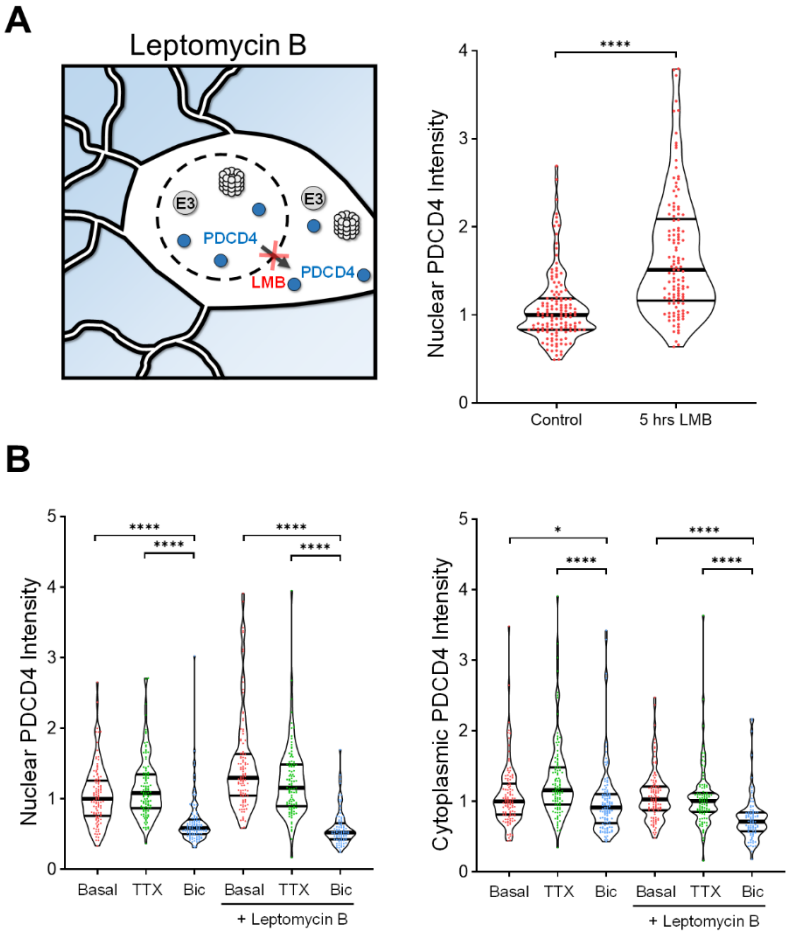
A
Leptomycin B
E3
E3
PDCD4
LMB
PDCD4
Nuclear PDCD4 Intensity
****
Control
5 hrs LMB
B
Nuclear PDCD4 Intensity
Basal
TTX
Bic
Basal
TTX
Bic
+ Leptomycin B
Cytoplasmic PDCD4 Intensity
*
****
****
****

Figure 3.6

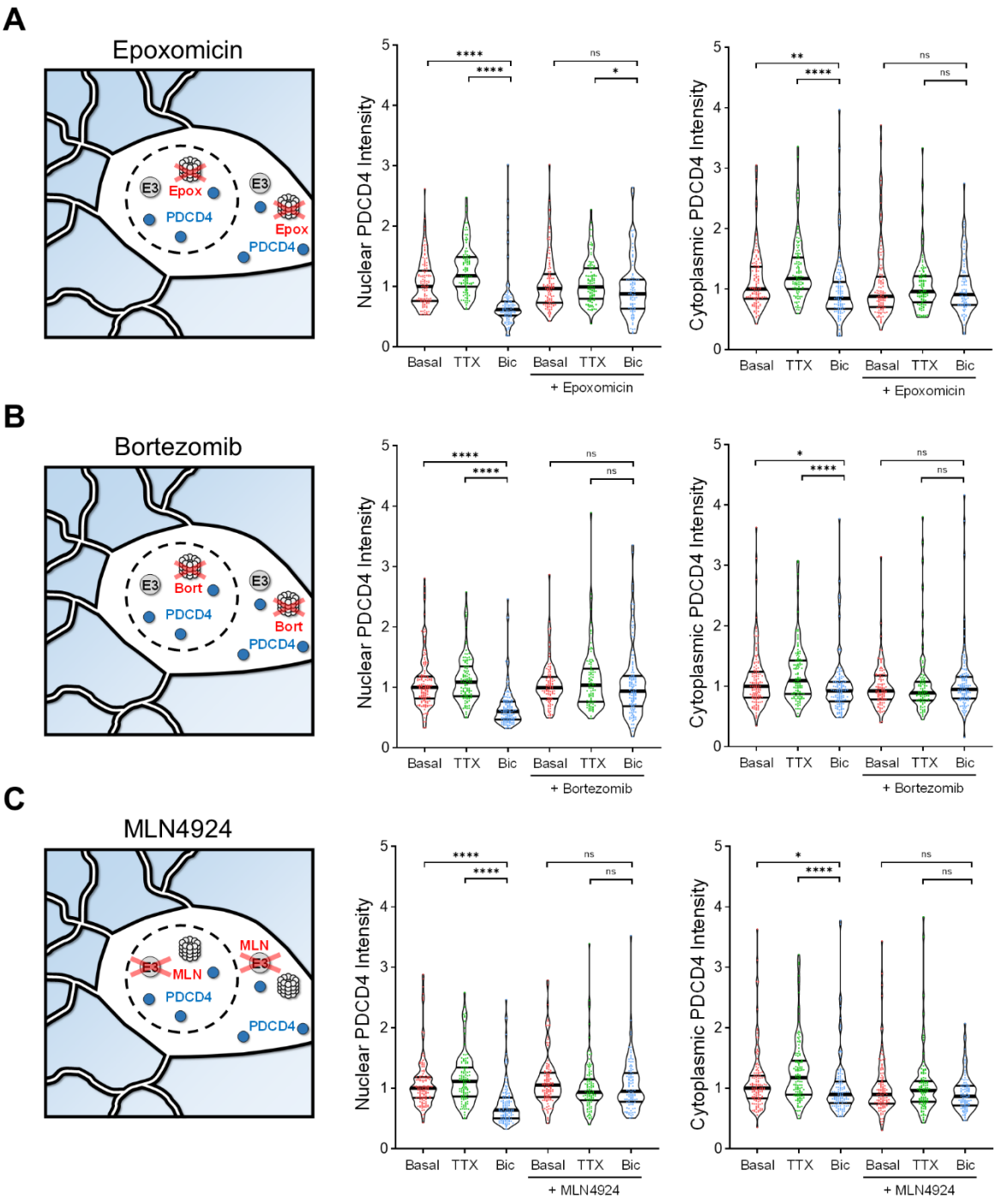
A
Epoxomicin
E3
Epox
PDCD4
Nuclear PDCD4 Intensity
Cytoplasmic PDCD4 Intensity
Basal
TTX
Bic
+ Epoxomicin
B
Bortezomib
Bort
+ Bortezomib
C
MLN4924
MLN
+ MLN4924
ns

Figure 3.7

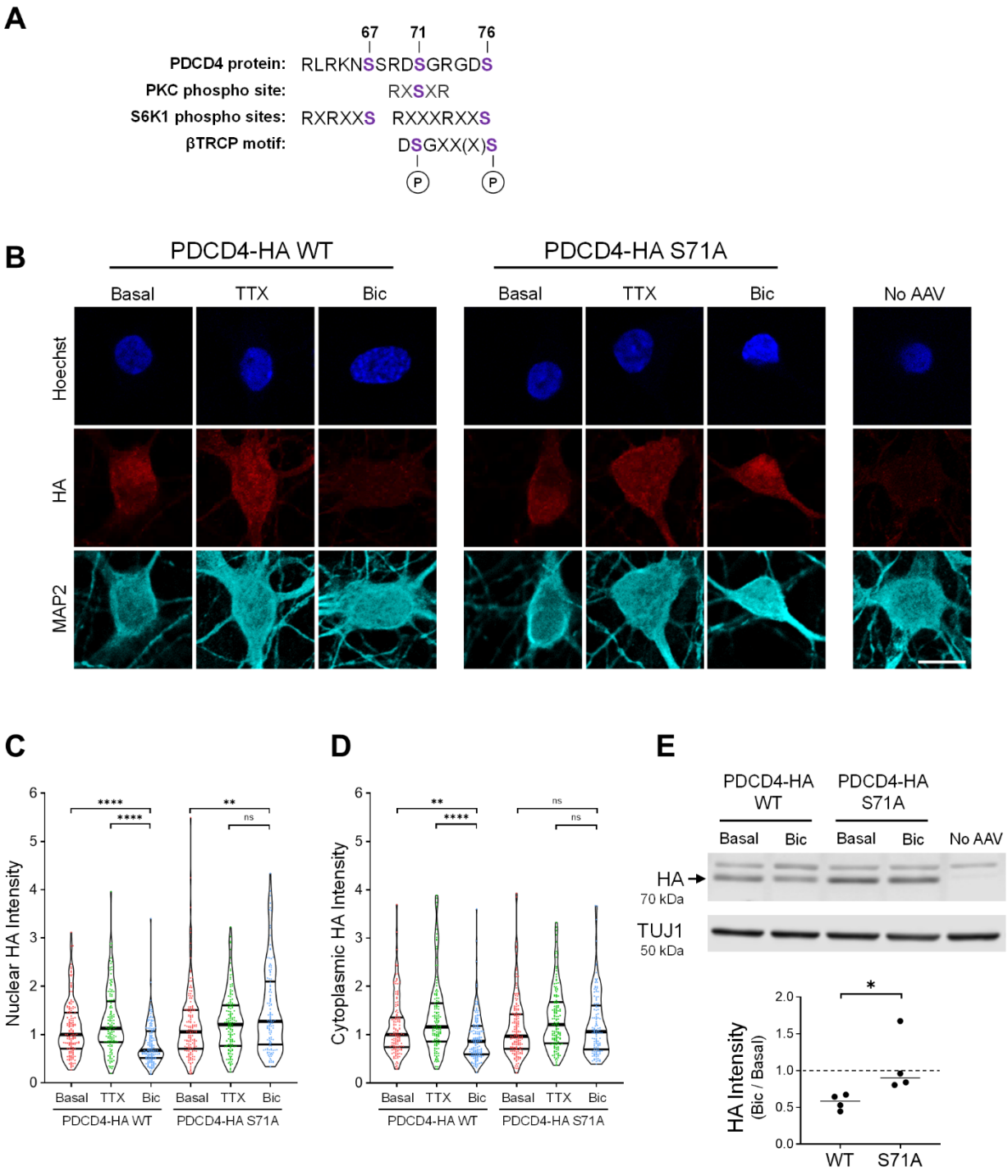
A
67
71
76
PDCD4 protein: RLRKNSSRDSGRGDS
PKC phospho site: RXSXR
S6K1 phospho sites: RXRXXS RXXXRXXS
βTRCP motif: DSGXX(X)S
P
P
B
PDCD4-HA WT
PDCD4-HA S71A
Basal
TTX
Bic
Basal
TTX
Bic
No AAV
Hoechst
HA
MAP2
C
Nuclear HA Intensity
****
****
**
ns
Basal TTX Bic Basal TTX Bic
PDCD4-HA WT
PDCD4-HA S71A
D
Cytoplasmic HA Intensity
**
****
ns
ns
Basal TTX Bic Basal TTX Bic
PDCD4-HA WT
PDCD4-HA S71A
E
PDCD4-HA WT
PDCD4-HA S71A
Basal
Bic
Basal
Bic
No AAV
HA
70 kDa
TUJ1
50 kDa
HA Intensity
(Bic / Basal)
*
WT
S71A

Figure 3.8

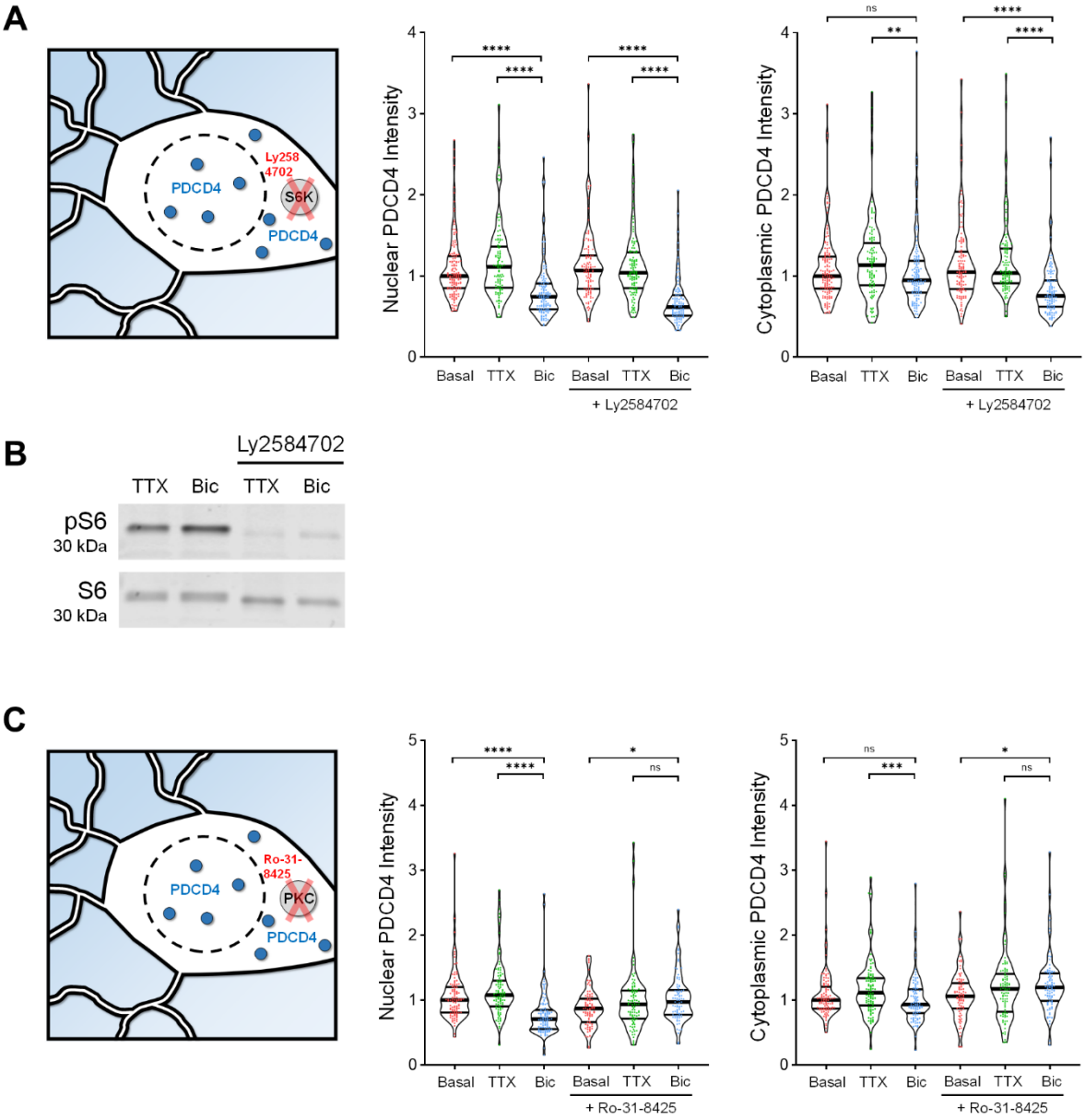
A
Ly258
4702
PDCD4
S6K
PDCD4
Nuclear PDCD4 Intensity
Cytoplasmic PDCD4 Intensity
Basal TTX Bic Basal TTX Bic
+ Ly2584702
B
Ly2584702
TTX Bic TTX Bic
pS6
30 kDa
S6
30 kDa
C
Ro-31-
8425
PDCD4
PKC
PDCD4
Nuclear PDCD4 Intensity
Cytoplasmic PDCD4 Intensity
Basal TTX Bic Basal TTX Bic
+ Ro-31-8425

Figure 3.9

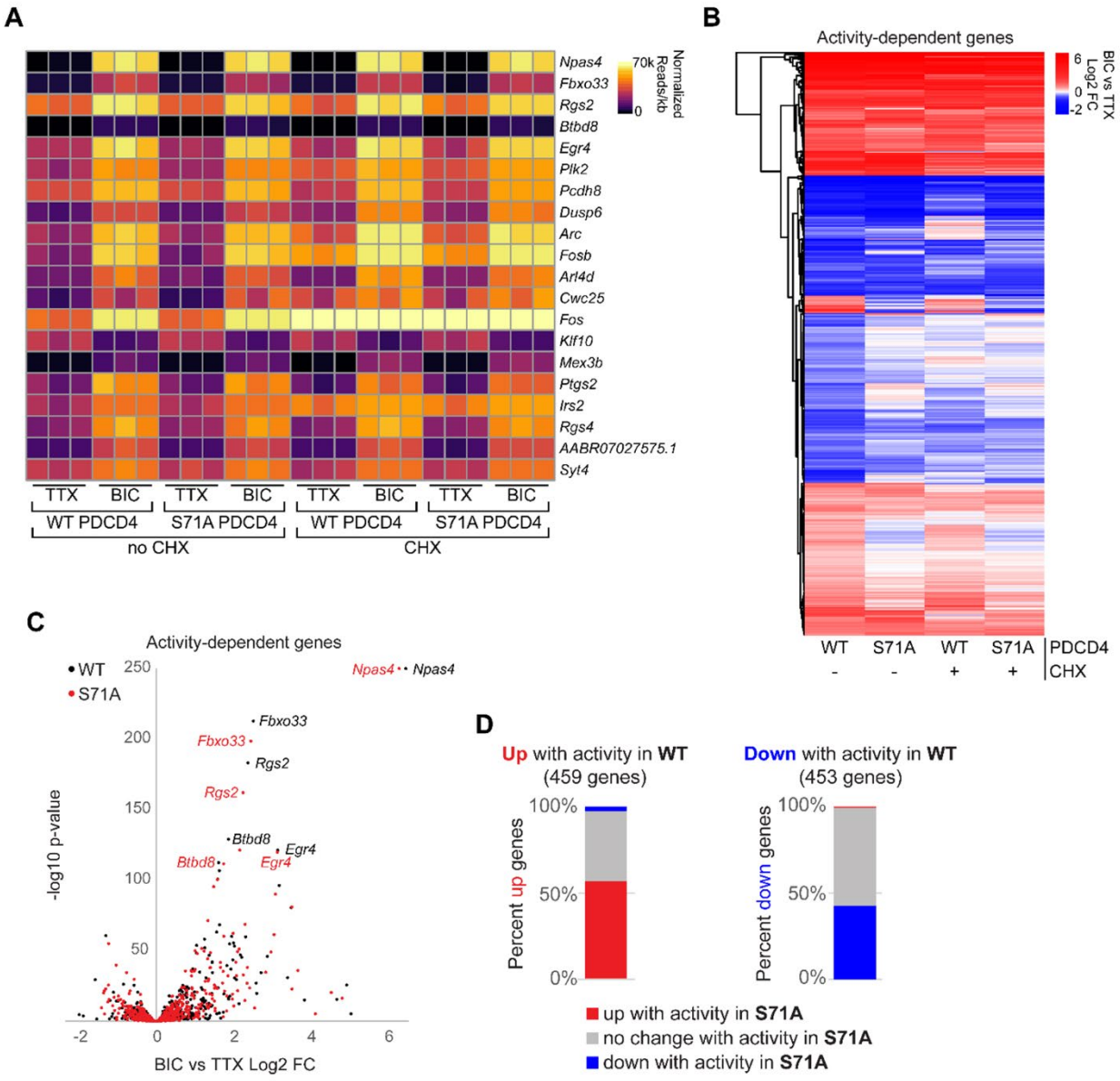
A
Npas4
Fbxo33
Rgs2
Btbd8
Egr4
Plk2
Pcdh8
Dusp6
Arc
Fosb
Arl4d
Cwc25
Fos
Klf10
Mex3b
Ptgs2
Irs2
Rgs4
AABR07027575.1
Syt4
70k
0
Normalized Reads/kb
TTX
BIC
WT PDCD4
S71A PDCD4
no CHX
CHX
B
Activity-dependent genes
6
0
-2
BIC vs TTX Log2 FC
WT
S71A
PDCD4
CHX
C
Activity-dependent genes
WT
S71A
-log10 p-value
BIC vs TTX Log2 FC
Npas4
Fbxo33
Rgs2
Btbd8
Egr4
D
Up with activity in WT
(459 genes)
Down with activity in WT
(453 genes)
Percent up genes
Percent down genes
100%
50%
0%
up with activity in S71A
no change with activity in S71A
down with activity in S71A

Figure 3.10

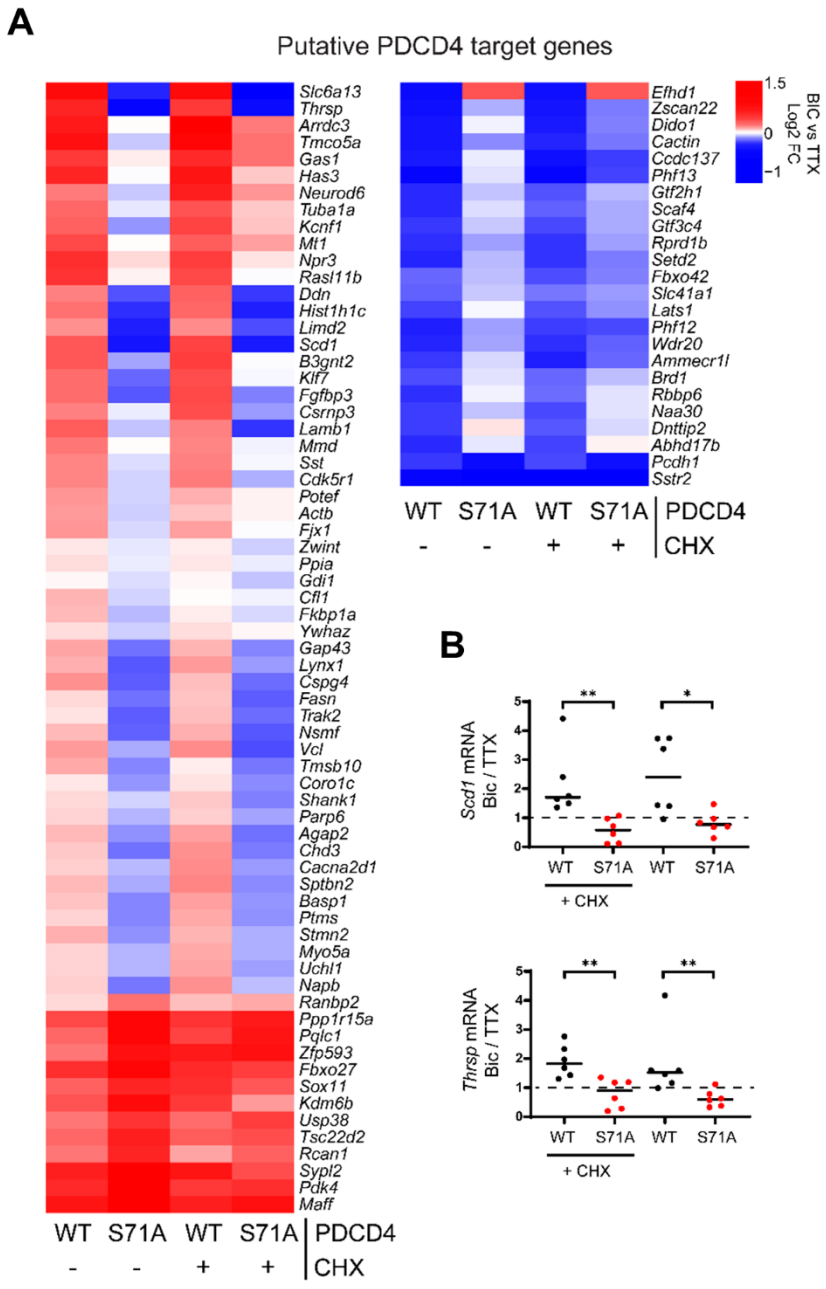
A
Putative PDCD4 target genes
Slc6a13
Thrsp
Arrdc3
Tmco5a
Gas1
Has3
Neurod6
Tuba1a
Kcnf1
Mt1
Npr3
Rasl11b
Ddn
Hist1h1c
Limd2
Scd1
B3gnt2
Klf7
Fgfbp3
Csrnp3
Lamb1
Mmd
Sst
Cdk5r1
Potef
Actb
Fjx1
Zwint
Ppia
Gdi1
Cfl1
Fkbp1a
Ywhaz
Gap43
Lynx1
Cspg4
Fasn
Trak2
Nsmf
Vcl
Tmsb10
Coro1c
Shank1
Parp6
Agap2
Chd3
Cacna2d1
Sptbn2
Basp1
Ptms
Stmn2
Myo5a
Uchl1
Napb
Ranbp2
Ppp1r15a
Pqlc1
Zfp593
Fbxo27
Sox11
Kdm6b
Usp38
Tsc22d2
Rcan1
Sypl2
Pdk4
Maff
WT S71A WT S71A PDCD4
- - + + CHX
Efhd1
Zscan22
Dido1
Cactin
Ccdc137
Phf13
Gtf2h1
Scaf4
Gtf3c4
Rprd1b
Setd2
Fbxo42
Slc41a1
Lats1
Phf12
Wdr20
Ammecr1l
Brd1
Rbbp6
Naa30
Dnttip2
Abhd17b
Pcdh1
Sstr2
1.5
0
−1
Bic vs TTX
Log2 FC
WT S71A WT S71A PDCD4
- - + + CHX
B
Scd1 mRNA
Bic / TTX
**
*
WT S71A WT S71A
+ CHX
Thrsp mRNA
Bic / TTX
**
**
WT S71A WT S71A
+ CHX

Figure 3.11

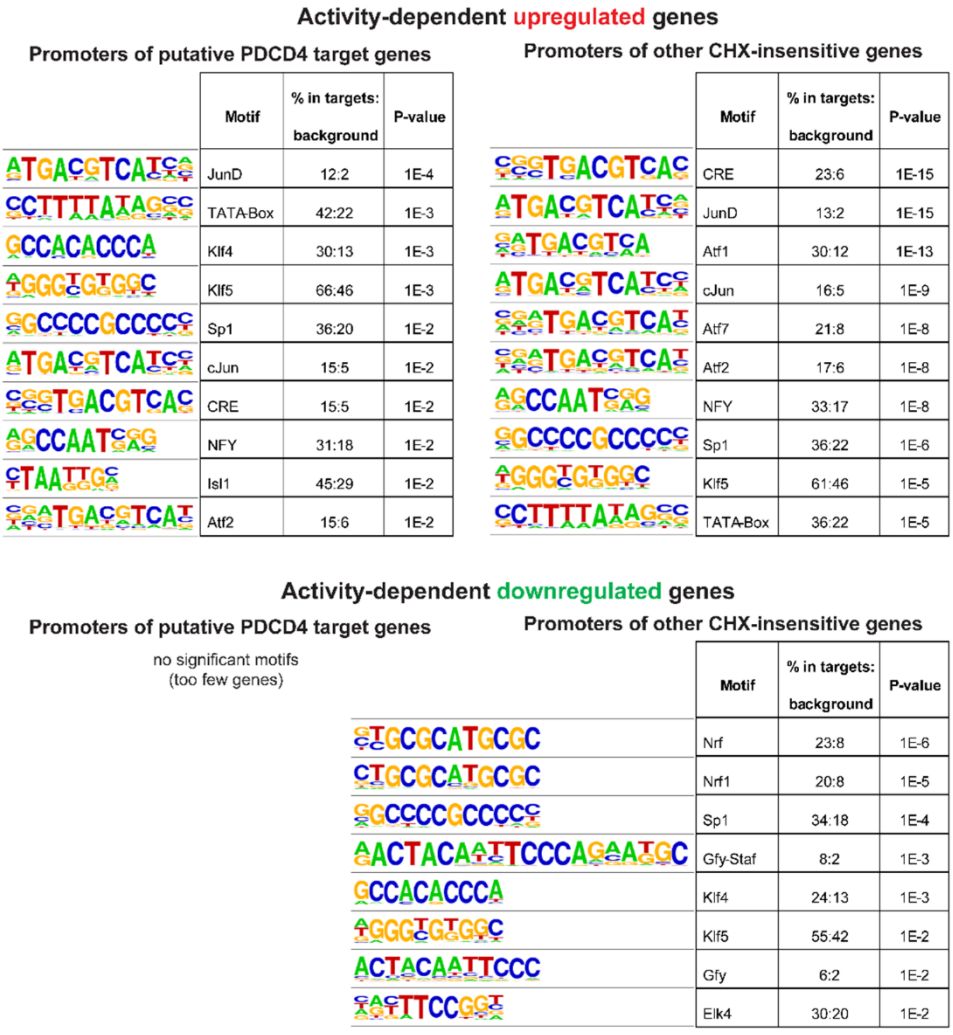
Activity-dependent upregulated genes
Promoters of putative PDCD4 target genes
Motif
% in targets: background
P-value
JunD 12:2 1E-4
TATA-Box 42:22 1E-3
Klf4 30:13 1E-3
Klf5 66:46 1E-3
Sp1 36:20 1E-2
cJun 15:5 1E-2
CRE 15:5 1E-2
NFY 31:18 1E-2
Isl1 45:29 1E-2
Atf2 15:6 1E-2
Promoters of other CHX-insensitive genes
Motif
% in targets: background
P-value
CRE 23:6 1E-15
JunD 13:2 1E-15
Atf1 30:12 1E-13
cJun 16:5 1E-9
Atf7 21:8 1E-8
Atf2 17:6 1E-8
NFY 33:17 1E-8
Sp1 36:22 1E-6
Klf5 61:46 1E-5
TATA-Box 36:22 1E-5
Activity-dependent downregulated genes
Promoters of putative PDCD4 target genes
no significant motifs (too few genes)
Promoters of other CHX-insensitive genes
Motif
% in targets: background
P-value
Nrf 23:8 1E-6
Nrf1 20:8 1E-5
Sp1 34:18 1E-4
Gfy-Staf 8:2 1E-3
Klf4 24:13 1E-3
Klf5 55:42 1E-2
Gfy 6:2 1E-2
Elk4 30:20 1E-2

Figure 3.12

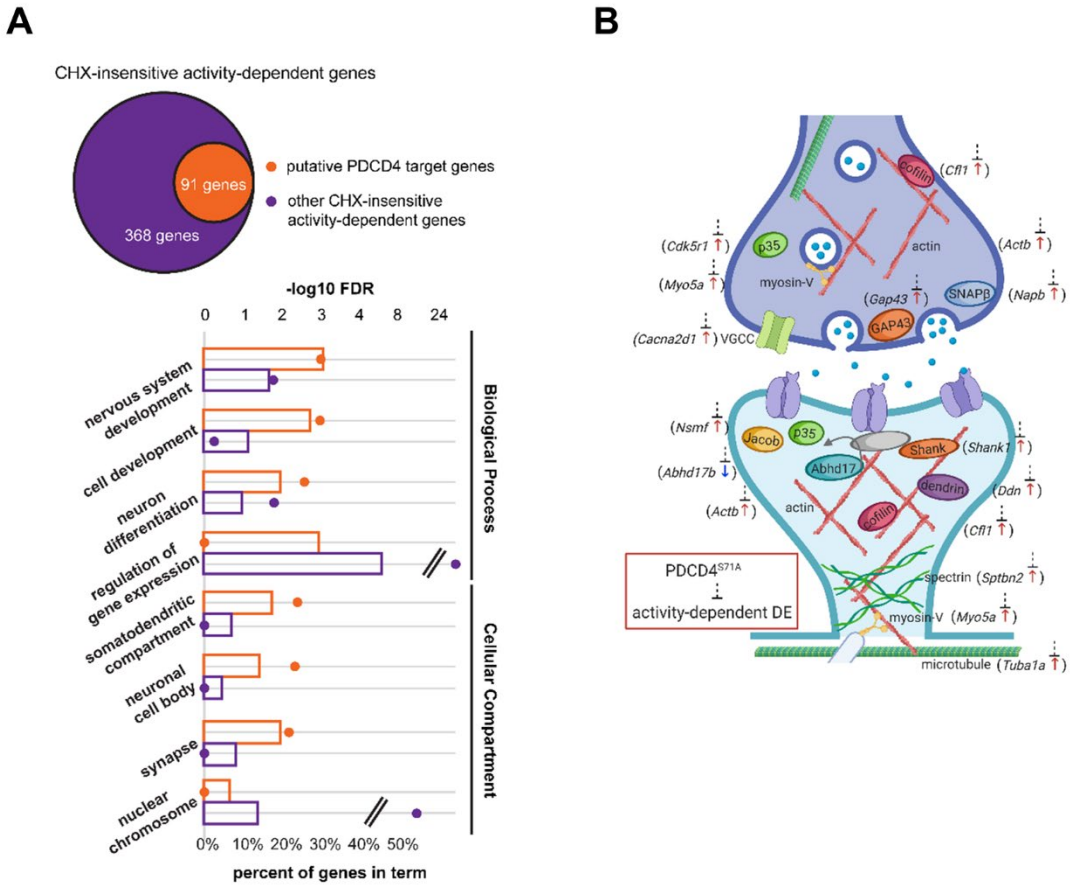
A
CHX-insensitive activity-dependent genes
91 genes
368 genes
putative PDCD4 target genes
other CHX-insensitive activity-dependent genes
-log10 FDR
0 1 2 3 4 8 24
nervous system development
cell development
neuron differentiation
regulation of gene expression
somatodendritic compartment
neuronal cell body
synapse
nuclear chromosome
Biological Process
Cellular Compartment
0% 10% 20% 30% 40% 50%
percent of genes in term
B
cofilin
(Cfl1 ↑)
(Cdk5r1 ↑)
p35
actin
(Actb ↑)
(Myo5a ↑)
myosin-V
(Gap43 ↑)
SNAPβ
(Napb ↑)
(Cacna2d1 ↑) VGCC
GAP43
(Nsmf ↑)
Jacob
p35
Shank
(Shank1 ↑)
(Abhd17b ↓)
Abhd17
dendrin
(Ddn ↑)
(Actb ↑)
actin
cofilin
(Cfl1 ↑)
PDCD4S71A
activity-dependent DE
spectrin (Sptbn2 ↑)
myosin-V (Myo5a ↑)
microtubule (Tuba1a ↑)

Figure 3.13

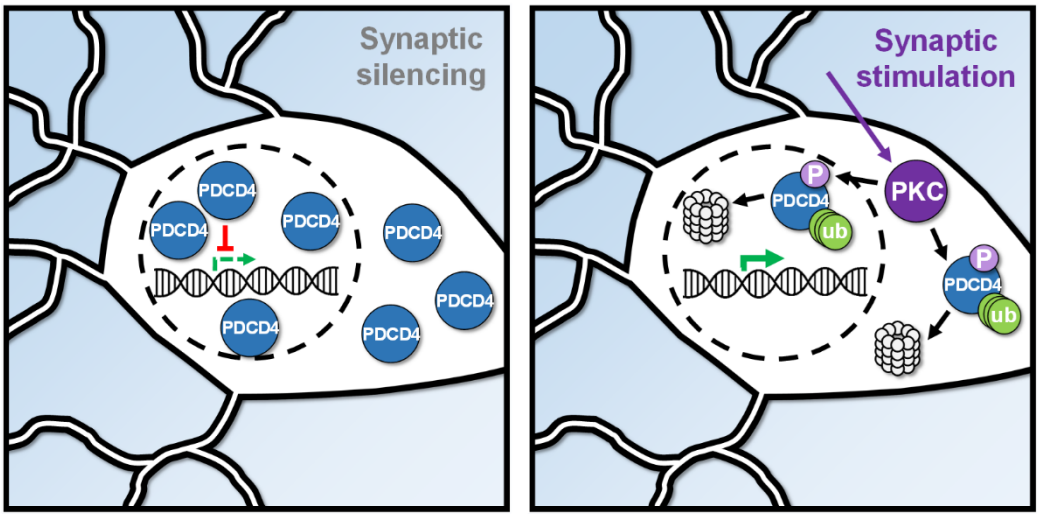
Synaptic silencing
PDCD4
PDCD4
PDCD4
PDCD4
PDCD4
PDCD4
PDCD4
Synaptic stimulation
PKC
P
PDCD4
ub
P
PDCD4
ub

Chapter 4:

Generation of CRTC1 conditional knockout mice

INTRODUCTION

CRTC1 is a transcriptional co-activator for CREB:

CREB-**R**egulated **T**ranscription **C**o-activator **1**, also known as CRTC1 or TORC1 (**T**ransducer **O**f **R**egulated **C**REB activity **1**), was identified in a genome-wide functional screen for proteins that regulate CREB-dependent transcription in HEK293T cells (Conkright et al., 2003). CRTC1, CRTC2, and CRTC3 were identified as transcriptional co-activators for CREB, a transcription factor that is important for neuronal activity-dependent gene expression. CRTC1 is highly expressed in the brain (Watts et al., 2011). The CRTC1 protein contains a CREB-binding domain, a domain that regulates nuclear translocation, and a transactivation domain that regulates transcription (Saura and Cardinaux, 2017). CRTC1 binds to the bZIP domain of CREB and enhances CREB activity by enhancing the interaction of CREB with TAF4, a component of the RNA polymerase II pre-initiation complex (Conkright et al., 2003). CRTC2 can also facilitate CREB binding to DNA (Wang et al., 2010). CRTC1 may serve as a transcription co-activator for additional transcription factors, as CRTC1 can also bind to the bZIP domains of c-Fos and c-Jun, and enhance subsequent AP-1-dependent transcription in HeLa cells (Canettieri et al., 2009).

CRTC1 translocates from synapses to the nucleus in response to neuronal activity:

In unstimulated neurons, CRTC1 localizes to the cytoplasm, including in dendrites and at synapses (Ch'ng et al., 2012). Following neuronal stimulation, CRTC1 rapidly translocates into the nucleus. In cultured neurons, activity-dependent nuclear translocation of CRTC1 occurs in response to stimulation of glutamatergic transmission by the $GABA_A$ receptor antagonist bicuculline (Zhou et al., 2006; Ch'ng et al., 2012; Nonaka et al., 2014; Ch'ng et al., 2015), KCl-mediated depolarization (Zhou et al., 2006; Kovacs et al., 2007; Li et al., 2009; Ch'ng et al., 2015), or stimulation of cAMP signaling by forskolin (Zhou et al., 2006; Kovacs et al., 2007; Ch'ng et al., 2012). CRTC1 translocates to the nucleus within several minutes of stimulation (Ch'ng et al., 2012, 2015), remains in the nucleus for the duration of the stimulation, and exits the nucleus within 30 minutes following the cessation of stimulation (Ch'ng et al., 2012). Activation of AMPA and NMDA receptors, as well as subsequent influx of calcium through L-type voltage-gated calcium channels, trigger the activity-dependent translocation of CRTC1 (Ch'ng et al., 2015). The nuclear translocation of CRTC1 is initiated by local calcium elevations and the calcium chelator BAPTA effectively blocks CRTC1 translocation (Ch'ng et al., 2015). Elevated calcium concentration is important for activating the calcium-sensitive phosphatase calcineurin (Li et al., 2011) and the calcineurin antagonist cyclosporine A prevents nuclear translocation of CRTC1 (Kovacs et al., 2007; Li et al., 2009; Ch'ng et al., 2012; Nonaka et al., 2014; Ch'ng et al., 2015). This suggests that CRTC1 undergoes activity-dependent dephosphorylation by calcineurin in response to stimulation. Indeed, CRTC1 phosphorylation decreases after stimulation, as indicated by decreases in the detection of phospho-CRTC1 (Li et al., 2009; Ch'ng et al., 2012; Parra-Damas et al., 2014, 2017), increased SDS-PAGE mobility consistent with dephosphorylation (Ch'ng et al., 2012, 2015), and increased pH detected by two-dimensional gel electrophoresis consistent with dephosphorylation (Ch'ng et al., 2012).

Moreover, inhibition of calcineurin prevents the activity-dependent dephosphorylation of CRTC1 (Ch'ng et al., 2012). The dephosphorylation of CRTC1 is important for nuclear translocation, as phospho-null CRTC1 mutants are constitutively nuclear (Nonaka et al., 2014; Ch'ng et al., 2015). In unstimulated neurons, CRTC1 is localized to synapses, where it is tethered to the cytosolic protein 14-3-3 epsilon (Ch'ng et al., 2012). 14-3-3 epsilon is only able to bind to phosphorylated CRTC1 from silenced neurons and is unable to bind to dephosphorylated CRTC1 from stimulated neurons (Ch'ng et al., 2012) or to phospho-null CRTC1 (Ch'ng et al., 2015). As such, phosphorylated CRTC1 is tethered to 14-3-3 in the cytoplasm, until activity-dependent dephosphorylation releases CRTC1 from 14-3-3, enabling nuclear translocation.

Following dephosphorylation and release from 14-3-3, CRTC1 undergoes dynein- and microtubule-mediated active transport to the nucleus (Ch'ng et al., 2015). Importantly, the nuclear accumulation of CRTC1 is due to translocation of pre-existing protein and not due to a simple increase in the synthesis of CRTC1 protein, as protein synthesis inhibitors do not prevent the nuclear accumulation of CRTC1 (Li et al., 2009; Ch'ng et al., 2012; Uchida et al., 2017). Live-imaging experiments of fluorescently-tagged CRTC1 further confirmed that CRTC1 is transported from synapses into the nucleus (Ch'ng et al., 2015). CRTC1 contains a nuclear-localization signal (NLS) that, when mutated, prevents the nuclear translocation of CRTC1 (Ch'ng et al., 2015). However, the nuclear import of CRTC1 is not mediated by the canonical importin β1-mediated pathway (Ch'ng et al., 2012). The export of CRTC1 is mediated by the export protein CRM1, as the CRM1 inhibitor Leptomycin B facilitates nuclear accumulation of CRTC1 (Zhou et al., 2006; Kovacs et al., 2007). Inhibition of cAMP-sensitive, salt-inducible

kinases (SIKs) increases the persistence of CRTC1 in the nucleus (Ch'ng et al., 2012), further supporting the idea that only dephosphorylated CRTC1 localizes to the nucleus.

CRTC1 has also been shown to translocate to the nucleus following the induction of long-term potentiation in hippocampal slices. Zhou et al. found that CRTC1 translocates to the nucleus following a 4 x 100 Hz high-frequency stimulation that induces LTP (Zhou et al., 2006) and Ch'ng et al. reported that CRTC1 translocates to the nucleus following theta-burst stimulation or chemical induction of LTP (Ch'ng et al., 2012). CRTC1 also undergoes activity-dependent translocation to the nucleus *in vivo*. Uchida et al. and Parra Damas et al. reported that CRTC1 translocates to the nucleus in the CA1 and CA3 regions of the mouse hippocampus following contextual fear conditioning (Uchida et al., 2017; Parra-Damas et al., 2017), while Nonaka et al. reported that CRTC1 translocates to the nucleus in the amygdala –but not hippocampus– after fear conditioning (Nonaka et al., 2014). Moreover, CRTC1 translocates into the nucleus of hippocampal neurons following pilocarpine-induced seizure in rats (Dubey and Porter, 2016). Taken together, these finding demonstrate that CRTC1 translocates to the nucleus in response to stimuli that produce synaptic plasticity and memory formation.

CRTC1 regulates neuronal activity-dependent gene expression:

CRTC1 is important for the induction of many activity-dependent genes following neuronal stimulation, particularly CREB target genes. In cultured neurons, shRNA knockdown of CRTC1 impairs the activity of CREB following KCl-mediated depolarization, as indicated by reduced luciferase activity from a cAMP response element (CRE) reporter in the presence of CRTC1 shRNA (Li et al., 2009; Nonaka et al., 2014), whereas expression of a constitutively nuclear CRTC1 increases luciferase activity from the CRE reporter (Nonaka et al., 2014). siRNA

knockdown of CRTC1 impairs the activity-dependent induction of specific CREB targets, including *c-fos*, *Arc*, *Egr1*, and *Egr4* in cultured hippocampal neurons (Ch'ng et al., 2012) and shRNA knockdown of CRTC1 impairs the activity-dependent transcription of *c-fos*, *Arc*, *Bdnf*, and *Nr4a1-2* (Parra-Damas et al., 2017). Additionally, CRTC1 shRNA knockdown impairs activity-dependent transcription of *Bdnf* in developing cortical neurons in culture (Fukuchi et al., 2014). While knockdown of CRTC1 impairs activity-dependent gene expression, the expression of a constitutively nuclear CRTC1 enhances gene expression, as indicated by increased c-fos, Arc, and Bdnf protein expression *in vivo* in the mouse hippocampus (Nonaka et al., 2014).

Chromatin immunoprecipitation studies have revealed that CRTC1 is present at the promoters of these activity-dependent genes following neuronal stimulation, supporting the notion that the activity-dependent nuclear translocation of CRTC1 is important for regulating gene expression. In cultured neurons, CRTC1 was enriched at *Arc* and *Bdnf* promoters after stimulation (Nonaka et al., 2014). Additionally, CRTC1 was detected at CRE sites in the promoters for *c-fos* and *Nr4a1-2* after stimulation, whereas the transcription factor CREB was present at these CRE sites irrespective of stimulation (Parra-Damas et al., 2017). Co-immunoprecipitation revealed that CRTC1 was only bound to CREB after neuronal stimulation (Parra-Damas et al., 2017), further supporting the idea that CRTC1 undergoes an activity-dependent translocation into the nucleus to bind to CREB and regulate gene expression. CRTC1 was also detected at the promoters for *c-fos* and *Fgf1b* in mouse hippocampus following contextual fear conditioning and CRTC1 was required for the stimulus-induced expression of *Fgf1b* (Uchida et al., 2017), demonstrating the importance of CRTC1 for activity-dependent gene expression during learning.

While candidate CRTC1-dependent genes have been identified, little work has been done to characterize the entire CRTC1-dependent transcriptome in response to neuronal stimulation. The candidate genes that have been identified are targets of CREB, but it will be important to understand if CRTC1 only regulates CREB targets, or if CRTC1 also regulates targets independent of CREB. There is some evidence that CRTCs can regulate other bZIP transcription factors (Canettieri et al., 2009), and therefore CRTC1 may regulate a distinct set of CREB and non-CREB targets in response to neuronal activity.

CRTC1 regulates synaptic plasticity and memory:

CRTC1 has been demonstrated to be important for long-term potentiation (Zhou et al., 2006; Kovacs et al., 2007; Uchida et al., 2017). To test the role of CRTC1 in LTP, Zhou et al. used a dominant-negative CRTC1 construct to disrupt the function of CRTC1 in the hippocampus. The dominant-negative CRTC1 contains only the CREB-binding domain of CRTC1, so that CRTC1 may bind to CREB but is unable to promote transcription. The authors found that acute hippocampal slices expressing dominant-negative CRTC1 displayed normal induction of LTP, but maintenance was impaired and synaptic strength began to decline to baseline levels at 90 minutes after stimulation (Zhou et al., 2006). This finding is consistent with the role of CRTC1 as a transcriptional regulator, given that transcriptional inhibitors also cause LTP maintenance to decline with similar timing (Nguyen et al., 1994; Nguyen and Kandel, 1997; Chotiner et al., 2003). Kovács et al. similarly disrupted the function of CRTC1 using a dominant-negative construct containing only the CREB-binding domain and nuclear localization signal of CRTC1, and found that hippocampal slices treated with the dominant-negative CRTC1 construct displayed impaired maintenance of LTP beginning at 75 minutes after the stimulation (Kovacs et

al., 2007). In contrast, Uchida et al. found that slices expressing CRTC1 shRNA had impaired *induction* of CRTC1 and that synaptic strength barely increased following stimulation (Uchida et al., 2017). This result is surprising, because the primary function of CRTC1 is as a transcriptional regulator, and yet transcription is not required for LTP until at least one hour after stimulation (Nguyen and Kandel, 1997; Nguyen et al., 1994; Chotiner et al., 2003). In Uchida et al., the shRNA construct was introduced several weeks before the experiment (Uchida et al., 2017), while the dominant-negative constructs were introduced only an hour (Kovacs et al., 2007) or a day (Zhou et al., 2006) before the experiment. It is possible that the longer knockdown of CRTC1 chronically impaired gene expression and led to downstream changes in the expression of proteins that are important during early LTP. While knockdown of CRTC1 impairs LTP, overexpression of full-length CRTC1 can enhance LTP. Zhou et al. found that, in response to a 1 x 100 Hz stimulation that normally only produces brief synaptic potentiation, hippocampal slices with CRTC1 overexpression displayed longer-lasting synaptic potentiation (Zhou et al., 2006). While CRTC1 has been demonstrated to be important for long-term potentiation, it is unclear if CRTC1 is also involved in long-term depression. Preliminary studies from the Martin lab have demonstrated that CRTC1 does translocate to the nucleus in response to stimuli that induce LTD (data not shown), and it will be important to test the role of CRTC1 in LTD.

CRTC1 is also important for long-term memory, specifically, contextual fear memory. When control mice receive electrical shocks in a particular context, the mice display freezing behavior when returned to that context one day later, indicating that a memory of the event and context has been formed (Nonaka et al., 2014). However, when mice injected with CRTC1 shRNA AAV undergo the same paradigm, they display reduced freezing behavior, suggesting

impaired memory formation (Nonaka et al., 2014) The authors found that CRTC1 shRNA AAV injection into the amygdala, but not the hippocampus, impaired contextual fear memory. In contrast, Uchida et al. reported that shRNA knockdown of CRTC1 in the hippocampus also impairs contextual fear memory, as indicated by reduced freezing (Uchida et al., 2017). While knockdown of CRTC1 impairs contextual fear memory, overexpression of CRTC1 enhances the memory. Sekeres et al. overexpressed CRTC1 in the dentate gyrus of the hippocampus, and found that fear memory was enhanced, as indicated by increased freezing specifically in the context in which electrical shocks were delivered (Sekeres et al., 2012). Similarly, expression of constitutively nuclear CRTC1 in the CA1 region of the hippocampus enhanced contextual fear memory (Nonaka et al., 2014) and expression of constitutively nuclear CRTC in the mushroom body of *Drosophila melanogaster* enhanced aversive long-term memory, as indicated by increased avoidance of an odor previously paired with electrical shocks (Hirano et al., 2013). In contrast, expression of a constitutively cytoplasmic CRTC1 mutant did not enhance contextual fear memory (Uchida et al., 2017), further supporting the importance of the activity-dependent nuclear translocation of CRTC1.

Deletion of the *CRTC1* gene results in disruption of energy balance, circadian rhythm, fertility, mood, and social behavior:

In 2008, Altarejos et al. created the first CRTC1 knockout mice (Altarejos et al., 2008) using conventional embryonic stem cell-mediated knock-in to insert a gene trap following exon 4 of the CRTC1 gene, so that a truncated form of the CRTC1 protein would be produced. This truncated CRTC1 protein truncated would only contain the first 147 amino acids of CRTC1, instead of the full 631 amino acids. This region includes the CREB-binding domain and part of

the nuclear translocation domain, but does not include the transactivation domain (Saura and Cardinaux, 2017), and truncated CRTC1 is therefore unlikely to function as a transcriptional co-activator. CRTC1 knockout mice were reported to be hyperphagic, obese, and infertile, due to deficits in the hypothalamus resulting from loss of CRTC1-mediated gene expression (Altarejos et al., 2008).

Concurrently, Breuillaud et al. created CRTC1 knockout mice using the same technique as Altarejos et al. 2008 and also reported that CRTC1 knockout mice develop obesity (Breuillaud et al., 2009), with a large increase in weight in males due to hyperphagia, disrupted circadian activity, and impaired gene expression in the hypothalamus, while females displayed a mild late-onset increase in weight (Rossetti et al., 2017). However, the authors found no fertility deficits in their CRTC1 knockout mice. It is difficult to explain the discrepancy between the two studies given that they used very similar knockout strategies, but it is possible that the authors used slightly different strains of C57BL/6 mice (Breuillaud et al., 2009). Additional studies using this CRTC1 knockout mouse found that loss of CRTC1 resulted in increased aggression, increased depressive-like behaviors, and decreased CREB-mediated gene expression, including decreased expression of *Bdnf*, *Nr4a1-3,* and *c-fos* (Breuillaud et al., 2009). Deletion of the single CRTC homologue in *Drosophila melanogaster* produced phenotypes similar to those found in CRTC1 knockout mice, including altered energy balance including reduced glycogen and lipid stores (Wang et al., 2008) and disruptions to the circadian clock (Kim et al., 2016).

Given that loss of the CRTC1 gene produces such widespread impairments, we were concerned that these phenotypes would complicate studies of synaptic plasticity and gene expression in CRTC1 knockout mice. To minimize the developmental effects of deleting CRTC1

as well as the effects of deleting CRTC1 in other brain regions, we sought to create CRTC1 conditional knockout mice, so that CRTC1 could be deleted in a precise spatiotemporal manner.

RESULTS

Generation of CRTC1 conditional knockout and CRTC1 null mice using CRISPR/Cas9 genome editing:

As a strategy for creating CRTC1 conditional knockout mice, we flanked exon 6 of the *CRTC1* gene with LoxP sites, so that the Cre/Lox conditional knockout approach could be implemented. Deletion of exon 6 would produce a frameshift mutation and premature stop codon, triggering nonsense-mediated decay of the mRNA transcript (Hug et al., 2016). We collaborated with the Janelia Research Campus Gene Targeting & Transgenic Facility to create CRTC1 conditional knockout mice using CRISPR/Cas9 genome editing. We designed two sgRNAs targeting before and after exon 6 and a donor vector containing the genomic region of exon 6 with two LoxP sites flanking the exon (**Table 4.1**). The sgRNAs, Cas9, and donor vector were microinjected into C57BL/6J zygotes. The resulting pups were genotyped after birth, and many of the pups had successful insertion of the LoxP sites. Additionally, some of the other pups had a permanent deletion of exon 6. Deletion of the targeted region is an expected outcome, as non-homologous end joining occurs more easily than homology-directed repair (Hsu et al., 2014). Six mice with CRTC1 exon 6 floxed alleles and five mice with CRTC1 exon 6 deletion alleles were shipped from Janelia Research Campus to UCLA. Each founder was bred with a wildtype C57BL/6J mate, and the resulting pups were genotyped to test for germline transmission of the CRTC1 floxed or knockout allele. Potential CRTC1 floxed mice were genotyped using primers 1-2 and 3-4 to test for presence of the two LoxP sites (**Table 4.1**), while

potential CRTC1 knockout mice were genotyped using primers 1 and 4 to test for deletion of exon 6 (**Table 4.1**). Initial genotyping results were also sequenced to confirm the expected CRTC1 alleles (**Table 4.2**). We established three CRTC1 knockout lines (KO1, KO2, and KO3) and three CRTC1 floxed lines (Mut1, Mut2, and Mut3). Each line was bred to produce homozygous mice. Sperm from the KO2, KO3, Mut1, and Mut2 lines were cryopreserved at Charles River Laboratories (Wilmington, MA).

CRTC1 knockout mice display complete loss of CRTC1 protein

We first characterized the CRTC1 knockout mice, to confirm that deletion of exon 6 disrupted CRTC1 expression. By western blot, CRTC1 protein was completely absent in hippocampal lysates from CRTC1 knockout mice, as detected by both C-terminal and N-terminal antibodies (**Fig 4.1A**). Similarly, CRTC1 was not detected in the hippocampus using immunohistochemistry (**Fig 4.1B**). We also characterized the expression of *CRTC1*, *CRTC2*, and *CRTC3* mRNA using qPCR. *CRTC1* mRNA was reduced by 80%, while *CRTC2* and *CRTC3* mRNA remained unchanged (**Fig 4.1C**), indicating that CRTC2/3 are not upregulated to compensate for loss of CRTC1. It has previously been reported that CRTC1 null mice develop obesity (Altarejos et al., 2008; Breuillaud et al., 2009; Rossetti et al., 2017). At four months old, our male CRTC1 knockout mice weighed on average 7 grams more than littermate controls (**Fig 4.1D**). Conflicting reports have found CRTC1 null mice to be infertile (Altarejos et al., 2008) or fertile (Breuillaud et al., 2009). We were able to successfully breed our CRTC1 knockout mice, although many of the breeding pairs never produced pups. Therefore, multiple breeding pairs were needed to maintain the line.

Previous studies have reported impaired maintenance of long-term potentiation (LTP) in the hippocampus of mice expressing dominant-negative CRTC1 constructs (Zhou et al., 2006; Kovacs et al., 2007) and impaired induction and maintenance of LTP after shRNA knockdown of CRTC1 (Uchida et al., 2017). In preliminary tests, we found that CRTC1 knockout mice display normal LTP for 4 hours after stimulation (data not shown).

CRTC1 conditional knockout mice display incomplete loss of CRTC1 protein

To confirm that the placement of the LoxP sites did not disrupt the expression of CRTC1, we first tested the expression of CRTC1 in floxed mice in the absence of Cre. CRTC1 floxed mice displayed similar levels of expression of CRTC1 as wildtype controls (**Fig 4.2A**). To conditionally delete CRTC1 from mature excitatory neurons, we used the T29 Camk2a-Cre strain (Tsien et al., 1996a). Our lab had previously found that Camk2a-Cre was expressed in ~95% of pyramidal neurons in the CA1 region of the hippocampus in this mouse strain (Chen et al., 2017). We crossed the CRTC1 floxed mice to the Camk2a-Cre mice to produce conditional knockout mice (Camk2a-Cre $CRTC1^{flox}/CRTC1^{flox}$) and Cre-negative littermate controls ($CRTC1^{flox}/CRTC1^{flox}$). We found that CRTC1 was only reduced by ~50% by western blot of hippocampal lysates (**Fig 4.2B**). Moreover, we still detected CRTC1 expression in most of the pyramidal neurons in CA1 using immunohistochemistry (**Fig 4.2C**). We suspected that the Camk2a-Cre line was inefficient at producing conditional knockout.

To achieve better knockout efficiency, we crossed the CRTC1 floxed mice to a different Cre line. We selected the Vglut2-Cre strain (Vong et al., 2011) because it had been previously reported to produce efficient conditional knockout (Meng et al., 2016). We crossed the Vglut2-Cre mice to mice with a floxed HA transgene (**Gay 2013**) and found that HA was expressed in

the pyramidal neurons in CA1 (**Fig 4.2D**). We then crossed the CRTC1 floxed mice to the Vglut2-Cre mice to produce conditional knockout mice (Vglut2-Cre $CRTC1^{flox}/CRTC1^{flox}$) and littermate controls ($CRTC1^{flox}/CRTC1^{flox}$). We found that CRTC1 was reduced by ~85% by western blot of hippocampal lysates (**Fig 4.2E**). Although knockout efficiency was improved using this Cre line, many pyramidal neurons in CA1 still expressed CRTC1, as detected by immunohistochemistry (**Fig 4.2F**).

In an attempt to further improve the knockout efficiency, we bred conditional knockout mice on a hemi-null CRTC1 knockout background, so that only one allele would need to be conditionally deleted instead of both. We bred Vglut2-Cre $CRTC1^{flox}/CRTC1^{flox}$ mice to $CRTC1^{KO}/CRTC1^{KO}$ mice. We generated hemi-null conditional knockout mice (Vglut2-Cre $CRTC1^{flox}/CRTC1^{KO}$), hemi-null littermate controls ($CRTC1^{flox}/CRTC1^{KO}$), and also compared to non-littermate controls ($CRTC1^{flox}/CRTC1^{flox}$). By western blot, the hemi-null conditional knockout mice had an ~85% decrease in CRTC1 protein expression compared to hemi-null littermate controls, while the hemi-null littermate controls had a ~50% decrease in CRTC1 protein expression compared to the control mice (**Fig 4.2G**). The knockout efficiency by immunohistochemistry was difficult to assess, as both the hemi-null conditional knockout mice and hemi-null littermate controls had extremely dim CRTC1 signal compared to the control mice, as detected by immunohistochemistry (**Fig 4.2H**).

DISCUSSION

To study the function of CRTC1 in long-term synaptic plasticity, activity-dependent gene expression, and memory, we generated CRTC1 knockout and conditional knockout mice. CRISPR/Cas9 genome editing proved to be a rapid method for generating floxed and knockout

mice, avoiding the need for lengthy procedures associated with embryonic stem cell-mediated knock-in, such as selection of ES cells or additional breeding due to chimeric mice (Burgio, 2018). In the span of three months, the CRISPR sgRNA and donor vector constructs were created, mouse zygotes were microinjected with the constructs, and the resulting mouse pups were genotyped to confirm successful creation of CRTC1 knockout and floxed alleles. CRISPR/Cas9 genome editing was highly efficient, as there were many mice created with CRTC1 floxed or CRTC1 knockout alleles from a single session of zygote microinjections. It has been reported that CRISPR/Cas9 genome editing strongly favors non-homologous end joining (NHEJ) over homology-directed repair (HDR) (Hsu et al., 2014), but fortunately, our injections produced a high number of both CRTC1 floxed mice (HDR) and CRTC1 knockout mice (NHEJ). Notably, our strategy inserted both LoxP sites simultaneously using one large donor vector containing a floxed exon 6, instead of separately inserting each LoxP site using two different single-stranded oligo donors (ssODNs). Interestingly, before successfully targeting exon 6, we had previously attempted to target exon 4 and were only able to produce knockout mice. The genomic region surrounding exon 6 might be more amenable to HDR than the region surrounding exon 4, as the efficiency of HDR is known to be dependent on the local chromatin structure (Janssen et al., 2019). One potential pitfall when creating knock-in and knockout mice is that there may not be germline transmission of the modified allele, if the editing occurs after cell division and the modified allele is not present in all cells (Mehravar et al., 2019). However, all of the CRTC1 floxed mice and CRTC1 knockout mice that we bred had successful transmission the modified allele to their offspring.

Upon obtaining homozygous CRTC1 knockout mice, we confirmed that the strategy of deleting exon 6 produced mice with complete loss of CRTC1 protein. Importantly, we confirmed

the loss of CRTC1 using an N-terminal antibody, to rule out the possibility that deletion of exon 6 created a truncated form of the CRTC1 protein instead of triggering nonsense-mediated decay of the *CRTC1* mRNA (Hug et al., 2016). Similar to what has been reported in the literature with CRTC1 exon 4 knockout mice, we found that exon 6 knockout mice were obese at 4 months old (Altarejos et al., 2008; Rossetti et al., 2017). Previous reports on the fertility of CRTC1 knockout mice have given conflicting results with Altarejos et al. reporting that CRTC1 knockout mice are infertile and Breuillard et al. reporting that CRTC1 knockout mice have completely normal fertility. Our finding was intermediate; we were able to breed the CRTC1 knockout mouse line, but many of the breeding pairs never produced pups. In preliminary tests, we also found that CRTC1 knockout mice displayed normal induction and maintenance of LTP for 4 hrs after stimulation, which is in contrast to previous reports that found impaired LTP using dominant-negative and shRNA constructs for CRTC1 (Zhou et al., 2006; Kovacs et al., 2007; Uchida et al., 2017). In these studies, the disruption of CRTC1 occurs on the order of hours (Kovacs et al., 2007), days (Zhou et al., 2006), or weeks (Uchida et al., 2017) before testing LTP, whereas in our study, CRTC1 is absent throughout the development and lifetime of the mouse. It is possible that there is developmental compensation for the loss of CRTC1, and that an acute loss of CRTC1 would be more informative when studying LTP. This underscores the need for Cre/LoxP conditional knockout mice for CRTC1, where Cre can be delivered at later timepoints using a promoter for mature neurons (such as Camk2a) or delivered days or weeks before the experiment using AAV injection.

When conditionally deleting floxed CRTC1 using the Camk2a-Cre mouse line, we detected only modest reduction of CRTC1 protein. This was a surprising result, as we had previously found this line to produce LoxP recombination in ~95% of CA1 pyramidal neurons

when crossed to mice with a conditional HA tag on the 60S ribosomal protein L22 (Chen et al., 2017). However, it may be more difficult to achieve efficient conditional knockout than conditional knock-in, as knock-in requires recombination in only one allele to detect the tagged protein, whereas recombination must occur in both alleles to achieve total knockout in the cell. Indeed, many studies that used the T29 Camk2a-Cre mice to conditionally delete genes had incomplete knockout of the target, especially as detected by immunohistochemistry (Stein et al., 2014; Jung et al., 2016; Lin et al., 2015; Barbarese et al., 2013). We next crossed the CRTC1 floxed mice to a Vglut2-Cre mouse line, as it had been previously reported to produced efficient conditional knockout (Meng et al., 2016). Vglut2-Cre is highly expressed in embryonic and early postnatal stages of development, whereas Camk2a-Cre is only expressed in mature, post-mitotic neurons (Tsien et al., 1996a). Chromatin accessibility changes during brain development (Trevino et al., 2020; de la Torre-Ubieta et al., 2018), and it is possible that LoxP recombination may occur more efficiently in certain chromatin states during development. Our CRTC1 knockout efficiency was improved with this Vglut2-Cre line, although many pyramidal neurons in the hippocampus still expressed CRTC1. In contrast, the Vglut2-Cre line has been reported to produce complete knockout of MeCP2 in Meng et al 2016. However, in that study the conditionally deleted allele was on the X chromosome and only male mice were used, meaning that LoxP recombination only needed to occur on one allele per cell to achieve complete knockout. To create a similar situation with our conditional knockout mice, we bred the Vglut2-Cre x CRTC1 floxed mice on a hemi-null background, to produce mice with one CRTC1 floxed allele and one CRTC1 knockout allele. This breeding strategy produced a similar knockout efficiency than that of the regular Cre/Lox breeding strategy.

One possible explanation for our difficulty in achieving high conditional knockout efficiency is that CRTC1 exon 6 is in a region of the genome that is particularly resistant to LoxP recombination due to the chromatin structure. Previous studies have reported that LoxP recombination efficiency is dependent on the position in the genome (Vooijs et al., 2001). However, LoxP recombination efficiency was improved when using the Vglut2-Cre line compared to the Camk2a-Cre line, suggesting that different expression and amount of Cre might be able to improve knockout efficiency. Viral delivery of Cre may be important for improving this knockout efficiency further, as viral Cre delivery can produce LoxP recombination with high efficiency (Kaspar et al., 2002; Ahmed et al., 2004). Additionally, viral delivery of Cre would allow for precise temporal deletion of CRTC1. Acute deletion of CRTC1 is of particular importance for our study, given that our CRTC1 null mice displayed normal LTP, whereas previous studies using short-term knockdown of CRTC1 found impaired LTP (Zhou et al., 2006; Kovacs et al., 2007; Uchida et al., 2017). Therefore, in future studies, acute deletion of CRTC1 using viral delivery might improve knockout efficiency and also enable us to observe CRTC1-mediated deficits in synaptic plasticity.

METHODS

Animals:

All experiments were performed using approaches approved by the UCLA Animal Research Committee. CRTC1 knockout and floxed mice were generated at Janelia Research Campus Gene Targeting & Transgenic Facility. Camk2a-Cre (stock #005359), Vglut2-Cre (stock #28863), and floxed UPRT-HA (stock #021469) mice were purchased from Jackson Laboratory. Female Camk2a-Cre mice were bred with male CRTC1 floxed mice, given that Camk2a-Cre is

expressed in testis and can cause germline recombination of the floxed allele (Kobayashi and Hensch, 2013). Male Vglut2-Cre mice were bred with female CRTC1 floxed mice, similar to previous studies (Meng et al., 2016).

Genotyping:

Tail biopsies were performed on postnatal day 7 mouse pups. DNA was extracted by boiling the biopsies in lysis buffer (25 mM NaOH, 0.2 mM ETDA) for 1 hr, neutralizing the samples with 40 mM Tris HCl, briefly vortexing the samples, centrifuging the samples at 2,000*g* for 3 minutes, and transferring the supernatant to a fresh tube. PCR was performed using Quick-Load Taq 2x Master Mix (New England Biolabs) according to manufacturer's instructions. To genotype CRTC1 knockout mice, primers 1 and 4 (**Table 4.1**) were used to test for a ~600 bp wildtype band or a ~300 bp band indicating deletion of exon 6. Heterozygous and homozygous CRTC1 knockout mice were difficult to distinguish using only this test, as the smaller knockout band amplified more readily than the longer wildtype band. To distinguish between heterozygous and homozygous CRTC1 knockout mice, primers 3-4 (**Table 4.1**) were used to test for any presence of exon 6. To genotype CRTC1 floxed mice, primers 1-2 and 3-4 (**Table 4.1**) were used to amplify the region containing each LoxP site, to test for the ~200 bp wildtype band or a longer ~300 bp band indicating the presence of a LoxP site. When genotyping the Cre x CRTC1 floxed line, primers 1 and 4 (**Table 4.1**) were used to confirm that both LoxP sites were intact as indicated by a ~800 bp band, and there was no germline recombination of the LoxP sites, as indicated by a ~300 bp band.

Isolation of hippocampal tissue:

8-12 week-old male and female mice were anaesthetized with isofluorane and sacrificed by cervical dislocation. Brains were dissected in cold, oxygenated artificial cerebrospinal fluid (ACSF: 124 mM NaCl, 4 mM KCl, 25 mM $NaHCO_3$, 1 mM NaH_2PO_4, 2 mM $CaCl_2$, 1.2 mM $MgSO_4$, and 10 mM glucose) to isolate the hippocampus, which was cut into 400 µm thick slices.

Protein extraction and western blot:

Hippocampal tissue was homogenized in RIPA buffer (50 mM Tris, 150 mM NaCl, 0.1% SDS, 0.5% sodium deoxycholate, 1% Triton X-100, pH 7.5), centrifuged at 10,000*g* for 10 min, and transferred to a fresh tube. Protein concentration was determined using the Pierce BCA Protein Assay Kit (Thermo Fisher). Protein lysates were boiled in loading buffer (10% glycerol, 1% SDS, 60 mM Tris HCl pH 7.0, 0.1 M DTT, 0.02% bromophenol blue) for 10 min at 95°C and 20 µg lysate per sample was run on at 8% polyacrylamide gel. Samples were wet-transferred onto a 0.2 µm nitrocellulose membrane. The membrane blocked with Odyssey Blocking Buffer (Licor) and incubated with primary antibodies: rabbit CRTC1 (Bethyl, C-term, 1:1000), rabbit CRTC1 (Rockland, N-term, 1:1000), and mouse TUJ1 (BioLegend, 1:1000). The membrane was washed with TBST and incubated with secondary antibodies: anti-rabbit IRDye 800CW (1:10,000) and anti-mouse IRDye 680CW (1:10,000). The membrane was imaged using the Odyssey Infrared imaging system (LI-COR).

Immunohistochemistry:

Hippocampal tissue was fixed in 4% paraformaldehyde in PBS for several hours at room temperature or overnight at 4°C. Samples were washed in PBS and covered in HistoGel (VWR).

Samples were serially dehydrated, cleared with xylene, embedded in paraffin, sectioned in 5 µm thick slices, and mounted on glass slides. Before staining the samples, paraffin was melted from the tissue and samples were cleared with xylene and serially re-hydrated. Antigen retrieval was performed by boiling samples in a pressure cooker in retrieval solution (8.2 mM sodium citrate, 1.8 mM citric acid). Samples were permeabilized with 0.1% Triton X-100 in PBS for 30 minutes and blocked in 10% goat serum in PBS for 1 hour. Samples were incubated with the following primary antibodies at 4°C overnight: rabbit CRTC1 (Bethyl, 1:500), mouse HA (BioLegend, 1:500), chicken Map2 (PhosphoSolutions, 1:500). Samples were washed with PBS and incubated at 1:1000 with the following secondary antibodies for 1 hour at room temperature: anti-rabbit Alexa Fluor 555, anti-mouse Alexa Fluor 555, anti-chicken Alexa Fluor 488, and Hoechst 33342 stain. Samples were washed with PBS and mounted with Aqua-Poly/Mount (Polysciences) and glass coverslips (Carolina Biologicals). Samples were imaged using a Zeiss LSM 700 confocal microscope with a 40x oil objective and 405 nm, 488 nm, 555 nm, and 639 nm lasers. Identical image acquisition settings were used for all images within an experiment.

RNA extraction, cDNA synthesis, and quantitative RT-PCR:

To extract RNA, mouse cortex was homogenized in TRIzol Reagent (Thermo Fisher), centrifuged at 12,000*g* for 5 minutes at 4°C, and supernatant was transferred to a fresh tube. Each 1 mL sample was mixed with 0.2 mL chloroform, centrifuged at 12,000*g* for 15 minutes at room temperature, and supernatant was transferred to a fresh tube. RNA was precipitated using 0.5 mL isopropanol per sample. Samples were centrifuged at 12,000*g* for 10 minutes at 4°C and the supernatant was discarded. Pellets were washed in 75% ethanol, dried, and re-suspended in RNase-free water

cDNA was synthesized from 50 ng RNA using Superscript III First Strand Synthesis (Thermo Fisher) with random hexamer primers according to manufacturer's instructions. A "No Reverse Transcriptase" sample was also prepared to serve as a negative control during qPCR experiments.

RT-qPCR was performed using SYBR Green PCR Master Mix (Applied Biosystems) and CFX Connect Real-Time System (Bio-Rad) according to manufacturer's instructions. CRTC qPCR primers were selected from PrimerBank (http://pga.mgh.harvard.edu/primerbank). Primer sequences were as follows: CRTC1 F (5' – TGCCCAACGTGAACCAGATT – 3'), CRTC1 R (5' – CCCATGATGTCGTGTGGTCC – 3'), CRTC2 F (5' – ATGAACCCTAACCCCCAAGAC – 3'), CRTC2 R (5' – CGTTCTCCTCAATAGCAGGGA – 3'), CRTC3 F (5' – GCGCCTTACCCAGTACCAC – 3'), CRTC3 R (5' – ATCGGCTTGATGAAGTGATGG – 3'), and loading control HPRT F (5' – TGTTGTTGGATATGCCCTTG – 3'), HPRT R (5' – GGCCACAGGACTAGAACACC – 3'). qPCR was performed on three biological replicates, with technical triplicate reactions for each sample. Cycle threshold (*Ct*) values were converted from logarithmic scale [2^(-*Ct*)] and CRTC values were normalized to the HPRT loading control. All values were then normalized to the median value of the control condition. CRTC values were compared between the control and CRTC1 KO conditions.

FIGURE LEGENDS

Figure 4.1 CRTC1 knockout mice display complete loss of CRTC1 protein.

A) Western blot of hippocampal lysates from control and CRTC1 KO mice.

B) Immunohistochemistry from CA1 region of the hippocampus in control and CRTC1 KO mice. Scale bar = 40 μm.

C) Quantitative RT-PCR of *CRTC1*, *CRTC2*, and *CRTC3* mRNA normalized to *HPRT* mRNA, from cortical lysates from control and CRTC1 KO mice.

D) Total body weight of male CRTC1 KO mice and male littermate control siblings at four months of age. ** indicates $p < 0.001$ from Mann Whitney test. N = 5 mice per genotype. Median weights: control mice = 29.1 g and knockout mice = 38.1g.

Figure 4.2 CRTC1 conditional knockout mice display incomplete loss of CRTC1 protein.

A) Western blot of hippocampal lysates from control and CRTC1 floxed mice.

B) Western blot of hippocampal lysates from control CRTC1 floxed mice and Camk2a-Cre CRTC1 floxed mice.

C) Immunohistochemistry from CA1 region of the hippocampus in control CRTC1 floxed mice and Camk2a-Cre CRTC1 floxed mice. Scale bar = 40 μm.

D) Immunohistochemistry from CA1 region of the hippocampus in control and Vglut2-Cre UPRT-HA floxed mice. Scale bar = 40 μm.

E) Western blot of hippocampal lysates from control CRTC1 floxed mice and Vglut2-Cre CRTC1 floxed mice.

F) Immunohistochemistry from CA1 region of the hippocampus in control CRTC1 floxed mice and Vglut2-Cre CRTC1 floxed mice. Scale bar = 40 μm.

G) Western blot of hippocampal lysates from control CRTC1 floxed mice, control CRTC1 floxed/KO mice, and Vglut2-Cre CRTC1 floxed/KO mice.

H) Immunohistochemistry from CA1 region of the hippocampus in control CRTC1 floxed mice, control CRTC1 floxed/KO mice, and Vglut2-Cre CRTC1 floxed/KO mice. Scale bar = 40 μm.

Table 4.1

sgRNA and primers sequences for creation and genotyping of CRTC1 mice.

Table 4.2

CRTC1 wildtype, knockout, and conditional knockout alleles.

Figure 4.1

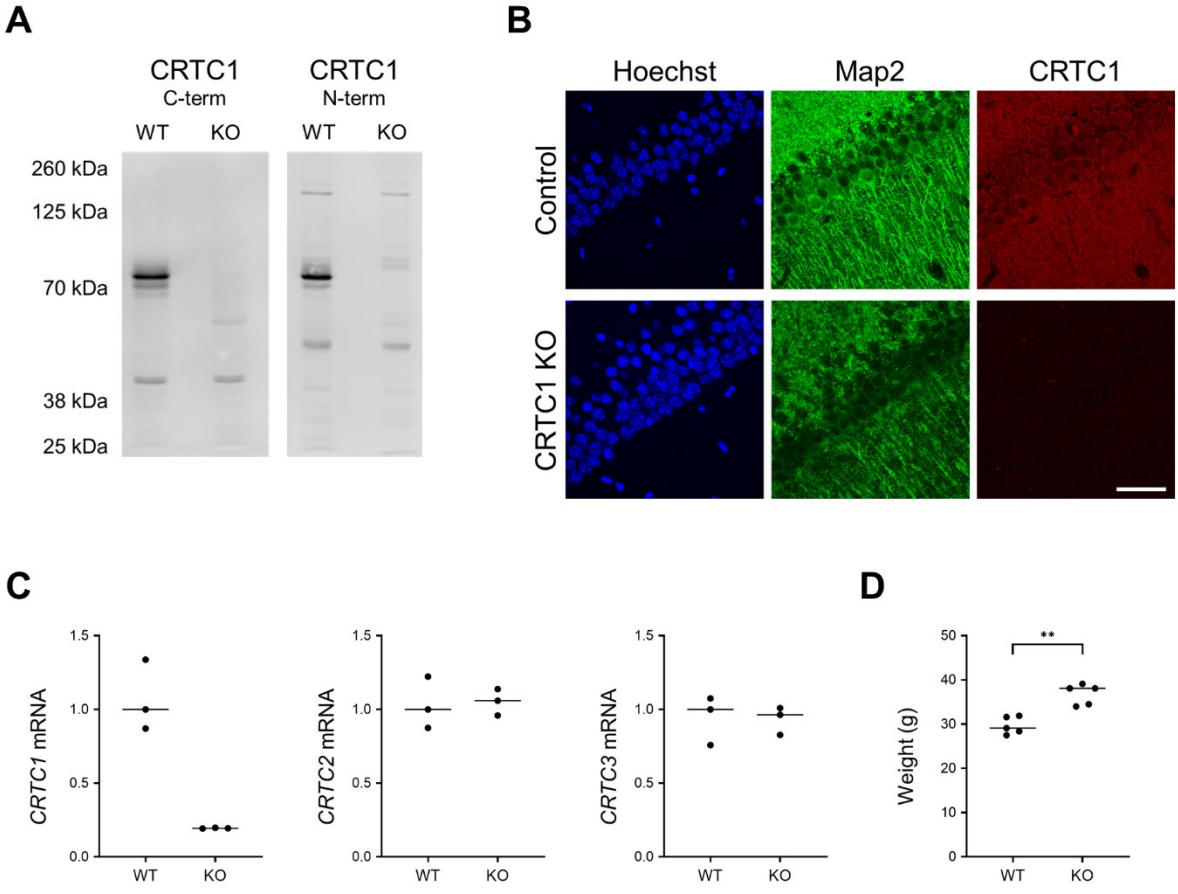
A
CRTC1
C-term
CRTC1
N-term
WT
KO
WT
KO
260 kDa
125 kDa
70 kDa
38 kDa
25 kDa
B
Hoechst
Map2
CRTC1
Control
CRTC1 KO
C
CRTC1 mRNA
CRTC2 mRNA
CRTC3 mRNA
1.5
1.0
0.5
0.0
WT
KO
D
Weight (g)
50
40
30
20
10
0
**
WT
KO

Figure 4.2

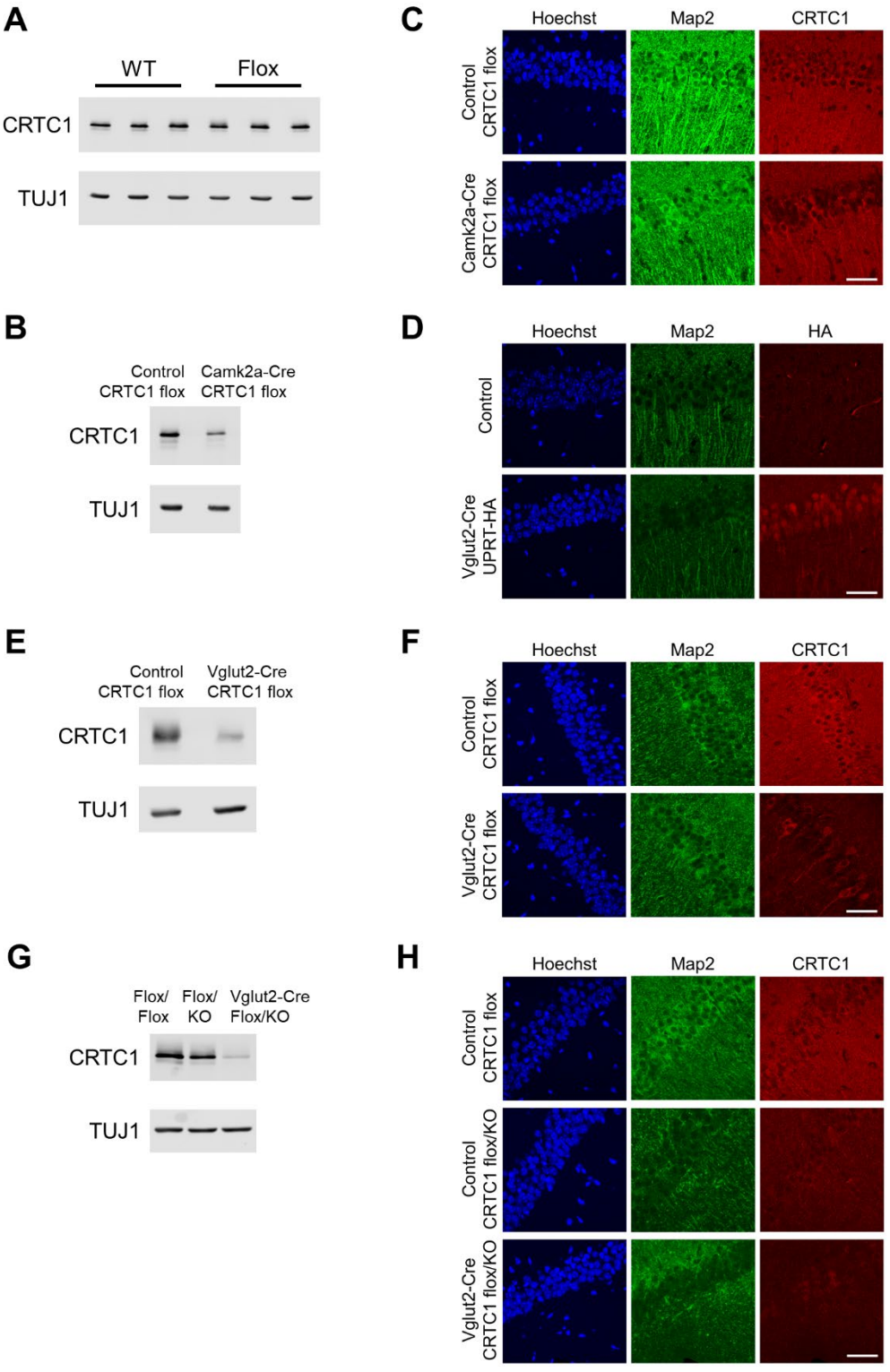
A
WT
Flox
CRTC1
TUJ1
B
Control CRTC1 flox
Camk2a-Cre CRTC1 flox
CRTC1
TUJ1
C
Hoechst
Map2
CRTC1
Control CRTC1 flox
Camk2a-Cre CRTC1 flox
D
Hoechst
Map2
HA
Control
Vglut2-Cre UPRT-HA
E
Control CRTC1 flox
Vglut2-Cre CRTC1 flox
CRTC1
TUJ1
F
Hoechst
Map2
CRTC1
Control CRTC1 flox
Vglut2-Cre CRTC1 flox
G
Flox/ Flox
Flox/ KO
Vglut2-Cre Flox/KO
CRTC1
TUJ1
H
Hoechst
Map2
CRTC1
Control CRTC1 flox
Control CRTC1 flox/KO
Vglut2-Cre CRTC1 flox/KO

Table 4.1

Name	**Sequence (5’ -> 3’)**
sgRNA 1: Pre-exon6	AGGATCATCAGTTGGCTATG
sgRNA 2: Post-exon6	CCAGGAATCACGTTGAGGTG
Primer 1: CRTC1 Lox1 F	TGCCAGCAATGCTGAGTGAT
Primer 2: CRTC1 Lox1 R	CTTGGAGGTTCTACTGAAGC
Primer 3: CRTC1 Lox2 F	CCTTTCTAAGCAGTCATGGG
Primer 4: CRTC1 Lox2 R	AGTGTCTGCTCTCATCAGCA
Primer 5: Cre F	GCATTACCGGTCGATGCAACGAGTG
Primer 6: Cre R	GAACGCTAGAGCCTGTTTTGCACGTTC

Table 4.2

Genotype	Sequence (5' -> 3')
Wildtype CRTC1 Blue = Exon6 Green = sgRNA site Orange = PAM sites	TGCCAGCAATGCTGAGTGATGGCAGATGATGGCAGGTGGCAG GCTCAGAGTCTCTGCTGACTTGTACAGCCAAGGTGCCCAGGGT CCCGGCCTGGGTGGGGGCCGGGGGGTACCCTGCTCAGCCTTGG CTCCCCACTCCAGCTGCTGTCTCAGCTCTTTGCTCCACATAGCC AACTGATGATCCTGGTGCAGGGTGTTCTTGTTAAGCCCCTCCCA CAGCTTCAGTAGAACCTCCAAGCCTGCTGTTAGGGCCCTGCGG TCTCTCTACTGTGTGGTCATGTCGCCCTGACCCTTCTCTCCCCCT ACATCCAGTCTTACTGCTAACTGTCCCAGGAATGGAGGACACC GGGGCTGAGACAGACAAGACCCTTTCTAAGCAGTCATGGGACT CAAAGAAGGTAAGGGCCACCGTGTGGGCCAACTGTTTCTTTTC ACACCCAGCCTGGAAGCAAACGACCAGGAATCACGTTGAGGT GAGGGCCTTGCTCAGCTTTACTGGGGCCCAGGCTTTGGCATCA ACAGCGGGCCTGTCAGACTGCCCAGAAACAGCTCAAAGTGTTA ACACGTGTGGCCGATCAGGGTGCTGATGAGAGCAGACACT
Knockout CRTC1	TGCCAGCAATGCTGAGTGATGGCAGATGATGGCAGGTGGCAG GCTCAGAGTCTCTGCTGACTTGTACAGCCAAGGTGCCCAGGGT CCCGGCCTGGGTGGGGGCCGGGGGGTACCCTGCTCAGCCTTGG CTCCCCACTCCAGCTGCTGTCTCAGCTCCTTGCTCAGCTTTACT GGGGCCCAGGCTTTGGCATCAACAGCGGGCCTGTCAGACTGCC CAGAAACAGCTCAAAGTGTTAACACGTGTGGCCGATCAGGGTG CTGATGAGAGCAGACACT
Floxed CRTC1 (no Cre) Blue = Exon6 Green = sgRNA site Orange = PAM sites Purple = LoxP sites Red = Additional new sequence	TGCCAGCAATGCTGAGTGATGGCAGATGATGGCAGGTGGCAG GCTCAGAGTCTCTGCTGACTTGTACAGCCAAGGTGCCCAGGGT CCCGGCCTGGGTGGGGGCCGGGGGGTACCCTGCTCAGCCTTGG CTCCCCACTCCAGCTGCTGTCTCAGCTCTTTGCTCCACAGAATT CCTAATATAACTTCGTATAATGTATGCTATACGAAGTTATTAAT GCAGCCAATTGCGATGATCTCGAGCATATGCAACTGATGATCC TGGTGCAGGGTGTTCTTGTTAAGCCCCTCCCACAGCTTCAGTAG AACCTCCAAGCCTGCTGTTAGGGCCCTGCGGTCTCTCTACTGTG TGGTCATGTCGCCCTGACCCTTCTCTCCCCCTACATCCAGTCTT ACTGCTAACTGTCCCAGGAATGGAGGACACCGGGGCTGAGAC AGACAAGACCCTTTCTAAGCAGTCATGGGACTCAAAGAAGGTA AGGGCCACCGTGTGGGCCAACTGTTTCTTTTCACACCCAGCCT GGAAGCAAACGACCAGGAATCACGTTGACATATGACCGGTGA TATTCCGAAGTTCCTATTCTCTAGAAAGTATAGGAACTTCATCA GTCAGGTACATAATATAACTTCGTATAATGTATGCTATACGAA GTTATTAGGTGGATCCAGGGCCTTGCTCAGCTTTACTGGGGCC CAGGCTTTGGCATCAACAGCGGGCCTGTCAGACTGCCCAGAAA CAGCTCAAAGTGTTAACACGTGTGGCCGATCAGGGTGCTGATG AGAGCAGACACT
Floxed CRTC1 (w/ Cre) Green = sgRNA site Orange = PAM sites Purple = LoxP sites Red = Additional new sequence	TGCCAGCAATGCTGAGTGATGGCAGATGATGGCAGGTGGCAG GCTCAGAGTCTCTGCTGACTTGTACAGCCAAGGTGCCCAGGGT CCCGGCCTGGGTGGGGGCCGGGGGGTACCCTGCTCAGCCTTGG CTCCCCACTCCAGCTGCTGTCTCAGCTCTTTGCTCCACAGAATT CCTAATATAACTTCGTATAATGTATGCTATACGAAGTTATTAGG TGGATCCAGGGCCTTGCTCAGCTTTACTGGGGCCCAGGCTTTG GCATCAACAGCGGGCCTGTCAGACTGCCCAGAAACAGCTCAA AGTGTTAACACGTGTGGCCGATCAGGGTGCTGATGAGAGCAGA CACT

Chapter 5: Concluding Remarks

Neuronal activity-dependent transcription is critical to the development and plasticity of synapses in the brain. To better understand how neuronal stimulation regulates transcription, we examined the cell biological mechanisms linking stimulation at neuronal synapses with transcriptional regulation in the nucleus. Neuronal stimulation activates a variety of proteins and signaling pathways at the synapse, which can then be relayed to the cell soma and nucleus to alter the nuclear proteome and trigger changes in transcription. The products of gene expression in turn function to alter the strength and number of connections between neurons.

Advances in next-generation sequencing technologies have enabled the identification of many genes that are up- or down-regulated following plasticity-inducing stimuli (Wu et al., 2017; Kim et al., 2010; Tyssowski et al., 2018). Less, however, is known about the cell biological mechanisms by which synaptic stimuli are coupled with transcriptional regulation. In part, this is due to limitations in biochemical screening technologies that identify activity-dependent proteomic changes at the level of specific subcellular compartments within neurons. Proximity-ligation approaches overcome this limitation by labeling proteins within specific subcellular compartments in a manner that can be detected by mass spectrometry, thereby achieving spatially resolved proteomic mapping (Hung et al., 2016). To ask whether and how synaptic stimulation changed the nuclear proteome, we coupled the APEX2 peroxidase to nuclear localization signals to restrict its localization to in the nucleus of with neurons and conducted mass spectrometry to characterize the nuclear proteome of silenced and stimulated neurons (**Chapter 2**).

We used a stimulation protocol we had previously shown triggers changes in the nuclear localization of the transcriptional co-regulator CRTC1 (Ch'ng et al., 2012) (**Chapter 4**)-silencing cultured forebrain neurons for 1 hour with tetrodotoxin (driving cytoplasmic localization of CRTC1) and stimulating cultured forebrain neurons for 1 hour with bicuculline (driving nuclear localization of CRTC1). Perhaps not surprisingly, since the parameters for our screen were selected based on activity-dependent changes in the nucleocytoplasmic ratio of CRTC1, the protein identified that underwent the largest increase in nuclear concentration in bicuculline-stimulated neurons was CRTC1. The proteins that underwent the largest increase in nuclear concentration in tetrodotoxin-silenced neurons, HDAC4 and HDAC5, have also previously been reported to undergo nuclear export following bicuculline-stimulation (Schlumm et al., 2013). In fact, the total number of proteins that underwent activity-dependent changes in their nuclear localization was smaller than we anticipated. While this could be due to technical limitations in the detection of proteins undergoing relatively small changes in subcellular localization, it is also possible that a limited number of proteins are altered by distinct stimuli.

The goal of an unbiased screen is to detect novel proteins and novel mechanisms, and our screen identified a few dozen proteins that were not previously known to undergo changes in nuclear localization following plasticity-inducing stimuli. We focused on one of the proteins that underwent an activity-dependent decrease in nuclear concentration following neuronal stimulation, the tumor suppressor protein PDCD4. In investigating the activity-dependent regulation of PDCD4 in neurons, we discovered an unanticipated role for proteasome-mediated degradation of PDCD4 in regulating transcription (**Chapter 3**). This body of work thus not only demonstrates the variety of proteins that undergo increases or decreases in nuclear concentration

in response to neuronal stimulation, but also highlights the variety of cell biological mechanisms by which stimuli can trigger changes in the proteome of subcellular compartments.

The studies described in **Chapter 3** indicate a role for PDCD4 as a transcriptional repressor of synaptic genes, in which PDCD4 serves as a brake on transcription that is removed after stimulation in order to facilitate activity-dependent expression of these genes. However, many questions remain regarding the specific mechanism by which PDCD4 regulates transcription. Further work is needed to identify potential binding partners of PDCD4 in the nucleus, which may provide insight into specific transcription factors or other proteins that PDCD4 is regulating in order to produce these changes in transcription. Moreover, given that PDCD4 regulates the expression of synaptic genes, it will be important to investigate if degradation of PDCD4 is required for synaptic plasticity. While there are paradigms for studying synaptic plasticity in primary neuronal cell culture, many of the stimuli that increase synaptic strength have not been confirmed to be transcription-dependent, which is critical for studying the role of potential transcriptional regulators in synaptic plasticity. Instead, it will be important to extend this work on PDCD4 to more physiologically relevant models, such as hippocampal slice preparations or *in vivo* rodent models. The long-term synaptic plasticity models in these systems have been demonstrated to be transcription-dependent (Nguyen et al., 1994; Nguyen and Kandel, 1997; Chotiner et al., 2003; Pedreira, 1996; Wüstenberg et al., 1998; Bailey et al., 1999), which is critical for investigating the role of PDCD4-mediated transcription in plasticity. Moreover, it will be important to confirm that PDCD4 is degraded by neuronal stimulation in these physiologically relevant models, via the same mechanisms we identified in primary neuronal cell culture.

This study provided a novel approach for identifying activity-dependent changes in the nuclear proteome, in order to understand how transcription is regulated in response to neuronal stimulation. This study focused on how the nuclear proteome changes in response to one particular stimulus, bicuculline stimulation, but it would be insightful to investigate the how the nuclear proteome changes in response to distinct types of stimulation and at different time points. Additionally, the use of different stimulation paradigms could help elucidate how the different synapse-to-nucleus signaling mechanisms (electrochemical signaling or synapto-nuclear messenger proteins) contribute to changes in the nuclear proteome. To identify how synapo-nuclear messenger proteins contribute to changes in the nucleus, local glutamate uncaging could be used to stimulate several select synapses. This type of local stimulation does not elicit global changes in depolarization or calcium influx that reach the cell body (Zhai et al., 2013), and so any changes detected in the nucleus would be due to the signaling proteins activated at those synapses. To identify how electrochemical signaling and calcium influx regulate the nuclear proteome, stimulation could be performed in the presence of dynein and kinesin inhibitors, to prevent active transport of signaling proteins from synapses to the nucleus. Such work would provide insight into the relative importance of various mechanisms of synapse-to-nucleus communication in regulating transcription.

The importance of activity-dependent transcription for synaptic plasticity has been established through experiments that either globally block transcription during the stimulation (Nguyen et al., 1994; Nguyen and Kandel, 1997; Chotiner et al., 2003), or experiments that delete key activity-dependent genes that are induced after stimulation (Fleischmann et al., 2003; Plath et al., 2006), both of which can impair synaptic plasticity. However, globally inhibiting transcription after stimulation inhibits both the transcription of activity-dependent genes, as well

as transcription of activity-*in*dependent genes that are continually transcribed. Additionally, deleting particular genes that are known to undergo activity-dependent changes in transcription does not distinguish between the role of these genes at baseline from the role of these genes after stimulation. An ideal manipulation would block the activity-dependent changes in transcription, while maintaining baseline levels of transcription. While this is a complicated task, understanding the mechanisms that link neuronal stimulation to changes in transcription provides an avenue for manipulating specifically *activity-dependent* transcription. For example, CRTC1 only translocates to the nucleus to promote transcription in response to stimulation, and so mutating phosphorylation sites to keep CRTC1 constitutively in the cytoplasm would specifically block activity-dependent CRTC1-mediated transcription. Similarly, PDCD4 is degraded after stimulation to promote activity-dependent transcription, and so mutating phosphorylation sites to prevent PDCD4 degradation blocks activity-dependent PDCD4-mediated transcription. Manipulating these types of proteins provides a way to study specifically activity-dependent transcription. This enables one to study the contribution of activity-dependent transcription to synaptic plasticity and other processes. In this manner, the identification of proteins that link stimulation to transcription provides insight into the importance of activity-dependent transcription in the brain.

References

Abel, T., and E. Kandel. 1998. Positive and negative regulatory mechanisms that mediate long-term memory storage. *In* Brain Research Reviews. 360–378.

Ahmed, B.Y., S. Chakravarthy, R. Eggers, W.T.J.M.C. Hermens, J.Y. Zhang, S.P. Niclou, C. Levelt, F. Sablitzky, P.N. Anderson, A.R. Lieberman, and J. Verhaagen. 2004. Efficient delivery of Cre-recombinase to neurons in vivo and stable transduction of neurons using adeno-associated and lentiviral vectors. *BMC Neurosci.* 5:4. doi:10.1186/1471-2202-5-4.

Aizawa, H., S.-C. Hu, K. Bobb, K. Balakrishnan, G. Ince, I. Gurevich, M. Cowan, and A. Ghosh. 2004. Dendrite development regulated by CREST, a calcium-regulated transcriptional activator. *Science*. 303:197–202. doi:10.1126/science.1089845.

Alberini, C.M. 2009. Transcription factors in long-term memory and synaptic plasticity. *Physiol. Rev.* 89:121–145. doi:10.1152/physrev.00017.2008.

Allgayer, H. 2010. Pdcd4, a colon cancer prognostic that is regulated by a microRNA. *Crit. Rev. Oncol. Hematol.* 73:185–191. doi:10.1016/j.critrevonc.2009.09.001.

Altarejos, J.Y., N. Goebel, M.D. Conkright, H. Inoue, J. Xie, C.M. Arias, P.E. Sawchenko, and M. Montminy. 2008. The Creb1 coactivator Crtc1 is required for energy balance and fertility. *Nat. Med.* 14:1112–1117. doi:10.1038/nm.1866.

Asangani, I.A., S.A.K. Rasheed, D.A. Nikolova, J.H. Leupold, N.H. Colburn, S. Post, and H. Allgayer. 2008. MicroRNA-21 (miR-21) post-transcriptionally downregulates tumor suppressor Pdcd4 and stimulates invasion, intravasation and metastasis in colorectal cancer. *Oncogene*. 27:2128–2136. doi:10.1038/sj.onc.1210856.

Ashburner, M., C.A. Ball, J.A. Blake, D. Botstein, H. Butler, J.M. Cherry, A.P. Davis, K.

Dolinski, S.S. Dwight, J.T. Eppig, M.A. Harris, D.P. Hill, L. Issel-Tarver, A. Kasarskis, S. Lewis, J.C. Matese, J.E. Richardson, M. Ringwald, G.M. Rubin, and G. Sherlock. 2000. Gene ontology: Tool for the unification of biology. *Nat. Genet.* 25:25–29. doi:10.1038/75556.

Bading, H. 2013. Nuclear calcium signalling in the regulation of brain function. *Nat. Rev. Neurosci.* 14:593–608. doi:10.1038/nrn3531.

Bailey, C.H., and M. Chen. 1988. Long-term memory in Aplysia modulates the total number of varicosities of single identified sensory neurons. *Proc. Natl. Acad. Sci.* 85:2373–2377. doi:10.1073/pnas.85.7.2373.

Bailey, D.J., J.J. Kim, W. Sun, R.F. Thompson, and F.J. Helmstetter. 1999. Acquisition of fear conditioning in rats requires the synthesis of mRNA in the amygdala. *Behav. Neurosci.* 113:276–282. doi:10.1037/0735-7044.113.2.276.

Banerjee, S., P. Neveu, and K.S. Kosik. 2009. A Coordinated Local Translational Control Point at the Synapse Involving Relief from Silencing and MOV10 Degradation. *Neuron*. 64:871–884. doi:10.1016/j.neuron.2009.11.023.

Barbarese, E., M.F. Ifrim, L. Hsieh, C. Guo, V. Tatavarty, M.J. Maggipinto, G. Korza, J.W. Tutolo, A. Giampetruzzi, H. Le, X.-M. Ma, E. Levine, B. Bishop, D.O. Kim, S. Kuwada, and J.H. Carson. 2013. Conditional Knockout of Tumor Overexpressed Gene in Mouse Neurons Affects RNA Granule Assembly, Granule Translation, LTP and Short Term Habituation. *PLoS One*. 8:e69989. doi:10.1371/journal.pone.0069989.

Bayraktar, G., P.A. Yuanxiang, A.D. Confettura, G.M. Gomes, S.A. Raza, O. Stork, S. Tajima, I. Suetake, A. Karpova, F. Yildirim, and M.R. Kreutz. 2020. Synaptic control of DNA methylation involves activity-dependent degradation of DNMT3A1 in the nucleus.

Neuropsychopharmacology. 45:2120–2130. doi:10.1038/s41386-020-0780-2.

Bengtson, C.P., and H. Bading. 2012. Nuclear Calcium Signaling. *In* Synaptic Plasticity. 377–405.

Benito, E., and A. Barco. 2015. The Neuronal Activity-Driven Transcriptome. *Mol. Neurobiol.* 51:1071–1088. doi:10.1007/s12035-014-8772-z.

Biever, A., E. Valjent, and E. Puighermanal. 2015. Ribosomal Protein S6 Phosphorylation in the Nervous System: From Regulation to Function. *Front. Mol. Neurosci.* 8. doi:10.3389/fnmol.2015.00075.

Bird, C.M., and N. Burgess. 2008. The hippocampus and memory: insights from spatial processing. *Nat. Rev. Neurosci.* 9:182–194. doi:10.1038/nrn2335.

Bitomsky, N., M. Böhm, and K.H. Klempnauer. 2004. Transformation suppressor protein Pdcd4 interferes with JNK-mediated phosphorylation of c-Jun and recruitment of the coactivator p300 by c-Jun. *Oncogene*. 23:7484–7493. doi:10.1038/sj.onc.1208064.

Bliss, T.V.P., and T. Lømo. 1973. Long-lasting potentiation of synaptic transmission in the dentate area of the anaesthetized rabbit following stimulation of the perforant path. *J. Physiol.* 232:331–356. doi:10.1113/jphysiol.1973.sp010273.

Bloodgood, B.L., N. Sharma, H.A. Browne, A.Z. Trepman, and M.E. Greenberg. 2013. The activity-dependent transcription factor NPAS4 regulates domain-specific inhibition. *Nature*. 503:121–125. doi:10.1038/nature12743.

Böhm, M., K. Sawicka, J.P. Siebrasse, A. Brehmer-Fastnacht, R. Peters, and K.H. Klempnauer. 2003. The transformation suppressor protein Pdcd4 shuttles between nucleus and cytoplasm and binds RNA. *Oncogene*. 22:4905–4910. doi:10.1038/sj.onc.1206710.

Breuillaud, L., O. Halfon, P.J. Magistretti, F.P. Pralong, and J.-R. Cardinaux. 2009. Mouse

fertility is not dependent on the CREB coactivator Crtc1. *Nat. Med.* 15:989–990. doi:10.1038/nm0909-989.

Brigidi, G.S., M.G.B. Hayes, N.P. Delos Santos, A.L. Hartzell, L. Texari, P.A. Lin, A. Bartlett, J.R. Ecker, C. Benner, S. Heinz, and B.L. Bloodgood. 2019. Genomic Decoding of Neuronal Depolarization by Stimulus-Specific NPAS4 Heterodimers. *Cell*. 179:373-391.e27. doi:10.1016/j.cell.2019.09.004.

Burgio, G. 2018. Redefining mouse transgenesis with CRISPR/Cas9 genome editing technology. *Genome Biol.* 19:27. doi:10.1186/s13059-018-1409-1.

Callender, J.A., and A.C. Newton. 2017. Conventional protein kinase C in the brain: 40 years later. *Neuronal Signal.* 1. doi:10.1042/NS20160005.

Canettieri, G., S. Coni, M. Della Guardia, V. Nocerino, L. Antonucci, L. Di Magno, R. Screaton, I. Screpanti, G. Giannini, and A. Gulino. 2009. The coactivator CRTC1 promotes cell proliferation and transformation via AP-1. *Proc. Natl. Acad. Sci.* 106:1445–1450. doi:10.1073/pnas.0808749106.

Carbon, S., E. Douglass, N. Dunn, B. Good, N.L. Harris, S.E. Lewis, C.J. Mungall, S. Basu, R.L. Chisholm, R.J. Dodson, E. Hartline, P. Fey, P.D. Thomas, L.P. Albou, D. Ebert, M.J. Kesling, H. Mi, A. Muruganujan, X. Huang, S. Poudel, T. Mushayahama, J.C. Hu, S.A. LaBonte, D.A. Siegele, G. Antonazzo, H. Attrill, N.H. Brown, S. Fexova, P. Garapati, T.E.M. Jones, S.J. Marygold, G.H. Millburn, A.J. Rey, V. Trovisco, G. Dos Santos, D.B. Emmert, K. Falls, P. Zhou, J.L. Goodman, V.B. Strelets, J. Thurmond, M. Courtot, D.S. Osumi, H. Parkinson, P. Roncaglia, M.L. Acencio, M. Kuiper, A. Lreid, C. Logie, R.C. Lovering, R.P. Huntley, P. Denny, N.H. Campbell, B. Kramarz, V. Acquaah, S.H. Ahmad, H. Chen, J.H. Rawson, M.C. Chibucos, M. Giglio, S. Nadendla, R. Tauber, M.J. Duesbury,

N.T. Del, B.H.M. Meldal, L. Perfetto, P. Porras, S. Orchard, A. Shrivastava, Z. Xie, H.Y. Chang, R.D. Finn, A.L. Mitchell, N.D. Rawlings, L. Richardson, A. Sangrador-Vegas, J.A. Blake, K.R. Christie, M.E. Dolan, H.J. Drabkin, D.P. Hill, L. Ni, D. Sitnikov, M.A. Harris, S.G. Oliver, K. Rutherford, V. Wood, J. Hayles, J. Bahler, A. Lock, E.R. Bolton, J. De Pons, M. Dwinell, G.T. Hayman, S.J.F. Laulederkind, M. Shimoyama, M. Tutaj, S.J. Wang, et al. 2019. The Gene Ontology Resource: 20 years and still GOing strong. *Nucleic Acids Res.* 47:D330–D338. doi:10.1093/nar/gky1055.

Cardozo, T., and M. Pagano. 2004. The SCF ubiquitin ligase: insights into a molecular machine. *Nat. Rev. Mol. Cell Biol.* 5:739–751. doi:10.1038/nrm1471.

Carrión, A.M., W.A. Link, F. Ledo, B. Mellström, and J.R. Naranjo. 1999. DREAM is a Ca2+-regulated transcriptional repressor. *Nature*. 398:80–84. doi:10.1038/18044.

Ch'ng, T.H., M. DeSalvo, P. Lin, A. Vashisht, J.A. Wohlschlegel, and K.C. Martin. 2015. Cell biological mechanisms of activity-dependent synapse to nucleus translocation of CRTC1 in neurons. *Front. Mol. Neurosci.* 8:48. doi:10.3389/fnmol.2015.00048.

Ch'ng, T.H., B. Uzgil, P. Lin, N.K. Avliyakulov, T.J. O'Dell, and K.C. Martin. 2012. Activity-dependent transport of the transcriptional coactivator CRTC1 from synapse to nucleus. *Cell*. 150:207–221. doi:10.1016/j.cell.2012.05.027.

Chawla, S., P. Vanhoutte, F.J.L. Arnold, C.L.H. Huang, and H. Bading. 2003. Neuronal activity-dependent nucleocytoplasmic shuttling of HDAC4 and HDAC5. *J. Neurochem.* 85:151–159. doi:10.1046/j.1471-4159.2003.01648.x.

Chen, P.B., R. Kawaguchi, C. Blum, J.M. Achiro, G. Coppola, T.J. O'Dell, and K.C. Martin. 2017. Mapping Gene Expression in Excitatory Neurons during Hippocampal Late-Phase Long-Term Potentiation. *Front. Mol. Neurosci.* 10. doi:10.3389/fnmol.2017.00039.

Chen, Y., T. Knösel, G. Kristiansen, A. Pietas, M.E. Garber, S. Matsuhashi, I. Ozaki, and I. Petersen. 2003. Loss of PDCD4 expression in human lung cancer correlates with tumour progression and prognosis. *J. Pathol.* 200:640–646. doi:10.1002/path.1378.

Cho, J.-H., B.S. Huang, and J.M. Gray. 2016. RNA sequencing from neural ensembles activated during fear conditioning in the mouse temporal association cortex. *Sci. Rep.* 6:31753. doi:10.1038/srep31753.

Cho, K.F., T.C. Branon, N.D. Udeshi, S.A. Myers, S.A. Carr, and A.Y. Ting. 2020. Proximity labeling in mammalian cells with TurboID and split-TurboID. *Nat. Protoc.* 15:3971–3999. doi:10.1038/s41596-020-0399-0.

Chotiner, J.K., H. Khorasani, A.C. Nairn, T.J. O'Dell, and J.B. Watson. 2003. Adenylyl cyclase-dependent form of chemical long-term potentiation triggers translational regulation at the elongation step. *Neuroscience*. 116:743–752. doi:10.1016/S0306-4522(02)00797-2.

Clarke, J.R., M. Cammarota, A. Gruart, I. Izquierdo, and J.M. Delgado-Garcia. 2010. Plastic modifications induced by object recognition memory processing. *Proc. Natl. Acad. Sci.* 107:2652–2657. doi:10.1073/pnas.0915059107.

Cmarik, J.L., H. Min, G. Hegamyer, S. Zhan, M. Kulesz-Martin, H. Yoshinaga, S. Matsuhashi, and N.H. Colburn. 1999. Differentially expressed protein Pdcd4 inhibits tumor promoter-induced neoplastic transformation. *Proc. Natl. Acad. Sci.* 96:14037–14042. doi:10.1073/pnas.96.24.14037.

Coba, M.P., L.M. Valor, M. V. Kopanitsa, N.O. Afinowi, and S.G.N. Grant. 2008. Kinase Networks Integrate Profiles of N-Methyl-d-aspartate Receptor-mediated Gene Expression in Hippocampus. *J. Biol. Chem.* 283:34101–34107. doi:10.1074/jbc.M804951200.

Cohen, S.M., B. Li, R.W. Tsien, and H. Ma. 2015. Evolutionary and functional perspectives on

signaling from neuronal surface to nucleus. *Biochem. Biophys. Res. Commun.* 460:88–99. doi:10.1016/j.bbrc.2015.02.146.

Conkright, M.D., G. Canettieri, R. Screaton, E. Guzman, L. Miraglia, J.B. Hogenesch, and M. Montminy. 2003. TORCs: Transducers of Regulated CREB Activity. *Mol. Cell*. 12:413–423. doi:10.1016/j.molcel.2003.08.013.

Cox, J., and M. Mann. 2008. MaxQuant enables high peptide identification rates, individualized p.p.b.-range mass accuracies and proteome-wide protein quantification. *Nat. Biotechnol.* 26:1367–1372. doi:10.1038/nbt.1511.

Deisseroth, K., P.G. Mermelstein, H. Xia, and R.W. Tsien. 2003. Signaling from synapse to nucleus: the logic behind the mechanisms. *Curr. Opin. Neurobiol.* 13:354–365. doi:10.1016/S0959-4388(03)00076-X.

Dieterich, D.C., A. Karpova, M. Mikhaylova, I. Zdobnova, I. König, M. Landwehr, M. Kreutz, K.H. Smalla, K. Richter, P. Landgraf, C. Reissner, T.M. Boeckers, W. Zuschratter, C. Spilker, C.I. Seidenbecher, C.C. Garner, E.D. Gundelfinger, and M.R. Kreutz. 2008. Caldendrin-Jacob: A protein liaison that couples NMDA receptor signalling to the nucleus. *PLoS Biol.* 6:0286–0306. doi:10.1371/journal.pbio.0060034.

Dinamarca, M.C., F. Guzzetti, A. Karpova, D. Lim, N. Mitro, S. Musardo, M. Mellone, E. Marcello, J. Stanic, T. Samaddar, A. Burguière, A. Caldarelli, A.A. Genazzani, J. Perroy, L. Fagni, P.L. Canonico, M.R. Kreutz, F. Gardoni, and M. Di Luca. 2016. Ring finger protein 10 is a novel synaptonuclear messenger encoding activation of NMDA receptors in hippocampus. *Elife*. 5. doi:10.7554/eLife.12430.

Dobin, A., C.A. Davis, F. Schlesinger, J. Drenkow, C. Zaleski, S. Jha, P. Batut, M. Chaisson, and T.R. Gingeras. 2013. STAR: Ultrafast universal RNA-seq aligner. *Bioinformatics*. 29:15–

21. doi:10.1093/bioinformatics/bts635.

Dörrbaum, A.R., B. Alvarez-Castelao, B. Nassim-Assir, J.D. Langer, and E.M. Schuman. 2020. Proteome dynamics during homeostatic scaling in cultured neurons. *Elife*. 9. doi:10.7554/eLife.52939.

Dorrello, N.V., A. Peschiaroli, D. Guardavaccaro, N.H. Colburn, N.E. Sherman, and M. Pagano. 2006. S6k1- and βTRCP-mediated degradation of PDCD4 promotes protein translation and cell growth. *Science (80-.).* 314:467–471. doi:10.1126/science.1130276.

Dubey, D., and B.E. Porter. 2016. CRTC1 nuclear localization in the hippocampus of the pilocarpine-induced status epilepticus model of temporal lobe epilepsy. *Neuroscience*. 320:57–68. doi:10.1016/j.neuroscience.2016.01.059.

Duclot, F., and M. Kabbaj. 2017. The Role of Early Growth Response 1 (EGR1) in Brain Plasticity and Neuropsychiatric Disorders. *Front. Behav. Neurosci.* 11. doi:10.3389/fnbeh.2017.00035.

Dudek, S.M., and M.F. Bear. 1992. Homosynaptic long-term depression in area CA1 of hippocampus and effects of N-methyl-D-aspartate receptor blockade. *Proc. Natl. Acad. Sci.* 89:4363–4367. doi:10.1073/pnas.89.10.4363.

Edgar, R., M. Domrachev, and A.E. Lash. 2002. Gene Expression Omnibus: NCBI gene expression and hybridization array data repository. *Nucleic Acids Res.* 30:207–210. doi:10.1093/nar/30.1.207.

Eshete, F., and R.D. Fields. 2001. Spike frequency decoding and autonomous activation of Ca2+-calmodulin-dependent protein kinase II in dorsal root ganglion neurons. *J. Neurosci.* 21:6694–6705. doi:21/17/6694 [pii].

Eto, K., S. Goto, W. Nakashima, Y. Ura, and S.-I. Abe. 2012. Loss of programmed cell death 4

induces apoptosis by promoting the translation of procaspase-3 mRNA. *Cell Death Differ.* 19:573–581. doi:10.1038/cdd.2011.126.

Fassan, M., M. Pizzi, L. Giacomelli, C. Mescoli, K. Ludwig, S. Pucciarelli, and M. Rugge. 2011. PDCD4 nuclear loss inversely correlates with miR-21 levels in colon carcinogenesis. *Virchows Arch.* 458:413–419. doi:10.1007/s00428-011-1046-5.

Fernandez-Albert, J., M. Lipinski, M.T. Lopez-Cascales, M.J. Rowley, A.M. Martin-Gonzalez, B. del Blanco, V.G. Corces, and A. Barco. 2019. Immediate and deferred epigenomic signatures of in vivo neuronal activation in mouse hippocampus. *Nat. Neurosci.* 22:1718–1730. doi:10.1038/s41593-019-0476-2.

Flavell, S.W., C.W. Cowan, T.K. Kim, P.L. Greer, Y. Lin, S. Paradis, E.C. Griffith, L.S. Hu, C. Chen, and M.E. Greenberg. 2006. Activity-dependent regulation of MEF2 transcription factors suppresses excitatory synapse number. *Science (80-.).* 311:1008–1012. doi:10.1126/science.1122511.

Fleischmann, A., O. Hvalby, V. Jensen, T. Strekalova, C. Zacher, L.E. Layer, A. Kvello, M. Reschke, R. Spanagel, R. Sprengel, E.F. Wagner, and P. Gass. 2003. Impaired Long-Term Memory and NR2A-Type NMDA Receptor-Dependent Synaptic Plasticity in Mice Lacking c-Fos in the CNS. *J. Neurosci.* 23:9116–9122. doi:10.1523/JNEUROSCI.23-27-09116.2003.

Frankel, L.B., N.R. Christoffersen, A. Jacobsen, M. Lindow, A. Krogh, and A.H. Lund. 2008. Programmed cell death 4 (PDCD4) is an important functional target of the microRNA miR-21 in breast cancer cells. *J. Biol. Chem.* 283:1026–1033. doi:10.1074/jbc.M707224200.

Fukuchi, M., Y. Kirikoshi, A. Mori, R. Eda, D. Ihara, I. Takasaki, A. Tabuchi, and M. Tsuda. 2014. Excitatory GABA induces BDNF transcription via CRTC1 and phosphorylated

CREB-related pathways in immature cortical cells. *J. Neurochem.* 131:134–146. doi:10.1111/jnc.12801.

Gallegos, D.A., U. Chan, L.F. Chen, and A.E. West. 2018. Chromatin Regulation of Neuronal Maturation and Plasticity. *Trends Neurosci.* 41:311–324. doi:10.1016/j.tins.2018.02.009.

Gaudillière, B., Y. Konishi, N. de la Iglesia, G. Yao, and A. Bonni. 2004. A CaMKII-NeuroD Signaling Pathway Specifies Dendritic Morphogenesis. *Neuron*. 41:229–241. doi:10.1016/S0896-6273(03)00841-9.

Giachero, M., G.D. Calfa, and V.A. Molina. 2013. Hippocampal structural plasticity accompanies the resulting contextual fear memory following stress and fear conditioning. *Learn. Mem.* 20:611–616. doi:10.1101/lm.031724.113.

Gould, C., and A. Newton. 2008. The Life and Death of Protein Kinase C. *Curr. Drug Targets*. 9:614–625. doi:10.2174/138945008785132411.

Grabowski, P.J. 2005. Splicing-active nuclear extracts from rat brain. *Methods*. 37:323–330. doi:10.1016/j.ymeth.2005.07.014.

Graef, I.A., F. Wang, F. Charron, L. Chen, J. Neilson, M. Tessier-Lavigne, and G.R. Crabtree. 2003. Neurotrophins and Netrins Require Calcineurin/NFAT Signaling to Stimulate Outgrowth of Embryonic Axons. *Cell*. 113:657–670. doi:10.1016/S0092-8674(03)00390-8.

Gruart, A. 2006. Involvement of the CA3-CA1 Synapse in the Acquisition of Associative Learning in Behaving Mice. *J. Neurosci.* 26:1077–1087. doi:10.1523/JNEUROSCI.2834-05.2006.

Guimarães de Araújo, M.E., and L.A. Huber. 2007. Subcellular Fractionation. *In* Cardiovascular Proteomics. Humana Press, New Jersey. 73–86.

Haas, A., B.S. Nilges, S.A. Leidel, and K.-H. Klempnauer. 2020. PDCD4 controls the G1/S-

phase transition in a telomerase-immortalized epithelial cell line and affects the expression level and translation of multiple mRNAs. *Sci. Rep.* 10:2758. doi:10.1038/s41598-020-59678-w.

Hebb, D.O. 1949. The Organization of Behavior. A Neuropsychological Theory. John Wiley & Sons, New York.

Hegde, A.N., A.L. Goldberg, and J.H. Schwartz. 1993. Regulatory subunits of cAMP-dependent protein kinases are degraded after conjugation to ubiquitin: A molecular mechanism underlying long-term synaptic plasticity. *Proc. Natl. Acad. Sci. U. S. A.* 90:7436–7440. doi:10.1073/pnas.90.16.7436.

Heinrichs, S.C., K.A. Leite-Morris, M.D. Guy, L.R. Goldberg, A.J. Young, and G.B. Kaplan. 2013. Dendritic structural plasticity in the basolateral amygdala after fear conditioning and its extinction in mice. *Behav. Brain Res.* 248:80–84. doi:10.1016/j.bbr.2013.03.048.

Heinz, D.A., and B.L. Bloodgood. 2020. Mechanisms that communicate features of neuronal activity to the genome. *Curr. Opin. Neurobiol.* 63:131–136. doi:10.1016/j.conb.2020.03.002.

Heinz, S., C. Benner, N. Spann, E. Bertolino, Y.C. Lin, P. Laslo, J.X. Cheng, C. Murre, H. Singh, and C.K. Glass. 2010. Simple Combinations of Lineage-Determining Transcription Factors Prime cis-Regulatory Elements Required for Macrophage and B Cell Identities. *Mol. Cell*. 38:576–589. doi:10.1016/j.molcel.2010.05.004.

Herbst, W.A., and K.C. Martin. 2017. Regulated transport of signaling proteins from synapse to nucleus. *Curr. Opin. Neurobiol.* 45:78–84. doi:10.1016/j.conb.2017.04.006.

Hirano, Y., T. Masuda, S. Naganos, M. Matsuno, K. Ueno, T. Miyashita, J. Horiuchi, and M. Saitoe. 2013. Fasting Launches CRTC to Facilitate Long-Term Memory Formation in

Drosophila. *Science (80-.).* 339:443–446. doi:10.1126/science.1227170.

Holt, C.E., K.C. Martin, and E.M. Schuman. 2019. Local translation in neurons: visualization and function. *Nat. Struct. Mol. Biol.* 26:557–566. doi:10.1038/s41594-019-0263-5.

Hrvatin, S., D.R. Hochbaum, M.A. Nagy, M. Cicconet, K. Robertson, L. Cheadle, R. Zilionis, A. Ratner, R. Borges-Monroy, A.M. Klein, B.L. Sabatini, and M.E. Greenberg. 2018. Single-cell analysis of experience-dependent transcriptomic states in the mouse visual cortex. *Nat. Neurosci.* 21:120–129. doi:10.1038/s41593-017-0029-5.

Hsu, P.D., E.S. Lander, and F. Zhang. 2014. Development and Applications of CRISPR-Cas9 for Genome Engineering. *Cell*. 157:1262–1278. doi:10.1016/j.cell.2014.05.010.

Huang, T., M. Choi, M. Tzouros, S. Golling, N.J. Pandya, B. Banfai, T. Dunkley, and O. Vitek. 2020. MSstatsTMT: Statistical Detection of Differentially Abundant Proteins in Experiments with Isobaric Labeling and Multiple Mixtures. *Mol. Cell. Proteomics*. 19:1706–1723. doi:10.1074/mcp.RA120.002105.

Hug, N., D. Longman, and J.F. Cáceres. 2016. Mechanism and regulation of the nonsense-mediated decay pathway. *Nucleic Acids Res.* 44:1483–1495. doi:10.1093/nar/gkw010.

Hung, V., N.D. Udeshi, S.S. Lam, K.H. Loh, K.J. Cox, K. Pedram, S.A. Carr, and A.Y. Ting. 2016. Spatially resolved proteomic mapping in living cells with the engineered peroxidase APEX2. *Nat. Protoc.* 11:456–475. doi:10.1038/nprot.2016.018.

Hwang, S.-K., A.R. Baker, M.R. Young, and N.H. Colburn. 2014. Tumor suppressor PDCD4 inhibits NF-κB-dependent transcription in human glioblastoma cells by direct interaction with p65. *Carcinogenesis*. 35:1469–1480. doi:10.1093/carcin/bgu008.

Ito, M., and M. Kano. 1982. Long-lasting depression of parallel fiber-Purkinje cell transmission induced by conjunctive stimulation of parallel fibers and climbing fibers in the cerebellar

cortex. *Neurosci. Lett.* 33:253–258. doi:10.1016/0304-3940(82)90380-9.

Ivanova, D., A. Dirks, C. Montenegro-Venegas, C. Schone, W.D. Altrock, C. Marini, R. Frischknecht, D. Schanze, M. Zenker, E.D. Gundelfinger, and A. Fejtova. 2015. Synaptic activity controls localization and function of CtBP1 via binding to Bassoon and Piccolo. *EMBO J*. 34:1056–1077. doi:10.15252/embj.201488796.

Jansen, A.P., C.E. Camalier, and N.H. Colburn. 2005. Epidermal Expression of the Translation Inhibitor Programmed Cell Death 4 Suppresses Tumorigenesis. *Cancer Res.* 65:6034–6041. doi:10.1158/0008-5472.CAN-04-2119.

Janssen, J.M., X. Chen, J. Liu, and M.A.F.V. Gonçalves. 2019. The Chromatin Structure of CRISPR-Cas9 Target DNA Controls the Balance between Mutagenic and Homology-Directed Gene-Editing Events. *Mol. Ther. - Nucleic Acids*. 16:141–154. doi:10.1016/j.omtn.2019.02.009.

Jarome, T.J., C.T. Werner, J.L. Kwapis, and F.J. Helmstetter. 2011. Activity Dependent Protein Degradation Is Critical for the Formation and Stability of Fear Memory in the Amygdala. *PLoS One*. 6. doi:10.1371/journal.pone.0024349.

Jiang, Y., S. Zhao, Y. Ding, L. Nong, H. Li, G. Gao, D. Zhou, and N. Xu. 2017. MicroRNA-21 promotes neurite outgrowth by regulating PDCD4 in a rat model of spinal cord injury. *Mol. Med. Rep.* 16:2522–2528. doi:10.3892/mmr.2017.6862.

Jo, S.H., D.E. Kim, A. Clocchiatti, and G.P. Dotto. 2016. PDCD4 is a CSL associated protein with a transcription repressive function in cancer associated fibroblast activation. *Oncotarget*. 7:58717–58727. doi:10.18632/oncotarget.11227.

Jordan, B. a, B.D. Fernholz, L. Khatri, and E.B. Ziff. 2007. Activity-dependent AIDA-1 nuclear signaling regulates nucleolar numbers and protein synthesis in neurons. *Nat. Neurosci.*

10:427–435. doi:10.1038/nn1867.

Jung, D., Y.J. Hwang, H. Ryu, M. Kano, K. Sakimura, and J. Cho. 2016. Conditional Knockout of Cav2.1 Disrupts the Accuracy of Spatial Recognition of CA1 Place Cells and Spatial/Contextual Recognition Behavior. *Front. Behav. Neurosci.* 10. doi:10.3389/fnbeh.2016.00214.

Kalderon, D., B.L. Roberts, W.D. Richardson, and A.E. Smith. 1984. A short amino acid sequence able to specify nuclear location. *Cell*. 39:499–509. doi:10.1016/0092-8674(84)90457-4.

Karpova, A., M. Mikhaylova, S. Bera, J. Bär, P.P. Reddy, T. Behnisch, V. Rankovic, C. Spilker, P. Bethge, J. Sahin, R. Kaushik, W. Zuschratter, T. Kähne, M. Naumann, E.D. Gundelfinger, and M.R. Kreutz. 2013. Encoding and transducing the synaptic or extrasynaptic origin of NMDA receptor signals to the nucleus. *Cell*. 152:1119–1133. doi:10.1016/j.cell.2013.02.002.

Kashani, A.H., Z. Qiu, L. Jurata, S.-K. Lee, S. Pfaff, S. Goebbels, K.-A. Nave, and A. Ghosh. 2006. Calcium Activation of the LMO4 Transcription Complex and Its Role in the Patterning of Thalamocortical Connections. *J. Neurosci.* 26:8398–8408. doi:10.1523/JNEUROSCI.0618-06.2006.

Kaspar, B.K., B. Vissel, T. Bengoechea, S. Crone, L. Randolph-Moore, R. Muller, E.P. Brandon, D. Schaffer, I.M. Verma, K.-F. Lee, S.F. Heinemann, and F.H. Gage. 2002. Adeno-associated virus effectively mediates conditional gene modification in the brain. *Proc. Natl. Acad. Sci.* 99:2320–2325. doi:10.1073/pnas.042678699.

Kim, M., H. Lee, J.-H. Hur, J. Choe, and C. Lim. 2016. CRTC Potentiates Light-independent timeless Transcription to Sustain Circadian Rhythms in Drosophila. *Sci. Rep.* 6:32113.

doi:10.1038/srep32113.

Kim, T.-K., M. Hemberg, J.M. Gray, A.M. Costa, D.M. Bear, J. Wu, D.A. Harmin, M. Laptewicz, K. Barbara-Haley, S. Kuersten, E. Markenscoff-Papadimitriou, D. Kuhl, H. Bito, P.F. Worley, G. Kreiman, and M.E. Greenberg. 2010. Widespread transcription at neuronal activity-regulated enhancers. *Nature*. 465:182–187. doi:10.1038/nature09033.

Kobayashi, Y., and T.K. Hensch. 2013. Germline recombination by conditional gene targeting with Parvalbumin-Cre lines. *Front. Neural Circuits*. 7. doi:10.3389/fncir.2013.00168.

Konorski, J. 1948. Conditioned Reflexes and Neuron Organization. Cambridge University Press, Cambridge.

Kovacs, K.A., P. Steullet, M. Steinmann, K.Q. Do, P.J. Magistretti, O. Halfon, and J.-R. Cardinaux. 2007. TORC1 is a calcium- and cAMP-sensitive coincidence detector involved in hippocampal long-term synaptic plasticity. *Proc. Natl. Acad. Sci.* 104:4700–4705. doi:10.1073/pnas.0607524104.

Kravchick, D.O., A. Karpova, M. Hrdinka, J. Lopez-rojas, S. Iacobas, A.U. Carbonell, D.A. Iacobas, M.R. Kreutz, and B.A. Jordan. 2016a. Synaptonuclear messenger PRR 7 inhibits c-Jun ubiquitination and regulates NMDA-mediated excitotoxicity. *EMBO J.* 35:1923–34. doi:10.15252/embj.201593070.

Kravchick, D.O., A. Karpova, M. Hrdinka, J. Lopez-Rojas, S. Iacobas, A.U. Carbonell, D.A. Iacobas, M.R. Kreutz, and B.A. Jordan. 2016b. Synaptonuclear messenger PRR 7 inhibits c-Jun ubiquitination and regulates NMDA -mediated excitotoxicity . *EMBO J.* 35:1923–1934. doi:10.15252/embj.201593070.

Kumar, N., N. Wethkamp, L.C. Waters, M.D. Carr, and K.-H. Klempnauer. 2013. Tumor suppressor protein Pdcd4 interacts with Daxx and modulates the stability of Daxx and the

Hipk2-dependent phosphorylation of p53 at serine 46. *Oncogenesis*. 2:e37–e37. doi:10.1038/oncsis.2012.37.

de la Torre-Ubieta, L., J.L. Stein, H. Won, C.K. Opland, D. Liang, D. Lu, and D.H. Geschwind. 2018. The Dynamic Landscape of Open Chromatin during Human Cortical Neurogenesis. *Cell*. 172:289-304.e18. doi:10.1016/j.cell.2017.12.014.

Lacar, B., S.B. Linker, B.N. Jaeger, S.R. Krishnaswami, J.J. Barron, M.J.E. Kelder, S.L. Parylak, A.C.M. Paquola, P. Venepally, M. Novotny, C. O'Connor, C. Fitzpatrick, J.A. Erwin, J.Y. Hsu, D. Husband, M.J. McConnell, R. Lasken, and F.H. Gage. 2016. Nuclear RNA-seq of single neurons reveals molecular signatures of activation. *Nat. Commun.* 7. doi:10.1038/ncomms11022.

Lai, K.-O., Y. Zhao, T.H. Ch'ng, and K.C. Martin. 2008. Importin-mediated retrograde transport of CREB2 from distal processes to the nucleus in neurons. *Proc. Natl. Acad. Sci. U. S. A.* 105:17175–80. doi:10.1073/pnas.0803906105.

Lankat-Buttgereit, B., and R. Göke. 2009. The tumour suppressor Pdcd4: recent advances in the elucidation of function and regulation. *Biol. Cell*. 101:309–317. doi:10.1042/BC20080191.

Lee, Y.-S., and A.J. Silva. 2009. The molecular and cellular biology of enhanced cognition. *Nat. Rev. Neurosci.* 10:126–140. doi:10.1038/nrn2572.

Lein, E.S., M.J. Hawrylycz, N. Ao, M. Ayres, A. Bensinger, A. Bernard, A.F. Boe, M.S. Boguski, K.S. Brockway, E.J. Byrnes, L. Chen, L. Chen, T.M. Chen, M.C. Chin, J. Chong, B.E. Crook, A. Czaplinska, C.N. Dang, S. Datta, N.R. Dee, A.L. Desaki, T. Desta, E. Diep, T.A. Dolbeare, M.J. Donelan, H.W. Dong, J.G. Dougherty, B.J. Duncan, A.J. Ebbert, G. Eichele, L.K. Estin, C. Faber, B.A. Facer, R. Fields, S.R. Fischer, T.P. Fliss, C. Frensley, S.N. Gates, K.J. Glattfelder, K.R. Halverson, M.R. Hart, J.G. Hohmann, M.P. Howell, D.P.

Jeung, R.A. Johnson, P.T. Karr, R. Kawal, J.M. Kidney, R.H. Knapik, C.L. Kuan, J.H. Lake, A.R. Laramee, K.D. Larsen, C. Lau, T.A. Lemon, A.J. Liang, Y. Liu, L.T. Luong, J. Michaels, J.J. Morgan, R.J. Morgan, M.T. Mortrud, N.F. Mosqueda, L.L. Ng, R. Ng, G.J. Orta, C.C. Overly, T.H. Pak, S.E. Parry, S.D. Pathak, O.C. Pearson, R.B. Puchalski, Z.L. Riley, H.R. Rockett, S.A. Rowland, J.J. Royall, M.J. Ruiz, N.R. Sarno, K. Schaffnit, N. V. Shapovalova, T. Sivisay, C.R. Slaughterbeck, S.C. Smith, K.A. Smith, B.I. Smith, A.J. Sodt, N.N. Stewart, K.R. Stumpf, S.M. Sunkin, M. Sutram, A. Tam, C.D. Teemer, C. Thaller, C.L. Thompson, L.R. Varnam, A. Visel, R.M. Whitlock, P.E. Wohnoutka, et al. 2007. Genome-wide atlas of gene expression in the adult mouse brain. *Nature*. 445:168–176. doi:10.1038/nature05453.

Li, H., A. Rao, and P.G. Hogan. 2011. Interaction of calcineurin with substrates and targeting proteins. *Trends Cell Biol.* 21:91–103. doi:10.1016/j.tcb.2010.09.011.

Li, J., S. Han, H. Li, N.D. Udeshi, T. Svinkina, D.R. Mani, C. Xu, R. Guajardo, Q. Xie, T. Li, D.J. Luginbuhl, B. Wu, C.N. McLaughlin, A. Xie, P. Kaewsapsak, S.R. Quake, S.A. Carr, A.Y. Ting, and L. Luo. 2020a. Cell-Surface Proteomic Profiling in the Fly Brain Uncovers Wiring Regulators. *Cell*. 180:373-386.e15. doi:10.1016/j.cell.2019.12.029.

Li, S., C. Zhang, H. Takemori, Y. Zhou, and Z.-Q. Xiong. 2009. TORC1 Regulates Activity-Dependent CREB-Target Gene Transcription and Dendritic Growth of Developing Cortical Neurons. *J. Neurosci.* 29:2334–2343. doi:10.1523/JNEUROSCI.2296-08.2009.

Li, Y., Y. Jia, D. Wang, X. Zhuang, Y. Li, C. Guo, H. Chu, F. Zhu, J. Wang, X. Wang, Q. Wang, W. Zhao, Y. Shi, W. Chen, and L. Zhang. 2020b. Programmed cell death 4 as an endogenous suppressor of BDNF translation is involved in stress-induced depression. *Mol. Psychiatry*. doi:10.1038/s41380-020-0692-x.

Lim, P.S., C.R. Sutton, and S. Rao. 2015. Protein kinase C in the immune system: From signalling to chromatin regulation. *Immunology*. 146:508–522. doi:10.1111/imm.12510.

Lin, W.-J., C. Jiang, M. Sadahiro, O. Bozdagi, L. Vulchanova, C.M. Alberini, and S.R. Salton. 2015. VGF and Its C-Terminal Peptide TLQP-62 Regulate Memory Formation in Hippocampus via a BDNF-TrkB-Dependent Mechanism. *J. Neurosci.* 35:10343–10356. doi:10.1523/JNEUROSCI.0584-15.2015.

Lin, Y., B.L. Bloodgood, J.L. Hauser, A.D. Lapan, A.C. Koon, T.K. Kim, L.S. Hu, A.N. Malik, and M.E. Greenberg. 2008. Activity-dependent regulation of inhibitory synapse development by Npas4. *Nature*. 455:1198–1204. doi:10.1038/nature07319.

Lisman, J., H. Schulman, and H. Cline. 2002. The molecular basis of CaMKII function in synaptic and behavioural memory. *Nat. Rev. Neurosci.* 3:175–190. doi:10.1038/nrn753.

Liu, X., S. Ramirez, and S. Tonegawa. 2014. Inception of a false memory by optogenetic manipulation of a hippocampal memory engram. *Philos. Trans. R. Soc. B Biol. Sci.* 369:20130142. doi:10.1098/rstb.2013.0142.

Liwak, U., N. Thakor, L.E. Jordan, R. Roy, S.M. Lewis, O.E. Pardo, M. Seckl, and M. Holcik. 2012. Tumor Suppressor PDCD4 Represses Internal Ribosome Entry Site-Mediated Translation of Antiapoptotic Proteins and Is Regulated by S6 Kinase 2. *Mol. Cell. Biol.* 32:1818–1829. doi:10.1128/MCB.06317-11.

Love, M.I., W. Huber, and S. Anders. 2014. Moderated estimation of fold change and dispersion for RNA-seq data with DESeq2. *Genome Biol.* 15. doi:10.1186/s13059-014-0550-8.

Lu, K., Q. Chen, M. Li, L. He, F. Riaz, T. Zhang, and D. Li. 2020. Programmed cell death factor 4 (PDCD4), a novel therapy target for metabolic diseases besides cancer. *Free Radic. Biol. Med.* 159:150–163. doi:10.1016/j.freeradbiomed.2020.06.016.

Ma, H., R.D. Groth, S.M. Cohen, J.F. Emery, B. Li, E. Hoedt, G. Zhang, T.A. Neubert, and R.W. Tsien. 2014. γcaMKII shuttles Ca2+/CaM to the nucleus to trigger CREB phosphorylation and gene expression. *Cell*. 159:281–294. doi:10.1016/j.cell.2014.09.019.

Madera, S., M.F. Chervo, V.A. Chiauzzi, M.G. Pereyra, L. Venturutti, F. Izzo, A. Roldán Deamicis, P. Guzman, A. Dupont, J.C. Roa, M.E. Cenciarini, S. Barchuk, S. Figurelli, D. Lopez Della Vecchia, C. Levit, G. Lebersztein, F. Anfuso, T. Castiglioni, E. Cortese, S. Ares, E.G. Deza, F.G. Gercovich, C.J. Proietti, R. Schillaci, R.I. Cordo Russo, and P. V. Elizalde. 2020. Nuclear PDCD4 Expression Defines a Subset of Luminal B-Like Breast Cancers with Good Prognosis. *Horm. Cancer*. 11:218–239. doi:10.1007/s12672-020-00392-4.

Mannix, K.M., R.M. Starble, R.S. Kaufman, and L. Cooley. 2019. Proximity labeling reveals novel interactomes in live Drosophila tissue. *Development*. doi:10.1242/dev.176644.

Martelli, A.M., C. Evangelisti, M. Nyakern, and F.A. Manzoli. 2006. Nuclear protein kinase C. *Biochim. Biophys. Acta - Mol. Cell Biol. Lipids*. 1761:542–551. doi:10.1016/j.bbalip.2006.02.009.

Martin, K.C., and A. Ephrussi. 2009. mRNA Localization: Gene Expression in the Spatial Dimension. *Cell*. 136:719–730. doi:10.1016/j.cell.2009.01.044.

Martin, K.C., D. Michael, J.C. Rose, M. Barad, A. Casadio, H. Zhu, and E.R. Kandel. 1997. MAP kinase translocates into the nucleus of the presynaptic cell and is required for long-term facilitation in Aplysia. *Neuron*. 18:899–912. doi:10.1016/S0896-6273(00)80330-X.

Matsuhashi, S., H. Hamajima, J.H. Xia, H. Zhang, T. Mizuta, K. Anzai, and I. Ozaki. 2014. Control of a tumor suppressor PDCD4: Degradation mechanisms of the protein in hepatocellular carcinoma cells. *Cell. Signal.* 26:603–610. doi:10.1016/j.cellsig.2013.11.038.

Matsuhashi, S., M. Manirujjaman, H. Hamajima, and I. Ozaki. 2019. Control Mechanisms of the Tumor Suppressor PDCD4: Expression and Functions. *Int. J. Mol. Sci.* 20. doi:10.3390/ijms20092304.

Mattson, M.P., and M.K. Meffert. 2006. Roles for NF-κB in nerve cell survival, plasticity, and disease. *Cell Death Differ.* 13:852–860. doi:10.1038/sj.cdd.4401837.

Mehravar, M., A. Shirazi, M. Nazari, and M. Banan. 2019. Mosaicism in CRISPR/Cas9-mediated genome editing. *Dev. Biol.* 445:156–162. doi:10.1016/j.ydbio.2018.10.008.

Meng, X., W. Wang, H. Lu, L. He, W. Chen, E.S. Chao, M.L. Fiorotto, B. Tang, J.A. Herrera, M.L. Seymour, J.L. Neul, F.A. Pereira, J. Tang, M. Xue, and H.Y. Zoghbi. 2016. Manipulations of MeCP2 in glutamatergic neurons highlight their contributions to Rett and other neurological disorders. *Elife*. 5. doi:10.7554/eLife.14199.

Mengual, E., P. Arizti, J. Rodrigo, J.M. Giménez-Amaya, and J.G. Castaño. 1996. Immunohistochemical distribution and electron microscopic subcellular localization of the proteasome in the rat CNS. *J. Neurosci.* 16:6331–6341. doi:10.1523/jneurosci.16-20-06331.1996.

Merlet, J., J. Burger, J.E. Gomes, and L. Pintard. 2009. Regulation of cullin-RING E3 ubiquitin-ligases by neddylation and dimerization. *Cell. Mol. Life Sci.* 66:1924–1938. doi:10.1007/s00018-009-8712-7.

Mi, H., A. Muruganujan, D. Ebert, X. Huang, and P.D. Thomas. 2019. PANTHER version 14: More genomes, a new PANTHER GO-slim and improvements in enrichment analysis tools. *Nucleic Acids Res.* 47:D419–D426. doi:10.1093/nar/gky1038.

von Mikecz, A. 2006. The nuclear ubiquitin-proteasome system. *J. Cell Sci.* 119:1977–1984. doi:10.1242/jcs.03008.

Mikenberg, I., D. Widera, A. Kaus, B. Kaltschmidt, and C. Kaltschmidt. 2007. Transcription Factor NF-κB Is Transported to the Nucleus via Cytoplasmic Dynein/Dynactin Motor Complex in Hippocampal Neurons. *PLoS One*. 2:e589. doi:10.1371/journal.pone.0000589.

Morris, R.G.M., E. Anderson, G.S. Lynch, and M. Baudry. 1986. Selective impairment of learning and blockade of long-term potentiation by an N-methyl-D-aspartate receptor antagonist, AP5. *Nature*. 319:774–776. doi:10.1038/319774a0.

Nakashima, M., H. Hamajima, J. Xia, S. Iwane, Y. Kwaguchi, Y. Eguchi, T. Mizuta, K. Fujimoto, I. Ozaki, and S. Matsuhashi. 2010. Regulation of tumor suppressor PDCD4 by novel protein kinase C isoforms. *Biochim. Biophys. Acta - Mol. Cell Res.* 1803:1020–1027. doi:10.1016/j.bbamcr.2010.05.002.

Narasimhan, M., M. Rathinam, A. Riar, D. Patel, S. Mummidi, H.S. Yang, N.H. Colburn, G.I. Henderson, and L. Mahimainathan. 2013. Programmed Cell Death 4 (PDCD4): A Novel Player in Ethanol-Mediated Suppression of Protein Translation in Primary Cortical Neurons and Developing Cerebral Cortex. *Alcohol. Clin. Exp. Res.* 37:96–109. doi:10.1111/j.1530-0277.2012.01850.x.

Nguyen, P. V., and E.R. Kandel. 1997. Brief theta-burst stimulation induces a transcription-dependent late phase of LTP requiring cAMP in area CA1 of the mouse hippocampus. *Learn. Mem.* 4:230–243. doi:10.1101/lm.4.2.230.

Nguyen, P. V, T. Abel, and E.R. Kandel. 1994. Requirement of a critical period of transcription for induction of a late phase of LTP. *Sci. (New York, NY)*. 265:1104–1107. doi:10.1126/science.8066450.

Nicoll, R.A. 2017. A Brief History of Long-Term Potentiation. *Neuron*. 93:281–290. doi:10.1016/j.neuron.2016.12.015.

Ning, F., F. Wang, M. Li, Z. Yu, Y. Hao, and S. Chen. 2014. MicroRNA-182 modulates chemosensitivity of human non-small cell lung cancer to cisplatin by targeting PDCD4. *Diagn. Pathol.* 9. doi:10.1186/1746-1596-9-143.

Nonaka, M., R. Kim, H. Fukushima, K. Sasaki, K. Suzuki, M. Okamura, Y. Ishii, T. Kawashima, S. Kamijo, S. Takemoto-Kimura, H. Okuno, S. Kida, and H. Bito. 2014. Region-Specific Activation of CRTC1-CREB Signaling Mediates Long-Term Fear Memory. *Neuron*. 84:92–106. doi:10.1016/j.neuron.2014.08.049.

Ortega-Martínez, S. 2015. A new perspective on the role of the CREB family of transcription factors in memory consolidation via adult hippocampal neurogenesis. *Front. Mol. Neurosci.* 8. doi:10.3389/fnmol.2015.00046.

Palamarchuk, A., A. Efanov, V. Maximov, R.I. Aqeilan, C.M. Croce, and Y. Pekarsky. 2005. Akt Phosphorylates and Regulates Pdcd4 Tumor Suppressor Protein. *Cancer Res.* 65:11282–11286. doi:10.1158/0008-5472.CAN-05-3469.

Di Paolo, A., G. Eastman, R. Mesquita-Ribeiro, J. Farias, A. Macklin, T. Kislinger, C. Nancy, D. Munroe, J.R.S. Sosa, F. Dajas-Bailador, and J.R. Sotelo-Silveira. 2020. PDCD4 regulates axonal growth by translational repression of neurite growth-related genes and is modulated during nerve injury responses. *RNA*. 26:1637–1653. doi:10.1261/rna.075424.120.

Parra-Damas, A., M. Chen, L. Enriquez-Barreto, L. Ortega, S. Acosta, J.C. Perna, M.N. Fullana, J. Aguilera, J. Rodríguez-Alvarez, and C.A. Saura. 2017. CRTC1 Function During Memory Encoding Is Disrupted in Neurodegeneration. *Biol. Psychiatry*. 81:111–123. doi:10.1016/j.biopsych.2016.06.025.

Parra-Damas, A., J. Valero, M. Chen, J. Espana, E. Martin, I. Ferrer, J. Rodriguez-Alvarez, and C.A. Saura. 2014. Crtc1 Activates a Transcriptional Program Deregulated at Early

Alzheimer's Disease-Related Stages. *J. Neurosci.* 34:5776–5787. doi:10.1523/JNEUROSCI.5288-13.2014.

Pedreira, M.E. 1996. Inhibitors of protein and RNA synthesis block context memory and long-term habituation in the crab Chasmagnathus. *Pharmacol. Biochem. Behav.* 54:611–617. doi:10.1016/0091-3057(95)02206-6.

Plath, N., O. Ohana, B. Dammermann, M.L. Errington, D. Schmitz, C. Gross, X. Mao, A. Engelsberg, C. Mahlke, H. Welzl, U. Kobalz, A. Stawrakakis, E. Fernandez, R. Waltereit, A. Bick-Sander, E. Therstappen, S.F. Cooke, V. Blanquet, W. Wurst, B. Salmen, M.R. Bösl, H.-P. Lipp, S.G.N. Grant, T.V.P. Bliss, D.P. Wolfer, and D. Kuhl. 2006. Arc/Arg3.1 Is Essential for the Consolidation of Synaptic Plasticity and Memories. *Neuron*. 52:437–444. doi:10.1016/j.neuron.2006.08.024.

Polleux, F., G. Ince-Dunn, and A. Ghosh. 2007. Transcriptional regulation of vertebrate axon guidance and synapse formation. *Nat. Rev. Neurosci.* 8:331–340. doi:10.1038/nrn2118.

Ramanan, N., Y. Shen, S. Sarsfield, T. Lemberger, G. Schütz, D.J. Linden, and D.D. Ginty. 2005. SRF mediates activity-induced gene expression and synaptic plasticity but not neuronal viability. *Nat. Neurosci.* 8:759–767. doi:10.1038/nn1462.

Ramón y Cajal, S. 1894. Consideraciones generales sobre la morfología de la célula nerviosa. *La Vet. Española*. 37:257–260, 273–275, 289–291.

Rao-Ruiz, P., J.J. Couey, I.M. Marcelo, C.G. Bouwkamp, D.E. Slump, M.R. Matos, R.J. van der Loo, G.J. Martins, M. van den Hout, W.F. van IJcken, R.M. Costa, M.C. van den Oever, and S.A. Kushner. 2019. Engram-specific transcriptome profiling of contextual memory consolidation. *Nat. Commun.* 10:2232. doi:10.1038/s41467-019-09960-x.

Rhee, H.-W., P. Zou, N.D. Udeshi, J.D. Martell, V.K. Mootha, S.A. Carr, and A.Y. Ting. 2013.

Proteomic Mapping of Mitochondria in Living Cells via Spatially Restricted Enzymatic Tagging. *Science (80-.).* 339:1328–1331. doi:10.1126/science.1230593.

Riar, A.K., M. Narasimhan, M.L. Rathinam, D. Vedpathak, S. Mummidi, G.I. Henderson, and L. Mahimainathan. 2014. Ethanol-Induced Transcriptional Activation of Programmed Cell Death 4 (Pdcd4) Is Mediated by GSK-3β Signaling in Rat Cortical Neuroblasts. *PLoS One*. 9. doi:10.1371/journal.pone.0098080.

Rossetti, C., D. Sciarra, J.-M. Petit, C.B. Eap, O. Halfon, P.J. Magistretti, B. Boutrel, and J.-R. Cardinaux. 2017. Gender-specific alteration of energy balance and circadian locomotor activity in the Crtc1 knockout mouse model of depression. *Transl. Psychiatry*. 7:1269. doi:10.1038/s41398-017-0023-4.

Sakimura, K., T. Kutsuwada, I. Ito, T. Manabe, C. Takayama, E. Kushiya, T. Yagi, S. Aizawa, Y. Inoue, H. Sugiyama, and M. Mishina. 1995. Reduced hippocampal LTP and spatial learning in mice lacking NMDA receptor ε1 subunit. *Nature*. 373:151–155. doi:10.1038/373151a0.

Saura, C.A., and J.-R. Cardinaux. 2017. Emerging Roles of CREB-Regulated Transcription Coactivators in Brain Physiology and Pathology. *Trends Neurosci.* 40:720–733. doi:10.1016/j.tins.2017.10.002.

Schindelin, J., I. Arganda-Carreras, E. Frise, V. Kaynig, M. Longair, T. Pietzsch, S. Preibisch, C. Rueden, S. Saalfeld, B. Schmid, J.Y. Tinevez, D.J. White, V. Hartenstein, K. Eliceiri, P. Tomancak, and A. Cardona. 2012. Fiji: An open-source platform for biological-image analysis. *Nat. Methods*. 9:676–682. doi:10.1038/nmeth.2019.

Schlumm, F., D. Mauceri, H.E. Freitag, and H. Bading. 2013. Nuclear calcium signaling regulates nuclear export of a subset of class iia histone deacetylases following synaptic

activity. *J. Biol. Chem.* 288:8074–8084. doi:10.1074/jbc.M112.432773.

Schmid, T., A.P. Jansen, A.R. Baker, G. Hegamyer, J.P. Hagan, and N.H. Colburn. 2008. Translation inhibitor Pdcd4 is targeted for degradation during tumor promotion. *Cancer Res.* 68:1254–1260. doi:10.1158/0008-5472.CAN-07-1719.

Scoville, W.B., and B. Milner. 1957. Loss of Recent Memory After Bilateral Hippocampal Lesions. *J. Neurol. Neurosurg. Psychiatry*. 20:11–21. doi:10.1136/jnnp.20.1.11.

Sears, R.M., D.G. May, and K.J. Roux. 2019. BioID as a Tool for Protein-Proximity Labeling in Living Cells. 299–313.

Sekeres, M.J., V. Mercaldo, B. Richards, D. Sargin, V. Mahadevan, M.A. Woodin, P.W. Frankland, and S.A. Josselyn. 2012. Increasing CRTC1 function in the dentate gyrus during memory formation or reactivation increases memory strength without compromising memory quality. *J. Neurosci.* 32:17857–17868. doi:10.1523/JNEUROSCI.1419-12.2012.

Shan, W., H. Ge, B. Chen, L. Huang, S. Zhu, and Y. Zhou. 2021. Upregulation of miR-499a-5p Decreases Cerebral Ischemia/Reperfusion Injury by Targeting PDCD4. *Cell. Mol. Neurobiol.* doi:10.1007/s10571-021-01085-4.

Sheng, M., G. McFadden, and M.E. Greenberg. 1990. Membrane depolarization and calcium induce c-fos transcription via phosphorylation of transcription factor CREB. *Neuron*. 4:571–582. doi:10.1016/0896-6273(90)90115-V.

Shibahara, K., M. Asano, Y. Ishida, T. Aoki, T. Koike, and T. Honjo. 1995. Isolation of a novel mouse gene MA-3 that is induced upon programmed cell death. *Gene*. 166:297–301. doi:10.1016/0378-1119(95)00607-9.

Shiota, M., M.H. Izumi, A. Tanimoto, M. Takahashi, N. Miyamoto, E. Kashiwagi, A. Kidani, G. Hirano, D. Masubuchi, Y. Fukunaka, Y. Yasuniwa, S. Naito, S. Nishizawa, Y. Sasaguri, and

K. Kohno. 2009. Programmed cell death protein 4 down-regulates Y-Box binding protein-1 expression via a direct interaction with twistl to suppress cancer cell growth. *Cancer Res.* 69:3148–3156. doi:10.1158/0008-5472.CAN-08-2334.

Stein, L.R., D.F. Wozniak, J.T. Dearborn, S. Kubota, R.S. Apte, Y. Izumi, C.F. Zorumski, and S. -i. Imai. 2014. Expression of Nampt in Hippocampal and Cortical Excitatory Neurons Is Critical for Cognitive Function. *J. Neurosci.* 34:5800–5815. doi:10.1523/JNEUROSCI.4730-13.2014.

Struhl, G., and A. Adachi. 1998. Nuclear access and action of notch in vivo. *Cell*. 93:649–60.

Swiech, L., M. Heidenreich, A. Banerjee, N. Habib, Y. Li, J. Trombetta, M. Sur, and F. Zhang. 2015. In vivo interrogation of gene function in the mammalian brain using CRISPR-Cas9. *Nat. Biotechnol.* 33:102–106. doi:10.1038/nbt.3055.

Takeuchi, T., A.J. Duszkiewicz, and R.G.M. Morris. 2014. The synaptic plasticity and memory hypothesis: encoding, storage and persistence. *Philos. Trans. R. Soc. B Biol. Sci.* 369:20130288. doi:10.1098/rstb.2013.0288.

Thompson, K.R., K.O. Otis, D.Y. Chen, Y. Zhao, T.J. O'Dell, and K.C. Martin. 2004. Synapse to nucleus signaling during long-term synaptic plasticity: A role for the classical active nuclear import pathway. *Neuron*. 44:997–1009. doi:10.1016/j.neuron.2004.11.025.

Ting, L., R. Rad, S.P. Gygi, and W. Haas. 2011. MS3 eliminates ratio distortion in isobaric multiplexed quantitative proteomics. *Nat. Methods*. 8:937–940. doi:10.1038/nmeth.1714.

Trevino, A.E., N. Sinnott-Armstrong, J. Andersen, S.-J. Yoon, N. Huber, J.K. Pritchard, H.Y. Chang, W.J. Greenleaf, and S.P. Pașca. 2020. Chromatin accessibility dynamics in a model of human forebrain development. *Science (80-.).* 367:eaay1645. doi:10.1126/science.aay1645.

Tsien, J.Z., D.F. Chen, D. Gerber, C. Tom, E.H. Mercer, D.J. Anderson, M. Mayford, E.R. Kandel, and S. Tonegawa. 1996a. Subregion- and Cell Type–Restricted Gene Knockout in Mouse Brain. *Cell*. 87:1317–1326. doi:10.1016/S0092-8674(00)81826-7.

Tsien, J.Z., P.T. Huerta, and S. Tonegawa. 1996b. The Essential Role of Hippocampal CA1 NMDA Receptor–Dependent Synaptic Plasticity in Spatial Memory. *Cell*. 87:1327–1338. doi:10.1016/S0092-8674(00)81827-9.

Tydlacka, S., C.E. Wang, X. Wang, S. Li, and X.J. Li. 2008. Differential activities of the ubiquitin-proteasome system in neurons versus glia may account for the preferential accumulation of misfolded proteins in neurons. *J. Neurosci.* 28:13285–13295. doi:10.1523/JNEUROSCI.4393-08.2008.

Tyssowski, K.M., N.R. DeStefino, J.H. Cho, C.J. Dunn, R.G. Poston, C.E. Carty, R.D. Jones, S.M. Chang, P. Romeo, M.K. Wurzelmann, J.M. Ward, M.L. Andermann, R.N. Saha, S.M. Dudek, and J.M. Gray. 2018. Different Neuronal Activity Patterns Induce Different Gene Expression Programs. *Neuron*. 98:530-546.e11. doi:10.1016/j.neuron.2018.04.001.

Uchida, S., B.J.W. Teubner, C. Hevi, K. Hara, A. Kobayashi, R.M. Dave, T. Shintaku, P. Jaikhan, H. Yamagata, T. Suzuki, Y. Watanabe, S.S. Zakharenko, and G.P. Shumyatsky. 2017. CRTC1 Nuclear Translocation Following Learning Modulates Memory Strength via Exchange of Chromatin Remodeling Complexes on the Fgf1 Gene. *Cell Rep.* 18:352–366. doi:10.1016/j.celrep.2016.12.052.

Uezu, A., D. Kanak, T. Bradshaw, E. Soderblom, C. Catavero, A. Burette, R. Weinberg, and S. Soderling. 2016. Identification of an elaborate complex mediating postsynaptic inhibition. *Sci. (New York, NY)*. 353:1123–1129. doi:10.1126/science.aag0821.

Untergasser, A., I. Cutcutache, T. Koressaar, J. Ye, B.C. Faircloth, M. Remm, and S.G. Rozen.

2012. Primer3—new capabilities and interfaces. *Nucleic Acids Res.* 40. doi:10.1093/nar/gks596.

Upadhya, S.C., L. Ding, T.K. Smith, and A.N. Hegde. 2006. Differential regulation of proteasome activity in the nucleus and the synaptic terminals. *Neurochem. Int.* 48:296–305. doi:10.1016/j.neuint.2005.11.003.

Upadhya, S.C., T.K. Smith, and A.N. Hegde. 2004. Ubiquitin-proteasome-mediated CREB repressor degradation during induction of long-term facilitation. *J. Neurochem.* 91:210–219. doi:10.1111/j.1471-4159.2004.02707.x.

Vong, L., C. Ye, Z. Yang, B. Choi, S. Chua, and B.B. Lowell. 2011. Leptin Action on GABAergic Neurons Prevents Obesity and Reduces Inhibitory Tone to POMC Neurons. *Neuron*. 71:142–154. doi:10.1016/j.neuron.2011.05.028.

Vooijs, M., J. Jonkers, and A. Berns. 2001. A highly efficient ligand-regulated Cre recombinase mouse line shows that LoxP recombination is position dependent. *EMBO Rep.* 2:292–297. doi:10.1093/embo-reports/kve064.

Wang, B., J. Goode, J. Best, J. Meltzer, P.E. Schilman, J. Chen, D. Garza, J.B. Thomas, and M. Montminy. 2008. The Insulin-Regulated CREB Coactivator TORC Promotes Stress Resistance in Drosophila. *Cell Metab.* 7:434–444. doi:10.1016/j.cmet.2008.02.010.

Wang, Q., and H.S. Yang. 2018. The role of Pdcd4 in tumour suppression and protein translation. *Biol. Cell*. 110:169–177. doi:10.1111/boc.201800014.

Wang, Q., J. Zhu, Y.W. Wang, Y. Dai, Y.L. Wang, C. Wang, J. Liu, A. Baker, N.H. Colburn, and H.S. Yang. 2017. Tumor suppressor Pdcd4 attenuates Sin1 translation to inhibit invasion in colon carcinoma. *Oncogene*. 36:6225–62354. doi:10.1038/onc.2017.228.

Wang, Y., H. Inoue, K. Ravnskjaer, K. Viste, N. Miller, Y. Liu, S. Hedrick, L. Vera, and M.

Montminy. 2010. Targeted disruption of the CREB coactivator Crtc2 increases insulin sensitivity. *Proc. Natl. Acad. Sci.* 107:3087–3092. doi:10.1073/pnas.0914897107.

Watts, A.G., G. Sanchez-Watts, Y. Liu, and G. Aguilera. 2011. The Distribution of Messenger RNAs Encoding the Three Isoforms of the Transducer of Regulated cAMP Responsive Element Binding Protein Activity in the Rat Forebrain. *J. Neuroendocrinol.* 23:754–766. doi:10.1111/j.1365-2826.2011.02178.x.

Wayman, G.A., S. Impey, D. Marks, T. Saneyoshi, W.F. Grant, V. Derkach, and T.R. Soderling. 2006. Activity-Dependent Dendritic Arborization Mediated by CaM-Kinase I Activation and Enhanced CREB-Dependent Transcription of Wnt-2. *Neuron*. 50:897–909. doi:10.1016/j.neuron.2006.05.008.

Wedeken, L., P. Singh, and K.H. Klempnauer. 2011. Tumor suppressor protein Pdcd4 inhibits translation of p53 mRNA. *J. Biol. Chem.* 286:42855–42862. doi:10.1074/jbc.M111.269456.

Wei, N., S.S. Liu, K.K.L. Chan, and H.Y.S. Ngan. 2012. Tumour Suppressive Function and Modulation of Programmed Cell Death 4 (PDCD4) in Ovarian Cancer. *PLoS One*. 7. doi:10.1371/journal.pone.0030311.

West, A.E., W.G. Chen, M.B. Dalva, R.E. Dolmetsch, J.M. Kornhauser, A.J. Shaywitz, M.A. Takasu, X. Tao, and M.E. Greenberg. 2001. Calcium regulation of neuronal gene expression. *Proc. Natl. Acad. Sci.* 98:11024–11031. doi:10.1073/pnas.191352298.

West, A.E., and M.E. Greenberg. 2011. Neuronal activity-regulated gene transcription in synapse development and cognitive function. *Cold Spring Harb. Perspect. Biol.* 3:1–21. doi:10.1101/cshperspect.a005744.

Whitlock, J.R. 2006. Learning Induces Long-Term Potentiation in the Hippocampus. *Science (80-.).* 313:1093–1097. doi:10.1126/science.1128134.

Wild, A.R., B.L. Sinnen, P.J. Dittmer, M.J. Kennedy, W.A. Sather, and M.L. Dell'Acqua. 2019. Synapse-to-Nucleus Communication through NFAT Is Mediated by L-type Ca2+ Channel Ca2+ Spike Propagation to the Soma. *Cell Rep.* 26:3537-3550.e4. doi:10.1016/j.celrep.2019.03.005.

Wu, Y.E., L. Pan, Y. Zuo, X. Li, and W. Hong. 2017. Detecting Activated Cell Populations Using Single-Cell RNA-Seq. *Neuron*. 96:313-329.e6. doi:10.1016/j.neuron.2017.09.026.

Wüstenberg, D., B. Gerber, and R. Menzel. 1998. Long- but not medium-term retention of olfactory memories in honeybees is impaired by actinomycin D and anisomycin. *Eur. J. Neurosci.* 10:2742–2745. doi:10.1046/j.1460-9568.1998.00319.x.

Yang, H.-S., M.-H. Cho, H. Zakowicz, G. Hegamyer, N. Sonenberg, and N.H. Colburn. 2004. A Novel Function of the MA-3 Domains in Transformation and Translation Suppressor Pdcd4 Is Essential for Its Binding to Eukaryotic Translation Initiation Factor 4A. *Mol. Cell. Biol.* 24:3894–3906. doi:10.1128/mcb.24.9.3894-3906.2004.

Yang, H.-S., A.P. Jansen, A.A. Komar, X. Zheng, W.C. Merrick, S. Costes, S.J. Lockett, N. Sonenberg, and N.H. Colburn. 2003a. The Transformation Suppressor Pdcd4 Is a Novel Eukaryotic Translation Initiation Factor 4A Binding Protein That Inhibits Translation. *Mol. Cell. Biol.* 23:26–37. doi:10.1128/mcb.23.1.26-37.2003.

Yang, H.-S., J.L. Knies, C. Stark, and N.H. Colburn. 2003b. Pdcd4 suppresses tumor phenotype in JB6 cells by inhibiting AP-1 transactivation. *Oncogene*. 22:3712–3720. doi:10.1038/sj.onc.1206433.

Yang, H.-S., C.P. Matthews, T. Clair, Q. Wang, A.R. Baker, C.-C.H. Li, T.-H. Tan, and N.H. Colburn. 2006. Tumorigenesis Suppressor Pdcd4 Down-Regulates Mitogen-Activated Protein Kinase Kinase Kinase Kinase 1 Expression To Suppress Colon Carcinoma Cell

Invasion. *Mol. Cell. Biol.* 26:1297–1306. doi:10.1128/mcb.26.4.1297-1306.2006.

Yap, E.L., and M.E. Greenberg. 2018. Activity-Regulated Transcription: Bridging the Gap between Neural Activity and Behavior. *Neuron*. 100:330–348. doi:10.1016/j.neuron.2018.10.013.

Ye, J., G. Coulouris, I. Zaretskaya, I. Cutcutache, S. Rozen, and T.L. Madden. 2012. Primer-BLAST: a tool to design target-specific primers for polymerase chain reaction. *BMC Bioinformatics*. 13:134. doi:10.1186/1471-2105-13-134.

Yuanxiang, P., S. Bera, A. Karpova, M.R. Kreutz, and M. Mikhaylova. 2014. Isolation of CA1 Nuclear Enriched Fractions from Hippocampal Slices to Study Activity-dependent Nuclear Import of Synapto-nuclear Messenger Proteins. *J. Vis. Exp.* doi:10.3791/51310.

Zhai, S., E.D. Ark, P. Parra-Bueno, and R. Yasuda. 2013. Long-distance integration of nuclear ERK signaling triggered by activation of a few dendritic spines. *Science*. 342:1107–11. doi:10.1126/science.1245622.

Zhang, H., I. Ozaki, T. Mizuta, H. Hamajima, T. Yasutake, Y. Eguchi, H. Ideguchi, K. Yamamoto, and S. Matsuhashi. 2006. Involvement of programmed cell death 4 in transforming growth factor-β1-induced apoptosis in human hepatocellular carcinoma. *Oncogene*. 25:6101–6112. doi:10.1038/sj.onc.1209634.

Zhou, Y., H. Wu, S. Li, Q. Chen, X.-W. Cheng, J. Zheng, H. Takemori, and Z.-Q. Xiong. 2006. Requirement of TORC1 for Late-Phase Long-Term Potentiation in the Hippocampus. *PLoS One*. 1. doi:10.1371/journal.pone.0000016.